

Dissertation

Jessica Sze Ki Chan

Dissertation
submitted to the
Combined Faculty of Natural Sciences and Mathematics
of the Ruperto Carola University Heidelberg, Germany
for the degree of
Doctor of Natural Sciences

Presented by:

M.Sc. Jessica Sze Ki Chan

Born in: Hong Kong

Oral examination: 22nd June 2018

The Oncogenic Role of TRIP13 in Hepatocellular Carcinoma

Referees:

PD Dr. Karin Mueller-Decker

Prof. Dr. Stephan Herzig

Summary

Hepatocellular carcinoma (HCC) is the fifth most common cancer and the second leading cause of cancer-related mortality worldwide. The high mortality rates have been attributed to late diagnosis and limited treatment options available. Sorafenib, a multi-kinase inhibitor, is currently the only targeted therapy that has shown survival benefits in advanced HCC patients. Several other targeted therapies, which were successful in animal models of HCC and in human cancer of head and neck, were met with limited success in HCC patients. Due to the unmet medical needs, it is clear that characterization of the mechanisms during hepatocarcinogenesis is pivotal in identifying novel treatment targets and diagnostic biomarkers.

In an effort to identify novel targets during HCC, previous work from the lab has shown that TRIP13, a member of the AAA⁺-ATPase family was significantly upregulated in DEN-induced HCC in mice and in human HCC. TRIP13 has been described to be an important regulator of chromosomal events during meiosis and mitosis. An induced expression of TRIP13 has been reported in several cancer entities however its cancer-related role remains marginally understood. Interestingly, TRIP13 forms part of the chromosomal instability (CIN) gene signature that is commonly seen in tumour cells and has DNA-damage repair functions in head and neck carcinoma cells (SSCHN).

Unpublished data from the lab was the first to have confirmed the growth-promoting role of TRIP13 in liver, which was unveiled during hepatocyte regeneration and tumorigenesis using various mouse models of HCC. Here, we aim to dissect the mechanism through which TRIP13 exerts its pro-proliferative effects in HCC and to identify novel signalling pathways through which TRIP13 could exert its function.

In this study, we showed that TRIP13 is essential during cell growth and proliferation, proliferation was severely impaired by Trip13 knockdown in all mouse and human HCC cells lines under investigation. Conversely, the overexpression of Trip13 in non-tumourigenic AML12 liver cells stimulated cell proliferation significantly, with upregulated expression of oncogenic factors like c-MYC, EGFR and cyclin D1. We identified an unexpected functional relevance of the interaction between TRIP13 and SIN3A, which was enriched during a MS screen for Trip13 interaction partners previously performed in the lab. SIN3A has been commonly described as a transcriptional repressor due to its HDAC-related roles. Strikingly, a concomitant depletion of SIN3A reverses the growth defect of TRIP13-depleted HCC cells, despite accumulated DNA damages (from TRIP13 depletion) still apparent in these growth-rescued cells. This growth rescue was paralleled by a partial restoration of c-MYC expression levels, which were significantly depleted during TRIP13-KD alone. We further demonstrated that the overexpression of c-MYC was able to rescue the growth defect seen in TRIP13-depleted cells.

Taken together, this study is the first to report on an oncogenic, pro-proliferative role of TRIP13 in liver cancer using both human HCC cells and mice HCC models. An inhibition of c-MYC and its downstream targets might account for the growth arrest and apoptotic cell death during TRIP13-depletion. Along with the reported roles of SIN3A as a c-MYC antagonist, further work is required to decipher a possible cross talk between TRIP13, SIN3A and c-MYC and its functional relevance during hepatocarcinogenesis.

Zusammenfassung Summary

Das hepatozelluläre Karzinom (*hepatocellular carcinoma*, HCC) ist weltweit die fünfthäufigste Krebsart aber an zweiter Stelle was die Krebs-assoziierten Mortalität angeht. Für die hohe Sterbebrate werden insbesondere die späte Diagnose sowie die limitierten Behandlungsoptionen verantwortlich gemacht. Die Behandlung mit Sorafenib, einem Multikinase-Inhibitor, stellt zurzeit die einzige gerichtete Therapie dar, bei der ein Benefit bezüglich Überleben festgestellt werden konnte. Verschiedene andere Therapieansätze, die in HCC-Tiermodellen sowie z.B. beim humanen Kopf-Hals Karzinom erfolgreich eingesetzt wurden, zeigten bei HCC-Patienten nur eine sehr eingeschränkte Wirkung. Angesichts dieses ungedeckten klinischen Bedarfs ist eine weiterführende Charakterisierung der Mechanismen der hepatischen Karzinogenese von entscheidender Bedeutung für die Identifikation neuer Zielstrukturen für Therapie sowie von diagnostischen Biomarkern.

In vorherigen Arbeiten aus unserem Labor zur Identifikation neuer Zielstrukturen bei HCC wurde gezeigt, dass Trip13, ein Mitglied aus Proteinfamilie der AAA⁺-ATPasen, signifikant hochreguliert war beim hepatozellulären Karzinom im Menschen sowie bei Diethylnitrosamin-induziertem Leberkrebs in Mäusen. Trip13 war als wichtiger Regulator chromosomaler Prozesse während der Meiose und der Mitose beschrieben worden. Eine erhöhte Expression von Trip13 war zuvor in mehreren Krebsarten festgestellt worden, wobei die krebsfördernde Wirkung mechanistisch nur ansatzweise aufgeklärt wurde. Interessanterweise wurde Trip13 einer häufig in Tumorzellen festgestellten Gensignatur für chromosomale Instabilität (chromosomal instability, CIN) zugeordnet, sowie einer DNA-Reparatur-Funktion beim Kopf-Hals-Karzinom.

In bisher nicht publizierten Daten aus unserem Labor wurde zum ersten Mal eine wachstumsfördernde Wirkung von Trip13 in der Leber gezeigt, die sich sowohl bei Hepatozyten-Regenerationsprozessen als auch bei der Tumourgenese in verschiedenen Mausmodellen von HCC bestätigte. Ziel dieser Arbeit war die Aufklärung der Mechanismen durch die Trip13 seine pro-proliferative Wirkung ausübt, sowie die Identifikation von bisher unbekanntem Signalwegen, die daran beteiligt sein könnten.

In der vorliegenden Studie konnten wir zeigen, dass Trip13 von zentraler Bedeutung für Zellwachstum und Proliferation ist. Trip13-Defizienz reduzierte in erheblichem Maß das Zellwachstum bei allen untersuchten humanen und murinen HCC-Zelllinien. Umgekehrt führte die Überexpression of Trip13 in nicht-tumorbildenden AML12-Leberzellen zu einer signifikanten Erhöhung des Zellwachstums (Proliferation), die mit einer Erhöhung der Expression von onkogenen Faktoren wie c-MYC, EGFR und Cyclin D1 einher ging. Darüber hinaus konnten wir eine unerwartete funktionale Relevanz der Interaktion zwischen Trip13 und SIN3A feststellen. Der Interaktionspartner SIN3A war zuvor aus einem im Labor durchgeführten Screen nach Trip13-Interaktionsproteinen mittels Massenspektrometrie hervorgegangen und als transkriptioneller Korepressor in Komplexen mit Histon-deacetylasen beschrieben worden. Erstaunlicherweise führte die gleichzeitige Ausschaltung von SIN3A zu einer vollständigen Aufhebung des wachstumshemmenden Effekts der Trip13-Depletion in HCC-Zellen. Die Umkehrung des Wachstumseffekts hatte jedoch keinen Einfluss auf die Erhöhung der DNA-Schäden, die wir nach Trip13-Depletion detektieren konnten. Diese Aufhebung des Wachstumsdefekts ging mit einer zumindest teilweisen Wiederherstellung der c-MYC-Expressionslevel einher, die bei der alleinigen Depletion von Trip13 erheblich reduziert waren. Darüber hinaus konnten wir zeigen, dass eine

Überexpression von c-MYC in der Lage war, den Wachstumsdefekt nach Trip13-Depletion umzukehren.

Diese Arbeit zeigt zum ersten Mal eine onkogene, pro-proliferative Rolle von Trip13 bei Leberkrebs unter Verwendung von humanen und murinen HCC-Zelllinien und HCC-Maus-Modellen. Die Reduktion von c-MYC und dessen Zielgenen könnte dabei für die wachstumshemmende und Apoptose-auslösende Wirkung von Trip13-Depletion verantwortlich sein. Unter Berücksichtigung der zuvor berichteten Rolle von SIN3A als Inhibitor von c-MYC, sind weiterführende Untersuchungen notwendig um die funktionalen Zusammenhänge zwischen Trip13, SIN3A und c-MYC hinsichtlich ihrer Relevanz für die Hepatokarzinogenese umfassend zu definieren.

Acknowledgments

I would like to thank Prof. Stephan Herzig for giving me the opportunity to perform my doctoral study in his department and for his constant support throughout my studies. I am greatly indebted to Dr Mauricio Berriel Diaz for his relentless time and commitment in seeing me through my PhD studies, thank you for your guidance and mentorship. To my TAC committee members: Dr Karin Müller-Decker and Kai Breuhahn, thank you for taking the time through these few years to participate in the reviewing and constant discussions for my thesis.

I would like to also express my gratitude to Dr Adam Rose and Dr Adriano Maida whom provided me with great support and supervision during the early phases of my PhD studies. Thank you for not only being a great teacher but a great friend as well. To: Annika, Jonas, Jessie and Thomas, you have been awesome colleagues and friends. The times spent in our previous AJR group back in DKFZ will always remain a good part of my memories from Heidelberg.

Many thanks to the old colleagues from DKFZ and current ones from Helmholtz IDC Munich for the great working atmosphere and for the great support. A special thank you to Götz, Marcos and Sören for their critical inputs and proofreading the manuscript of this thesis. To: Eveline, Phivos, Ana, Maude, Asrar, Miriam, Bahar, Aish and so many more as well, you have been great colleagues and friends! I am extremely grateful to have met so many talented and dedicated colleagues, many of whom I was able to develop not only a professional relationship but an enduring friendship as well.

I would like to express my gratitude to Prof Birgit Lane and Prof Mark Featherstone who first ignited the curiosities in a fresh-faced undergrad student when they first demonstrated seemingly abstract findings in such simple and casual ways. Thank you for having shaped my decisions to eventually pursue my PhD studies.

Most of all I would like to thank my family for their relentless support and faith in me. Thank you for always believing in me and allowing your wilful child the freedom to pursue her dreams. To my family: thanks for always reminding me to keep a picture of the trophy ahead and to not get lost in the midst of my own little world. To Matthias: thanks for being a constant source of support and encouragement for me, I am really appreciative of that!

I am greatly indebted to the help and support from the many people throughout my PhD studies that have made this journey smoother and much more memorable.

Contents

Summary

Contents

List of figures and tables

Abbreviations

1 Introduction

1.1	Hepatocellular Carcinoma	1
1.2	Genetic landscape and altered cell signalling driver pathways in HCC	1
1.3	Signalling pathways altered in HCC	2
1.4	Metabolic syndrome and HCC burden	4
1.4.1	Obesity, inflammation and HCC	4
1.4.2	A potential link between metabolic syndrome and HCC	4
1.4.3	Genetic instability and hepatocyte apoptosis correlate with a risk for HCC	5

2 TRIP13- An overview of cellular functions

2.1	TRIP13 as a key regulator of chromosomal processes during cell division....	6
2.1.1	TRIP13 and p31comet during mitotic checkpoint silencing	7
2.2	Upregulated expression of TRIP13 in several human cancers.....	9
2.2.1	Genomic instability and aneuploidy in cancer	9
2.2.2	Chromosomal instability (CIN) in liver cancer	9
2.2.3	Role of TRIP13 in promoting DNA repair and chemoresistance	10
2.3	A novel role of TRIP13 in liver regeneration and HCC tumourigenesis	11
2.3.1	TRIP13 is upregulated in liver cancer	12
2.3.2	TRIP13 is induced in partial hepatectomy and fatty liver diseases...	17
2.3.3	Involvement of TRIP13 in the mTOR-signalling axis?	17
2.3.4	Identifying novel interaction partners of TRIP13 in HCC	17
2.4	SIN3A— role as a transcriptional regulator in the context of cancer?	19
2.4.1	Structure and function of SIN3A.....	19
2.4.2	SIN3A as a tumour suppressor in cancer	20
2.4.3	SIN3A as a tumor oncogene in promoting tumourigenesis in Triple negative Breast cancer (TNBC)	20

CONTENTS

Aims of the study	22
3 Results	
3.1 TRIP13 regulates cell growth and proliferation in HCC cells	23
3.2 TRIP13 as a regulator of EGFR	24
3.2.1 EGFR expression is dependent on cellular levels of TRIP13	26
3.2.2 The EGF pathway does not significantly contributes to TRIP13- dependent cell growth.....	28
3.3 Investigating the mechanistic role of TRIP13 in its tumour promoting functions	
3.3.1 Identification of TRIP13-interaction partners that could define involved regulatory complexes.....	31
3.3.2 Effects of TRIP13 and interaction partners of SIN3A/SAP130 in HCC cell proliferation.....	37
3.3.3 SIN3A knockdown reverses the anti-proliferative effects from TRIP13-depletion and is recapitulated in several HCC cell lines.....	42
3.3.4 The oncogenic c-MYC pathway in mediating anti proliferative effects upon TRIP13-depletion in HLF cells	44
3.3.5 Establishing stable cell lines with concomitant depletion of TRIP13 and SIN3A for in vivo tumour implantation models	46
3.4 Effects of overexpressing Trip13 in non-tumorigenic AML12 liver cells....	49
3.4.1 Overexpressing Trip13 in AML12 cells boosted an increase in cell proliferation	50
3.5 Role of TRIP13 in the DNA damage repair pathway	51
3.5.1 Chromosomal instability (CIN) and upstream regulation of TRIP13	
3.5.2 TRIP13 in DNA damage repair pathways	52
3.5.3 Accumulation of DNA damage does not play a central role in causing proliferation defect in TRIP13-KD cells	54
3.5.4 DNA damage persist despite a proliferation rescue during concomitant depletion of TRIP13+SIN3A	55
4 Discussion	
4.1 TRIP13 as an oncogenic regulator of tumour growth	60
4.1.1 TRIP13 in cell cycle checkpoint and cancer	61
4.1.2 A proliferation-promoting role of TRIP13 in liver cancer	61
4.2 The functional implications of an interaction between TRIP13 and its interaction partner, SIN3A	61
4.2.1 Validating an interaction between TRIP13 and interaction partners	
4.2.2 Depleting of SIN3A reverses the growth impairment of TRIP13- depleted cells	61

CONTENTS

4.3	Role of the proto-oncogene c-Myc in liver cancer	
4.3.1	Possible cross talk between TRIP13 and c-MYC signalling pathways?	64
4.3.2	A possible TRIP13- c-MYC-SIN3A axis in HCC?	66
4.4	The relevance of EGFR signalling pathway during liver homeostasis and tumourigenesis?	67
4.5	The role of TRIP13 in DNA damage repair pathway and the implications in liver diseases and tumourigenesis	67
4.5.1	YAP as a regulator of TRIP13 in CIN signatures	68
4.5.2	TRIP13 in DNA damage repair pathway	68
4.6	Concluding remarks and outlook	69
5	Material and Methods	
5.1	Methods	
5.1.1	Cell culture	71
5.1.2	Cell lines	71
5.1.3	Cultivation of cells	71
5.1.4	Freezing and thawing of cells	71
5.2	Cell-based assays	
5.2.1	Cell counting kit-8 (CCK8)	73
5.2.2	BrdU cell proliferation assay	73
5.2.3	Apoptosis detection assay	74
5.2.4	Immunohistochemistry (IHC) fluorescence staining	74
5.2.5	In-situ Proximity ligation assay (PLA)	75
5.2.6	Dual luminescence assay	76
5.3	Virus work	
5.3.1	Lentivirus shRNA vector constructs	77
5.3.2	shRNA transfections to pre-select constructs with a good Knockdown	77
5.3.3	Lentivirus production	78
5.3.4	Lentivirus titer calculations	78
5.3.5	Lentivirus transduction and establishing stable cell lines	78
5.5	RNA methods	
5.5.1	RNA extraction from cell culture samples	79
5.5.2	Reverse transcription of RNA to form cDNA	79
5.5.3	TaqMan qPCR to quantify for gene expression	79

CONTENTS

5.6	Protein method	
5.6.1	Protein extraction from cell culture	80
5.6.2	Determination of protein concentrations	80
5.6.3	SDS-polyacrylamide gel electrophoresis	80
5.6.4	Protein transfer and immunoblotting	80
5.7	Molecular Cloning	
5.7.1	Transformation of bacteria <i>E.coli</i> cells	81
5.7.2	Growing bacteria colonies for plasmid amplification	81
5.7.3	Plasmid DNA purification	81
5.8	Nomenclature of genes and proteins	81
5.9	Materials	
5.9.1	Equipment	82
5.10	Consumables	83
5.11	Kits	85
5.12	Enzymes	86
5.13	Plasmids	86
5.14	Chemicals	87
5.15	Cell culture reagents	88
5.16	Antibodies	90
5.17	Software	91
5.18	Commercial probes for TaqMan quantitative PCR	92
5.19	Solutions and Buffers	93
	Appendices	94
	References	97

List of Figures

1.1	Cirrhosis as a cancer field during malignant tumour transformation.....	2
1.2	The pathological progression from benign hepatic steatosis to NASH/cirrhosis and eventually to HCC formation	5
1.3	Schematic organization of the human TRIP13 and the proposed model for its role in mitotic checkpoint silencing	8
1.4	Expression of Trip13 in human HCC and mouse model of DEN-induced HCC... ..	12
1.5	Trip13 is upregulated in mouse models of fatty liver diseases and during liver regeneration	13
1.6	Trip13 is essential during hepatocyte regeneration after partial hepatectomy (PHX) operation in mice	14
1.7	Trip13 depletion inhibits tumor growth in a tumour xenograft model	15
1.8	Trip13 depletion in HCC cells affects cell cycle and cell invasiveness through transwell assays.....	16
1.9	TRIP13 depletion downregulates key regulators in the mTOR-signalling axis	17
1.10	Mass spectrometry-based identification of TRIP13 interaction partners	18
1.11	Schematic representation of structural domains in Sin3 protein	19
3.1	Validation of siRNA-mediated knockdown in human and mouse HCC cell lines.....	22
3.2	TRIP13 regulates cell proliferation in various HCC cells	24
3.3	TRIP13 regulates EGFR protein expression in HCC cells	26
3.4	Cellular levels of TRIP13 affect EGFR mRNA and promoter activity in HCC Cells	27
3.5	EGFR knockdown only has a minor effect on cell growth in HCC cells	29
3.6	TRIP13 and EGFR expression are not positively correlated in HCC cancer	30
3.7	Intracellular localization of TRIP13, SIN3A and SAP130 in HCC cells by confocal imaging	33
3.8	Proximity ligation assay (PLA) to validate an intracellular interaction between TRIP13 with SIN3A or SAP130 that were previously identified via a MS screen.....	35
3.9	Concomitant KD of SIN3A or SAP130 rescues the growth defect exerted by TRIP13 depletion in HLF cells	38
3.9D	Apoptotic levels in HLF cells depleted either with TRIP13 or SIN3A or both	39
3.10	Expression levels of TRIP13, SIN3A and c-MYC after combined siRNA transfection in HLF cells	40
3.11	Partial restoration of c-MYC and Cyclin D1 (CCND1) after concomitantly knockdown of TRIP13+SIN3A from 3 independent experiments	41
3.12	Cellular fractionation to determine cell localization of TRIP13 and SIN3A during single and combined knockdown of these genes	41
3.13	Concomitant KD of SIN3A rescues the growth defect in TRIP13-depleted human Huh7 and HepG2 but not mouse Hepa1-6 cells	43
3.14	Expression levels of c-MYC after depleting TRIP13 or SIN3A or both in Huh7 and Hepa1-6 cells	44

3.15 Overexpression of c-MYC rescues the growth defect in TRIP13 deficient HLF Cells	45
3.16A Planned tumor implantation study using shTRIP13+shSIN3A HCC cells	47
3.16B Generating stable HLF and Hepa1-6 cell lines with shR KD of SIN3A using a Lentiviral-mediated system	48
3.17 Overexpression of TRIP13 resulted in an increase in cell growth in non-tumorigenic AMI12 cells but not in HepG2 cells	50
3.18 YAP as a plausible upstream regulator of TRIP13	52
3.19 TRIP13 depletion triggered an increase in DNA damage	53
3.19D Growth defect in TRIP13-depleted cells are not dependent on the ATM DNA damage pathway	54
3.20A Accumulation of DNA damage in combined siTRIP13+SIN3A persisted in spite of a growth rescue	57
3.20B Detection of DNA-damage markers in HLF cells depleted either with TRIP13 or SIN3A or both	59
S1 Expression profiling of TRIP13 and EGFR in HCC patient cohorts from different etiology background.....	94
S2 Gene expression levels between 8 hrs-72 hrs post siRNA transfections to knockdown either TRIP13 or SIN3A or both.....	95
S3 Protein expression levels between 8 hrs-72 hrs post siRNA transfections to knockdown either TRIP13 or SIN3A or both.....	96

Abbreviations	Expansion
AAA+ ATPase	ATPase associated with various cellular activities
AKT	Protein kinase B (PKB)
ANOVA	Analysis of variance
ATCC	American tissue culture collection
BCA	Bicinchoninic acid
BMI	Basal metabolic index
bp	Base pairs
BrdU	5-Bromo-2'-deoxyuridine
BSA	Bovine serum albumin
Cat. No	Catalogue number
CCND1	Cyclin D1
cDNA	Complementary DNA
ChIP	Chromatin Immunoprecipitation
CO₂	Carbon dioxide
DDR	DNA damage response
DMSO	Dimethyl sulfoxide
DNA	Deoxyribonucleic acid
DPBS	Dulbecco's phosphate buffered saline
DTT	Dithiothreitol
EGFR	Epidermal growth factor receptor
ELISA	Enzyme-linked immunosorbent assay
Erk	Extracellular signal regulated kinase
FA	Formaldehyde
FBS	Fetal bovine serum
GFP	Green fluorescent protein
H2AX	H2A histone family, member X
HCC	Hepatocellular Carcinoma
HDAC	Histone deacetylase complex
HEK	Human embryonic kidney
HFD	High fat diet
HRP	Horseradish peroxidase
Hrs	Hours
IFU	Infectious units
IgG	Immunoglobulin G
IHC	Immunohistochemistry
IL	Interleukin
IR	Insulin resistance
KD	Knockdown
kDa	Kilo daltons
Mins	Minutes
ml	Milli liter
mM	Milli molar

MOI	Multiplicity of infection
mRNA	Messenger RNA
mTOR	Mammalian target of Rapamycin
N.S	Non-significant
nm	Nanometer (wavelength)
nM	Nano molar
NTC	Non-targeted control
OD	Optical density
OE	Overexpression
p-	Phospho-
P/S	Penicillin/Streptomycin
p53	Tumour protein p53
PAH	Paired amphipathic helix
PBS	Phosphate buffered saline
PCR	Polymerase chain reaction
PI3K	Phosphoinositide 3-kinase
PKA	Protein kinase A
qPCR	Quantitative polymerase chain reaction
RFP	red fluorescent protein
RIPA	Radioimmunoprecipitation assay
RNA	Ribonucleic acid
ROS	reactive oxygen species
RT	Room temperature
SAP130	SIN3A associated protein 130
SC	Subcutaneous
SD	Standard deviation
SEM	Standard error of means
shRNA	Small hairpin RNA
SID	Sin3-interacting domain
SIN3A	SIN3 transcription family regulator family member A
siNTC	Negative control siRNA
siRNA	Small interfering RNA
TBP	TATA-box-binding protein
TG	Triglyceride
TNBC	Triple negative breast cancer
TR	Thyroid hormone receptor
TRIP13	Thyroid hormone receptor interactor 13
VCP	Valosin-containing protein
VEGFR	Vascular endothelial growth factor receptor
WHO	World health organization
WT	Wild-type

μl

Micro liter

μM

Micro molar

μm

Micro meter

1 Introduction

1.1 Hepatocellular carcinoma

Hepatocellular carcinoma (HCC) is the fifth most prevalent cancer and the second leading cause of Cancer-related mortality [64]. Liver carcinogenesis is a highly complicated process, which results from a complex interplay between host genetic factors and environmental exposure. HCC arises from a plethora of etiological factors that originates with a background in chronic liver diseases (CLDs). Such risk factors for the occurrence of HCC include chronic Hepatitis B or C infections (HBV, HCV); excessive alcohol consumption, autoimmune Hepatitis and several metabolic diseases including Diabetes mellitus, diet-induced fatty liver diseases and obesity [65]. The initiation and progression of HCC is thought to be a multistep process, involving the progressive accumulation of genetic and epigenetic alterations, undermined from different molecular and cellular events that still remains poorly understood [66].

1.2 Genetic landscape and altered cell signaling driver pathways in HCC

The liver is rarely affected by classical germ line mutations that predispose during the development of colorectal, breast or ovarian cancer. Instead, the transformation/proliferation of hepatocytes are usually associated with several single nucleotide polymorphisms (SNPs) [67]. Amongst these polymorphisms, many alter the carcinogenic pathways and are related to predisposition to specific risk factors during chronic liver diseases. PNPL3 was first identified to be a gene encoding for a lipase that mediates triacylglycerol hydrolysis [68]. In this example, there is a strong association between the SNP of PNPL3 with fatty liver and alcohol induced chronic liver damage, alongside an increased risk of HCC occurrence [69].

Cirrhosis marks the late stages of chronic liver injury when fibrotic tissues overtakes the function of hepatocytes, as these cells are forced to chronically alternate between necrosis and regeneration and eventually senesces. Cirrhosis paves the way during which preneoplastic lesions eventually gives way to malignant transformation in a well defined sequence as shown in Fig. 1.1. Damaged cells possibly hepatocytes undergoes initial insults to form a low-grade dysplastic nodules (LGDN) which then switches to a high-grade dysplastic nodules (HGDN) [66]. Subsequently, early HCC cells are further transformed to become highly proliferative and invasive cells in advanced HCC.

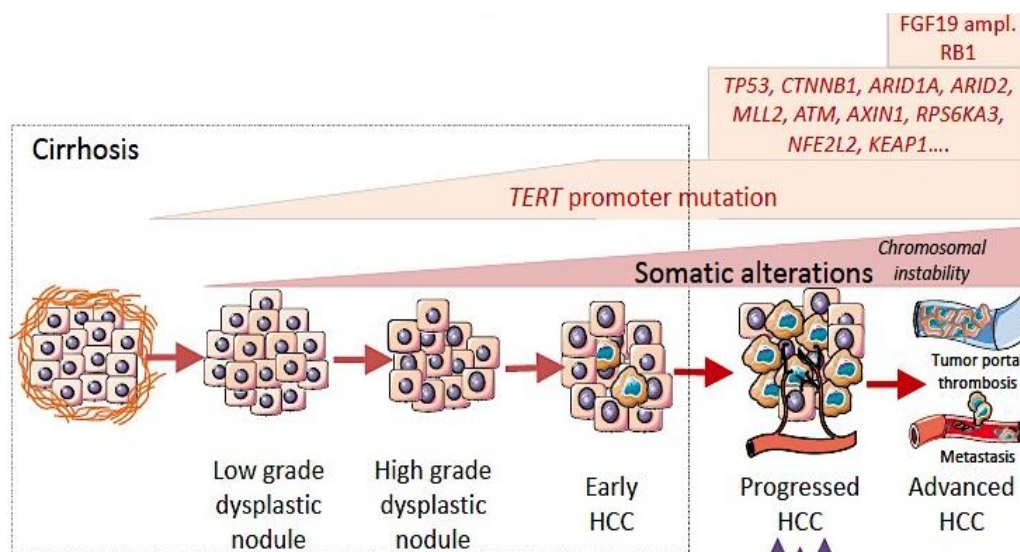


Fig. 1.1 Cirrhosis as a cancer field during malignant tumour transformation

A sequence of genetic events marks the malignant transformation of preneoplastic lesions in ultimately leading up to tumour initiation and progression. Figure adapted from [66]. In this paradigm, TERT promoter mutation is shown to occur early on during the transformation sequence, which progressively gives way to several more cancer gene mutations during advanced HCC

1.3 Signaling pathways altered in HCC

It has been predicted that the genome from each HCC tumour cell is uniquely complex and harbors between 35-80 somatic gene mutations. An overview of the recent whole-exome sequencing studies has identified the following 6 signaling pathways to be recurrently altered in HCC [66]. These are namely pathways regulating Telomerase maintenance; WNT/ β -catenin; p-53 cell cycle regulation, epigenetic modifiers, oxidative stress and the PI3K/AKT/mTOR, MAPK kinases and are briefly discussed below:

Telomeres are short DNA repeats that are located in chromosomal ends, which serves a protective role during cell division. Telomere shortening occurs with each round of cell division until a finite number of cycles have been reached before cell senescence and undergoes apoptosis. Telomerase is an enzymatic complex comprising of the TERT enzyme, which is responsible for telomere synthesis. In humans, telomerase are inactive in mature hepatocytes, whereby liver cells undergo normal replicative senescence and dies eventually. In HCC, frequent and a recurrent somatic mutation in the TERT promoter region results in reactivation of Telomerase in up to 59% of patients in a HCC cohort [70]. The reactivation of telomerase marks the key event during malignant transformation from a

1 INTRODUCTION

neoplastic lesion into a HCC [70,71]. Furthermore, TERT promoter mutations were proposed to be an early recurrent somatic gene mutation as observed by the progressive increase in gene mutations from 6% in LGDN to 19% in HGDN and eventually increasing to 61% in early HCC [70].

The **WNT/ β -catenin pathway** plays an indispensable role during embryonic development. This oncogenic pathway is frequently activated in HCC via an activating mutation of CTNNB1 (encoding for B-catenin) in 11%-37% of HCC patients and inactivating mutation of the inhibitory complexes of AXIN or APC [72, 73].

The **p53 cell cycle pathway** is altered in at least 50% of the HCC patients, with frequent inactivating mutations in the TP53 tumour suppressor gene [74]. Further genetic mutations in other component of this cell cycle pathway, like CDKN2A, and RB1 were found to be inactivated in HCC tumours characteristic of poor prognosis [75].

Epigenetic alterations allows for reversible modifications on the genomic level without changing the DNA sequence. Recent advances in sequencing technologies have made possible the identification of a novel class of non-coding RNAs (ncRNAs), the PIWI-interacting RNA (piRNA) piR-Hep1, which are upregulated in more than 50% of the HCC tumours being screened [80]. Inactivating mutations in HCC have also been seen in ARID1, ARID2 that are part of chromatin remodeling complexes [77]. Somatic alterations in the methylation writer family, mainly in MLL1, 2, 3, and 4 are similarly frequent in HCC. As limited work has been performed to explore the epigenetic aspects during HCC development, the functional consequences of a deregulation in these epigenetic modifiers in HCC awaits to be further explored [76, 77].

The Oxidative stress pathway is altered by recurrent activation of NRF2 or inactivating mutations of KEAP. Activation of NRF2 in tumour cells was shown to confer a protective role against chronic oxidative stress and cell death [78].

PI3K/AKT/mTOR and the RAS/MAPK growth factor receptor-signaling pathway are activated in around 5-10% of HCC cells. An activation of the AKT/mTOR pathway was shown to occur mainly via amplifications of the CCND1 locus, activating mutations of the PI3KCA and inactivating mutations of TSC1 or TSC2 [79]. Altogether, the activation of this growth factor signaling pathways in HCC likely accounts for the enhanced cell proliferative abilities of these tumour cells [79].

1.4 Metabolic syndrome and HCC burden

1.4.1 Obesity, inflammation and HCC

As previously mentioned, the risk of developing HCC are affected both by genetics and environmental factors including history of HBV or HCV infection, alcohol abuses as well as a conundrum of metabolic-related disorders like obesity, diabetes, fatty-liver diseases etc. In recent years, there has been a surge in the rates of obesity in both developing and developed nations, with one quarter of the population in the U.S deemed to be obese (BMI > 30 kg/m²) [1]. This obesity epidemic has been paralleled by a rise in prevalence of the metabolic syndrome, a collective term referring to disorders ranging from obesity to hypertension, hyperlipidaemia, insulin resistance to type-2 diabetes (T2D).

1.4.2 A potential link between metabolic syndrome and HCC

Several epidemiological and clinical studies have confirmed the importance of obesity as an independent risk factor for HCC [3, 4]. Notably, the risk of cancer-related death was significantly associated with obesity for multiple difference types of cancer. In a meta-analysis study, the relative risk for HCC-related death was reported to be 4,5 times higher in men with a high BMI $\geq 40\text{kg/m}^2$ [2].

Non-alcoholic fatty liver disease (NAFLD) is characterized by hepatic steatosis in the absence of alcohol abuse and other known liver disease and occurs commonly as a manifestation of obesity-related metabolic syndromes (6). Up to 90% of obese patients and 70% of T2D patients have been diagnosed with some sort of fatty liver diseases (5). In the absence of proper diet or weight management, 12-40% of the patients with NAFLD progresses to non-alcoholic steatohepatitis (NASH) and 15-33% of those with NASH develop cirrhosis, which paves the transformation from preneoplastic lesion towards HCC development [7, 8, 62] as outline in Fig. 1.2.

Obesity, as a state associated with chronic low-grade systemic inflammation, has been postulated to be a main contributor during this progression from NAFLD – NASH-fibrosis- cirrhosis and finally to HCC [9]. In obese individuals, adipocytes undergo hypertrophy due to the accumulation of excess lipids. These hypertrophic adipocytes secrete free fatty acids (FFA) into the surroundings, which can activate immune cells including liver macrophages and kupffer cells. Altogether, these adipocytes and immune cells secrete pro inflammatory cytokines like TNF- α , IL-6, IL-1 β , IL-8, IL-10, IL-17, IL-18, as well as adipokines-like leptin and adiponectin [10,11,12,13,14]. In the presence of excessive proinflammatory adipokines and cytokines, kupffer cells and hepatocytes are further stimulated to produce more cytokines, resulting in an inflammatory cascade in the liver. Several of these cytokine-signalling pathways have been separately demonstrated to be pivotal during this state of chronic liver injury, marking the progression from NAFLD to NASH, liver cirrhosis and finally towards liver carcinogenesis [15]. Furthermore, obesity-

1 INTRODUCTION

associated inflammation has also been identified to directly contribute to the development of metabolic disorders like atherosclerosis and insulin resistances during T2D [16, 17].

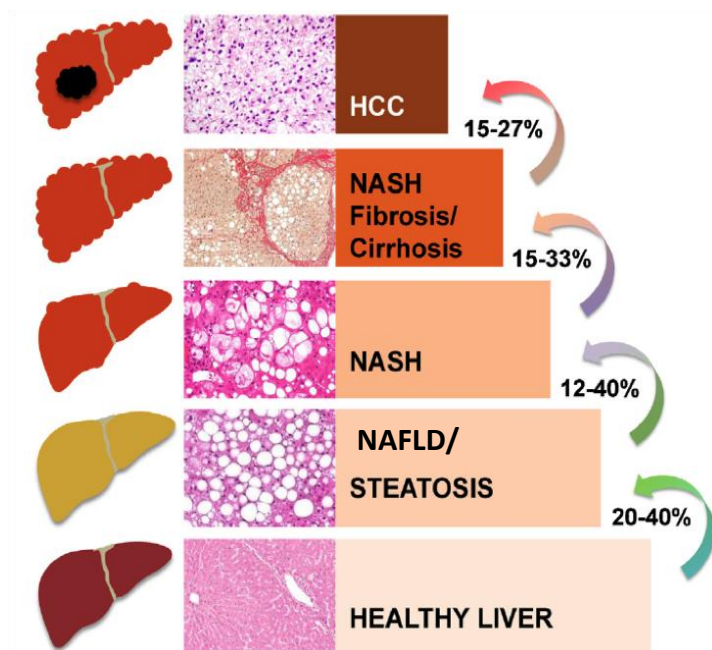


Fig. 1.2 The pathological progression from benign hepatic steatosis to NASH/cirrhosis and eventually to HCC formation

Non-alcoholic fatty liver disease (NAFLD) is a liver manifestation of the metabolic syndrome and is characterized by simple steatosis without obvious signs of necrosis and inflammatory activities. The percentages above provide an estimate of affected subjects at a current stage, which will progress onto the next clinical stage. Non-alcoholic steatohepatitis (NASH) is an aggressive form of hepatic steatosis marked by necroinflammatory activities. The sequential progression from NASH/cirrhosis to malignant transformation during HCC is believed to involve chronic cycles of inflammation-necrosis-regeneration along with mutation of tumour related genes. Figure adapted from [62]

1.4.3 Genetic instability and hepatocyte apoptosis correlate with a risk for HCC

Independent of all the underlying etiology leading up to chronic liver diseases (CLD), liver tissues from CLD patients all displayed varying degrees of chronic hepatocyte damage [18]. Mechanistically, it has been reported by the authors in [19] that the removal of damaged hepatocytes during the maintenance of liver homeostasis is regulated by factors involved in programmed cell death, namely Caspase 8 and receptor interacting kinase 1 (RIPK1). More recently in 2017, another group established that the concomitant hepatocyte apoptosis and proliferation seen during CLD acts as a decisive determinant of subsequent HCC development in mouse and human CLDs [20]. In these hyper-proliferative and hyper-apoptotic livers from CLD patients and mouse models, the carcinogenic effect from

replication errors that usually occurs stochastically is drastically increased [20]. The authors thereafter postulate that the levels of hepatocyte apoptosis and DNA damage serves as a predictive risk factor for subsequent HCC development in CLD patients. This finding further highlights and provides a mechanistic link for the correlation between CLD patients to develop HCC vs the severity and duration of their liver damage conditions as seen in most HCC epidemiological data [21,22,23].

2 TRIP13- An overview of key cellular functions

2.1 TRIP13 as a key regulator of chromosomal processes during cell division

Cell mitosis and meiosis are key events during development, where a series of tightly regulated chromosomal events occur to ensure a faithful transmission of genetic materials. AAA⁺-ATPase (ATPase Associated with diverse cellular Activities) are multi-subunit ATP hydrolases that mediate a conformational change in its targets, during which changes in the complex assembly in turn affect cellular signalling or activities [24]. TRIP13 is a member of this ATPase family and has been described to regulate key chromosomal events during cell meiosis and mitosis. Different studies have shown TRIP13 to be involved in a myriad of processes during G2/prophase of meiosis. These findings include its role as a checkpoint activator during synapsis defects and double strand break (DSB), which are intrinsically linked to its role in establishing homologous recombination and DSB repair strictly between homologous pairs [25, 26, 27].

TRIP13 has been recently described to be a novel mitotic checkpoint regulator during the transition from metaphase-to-anaphase and in promoting mitotic progression [28, 29]. The mitotic checkpoint is a fail-safe mechanism to ensure proper chromosomal segregation and genetic transmission to daughter cells during cell division. The spindle assembly checkpoint (SAC) is activated whilst its downstream mitotic checkpoint complex (MCC) is assembled when a defective kinetochore-microtubule attachment is detected [30]. The MCC is composed between BubR1, Bub3 and closed Mad2 (C-Mad2) which directly binds to Cdc20 (an APC activator) to inhibit the activity of the anaphase promoting complex/cyclosome (APC/C) [30]. The SAC is silenced once all the sister chromatids have been properly attached and bi-oriented at the metaphase plate, as shown in Fig. 1.3.

2 INTRODUCTION

2.1.1 TRIP13 and p31^{comet} during mitotic checkpoint silencing

P31^{comet} is a mitotic checkpoint silencing protein that can initiate the disassembly of the MCC by directly binding to C-Mad2 and displacing BubR1/Bub3 from this complex [31, 32]. A picture emerges such that P31^{comet} recruits TRIP13 to the kinetochores during which these two factors coordinate the disassembling and silencing of the mitotic checkpoint signals [28, 29]. In order for Cdc20 to be released during MCC disassembly, C-Mad2 needs to be actively remodelled into the inactive open conformation of O-Mad2. The ATPase activity of TRIP13 was found to be essential in driving this ATP-dependent conformational transition from C-Mad2 to O-Mad2 [33]. After Cdc20 is released following a disassembly of MCC and a halt in the checkpoint signalling, the activated APC/C then drives the transition from metaphase to anaphase [28, 29] as seen in Fig. 1.3. Further highlighting the essential role of TRIP13 during checkpoint exit, authors from [34] found that besides the inability to inactivate MAD2, TRIP13-depleted cells were similarly unable to activate the SAC. In other words, the activation and inactivation of the SAC were both dependent on TRIP13-mediated activities [34].

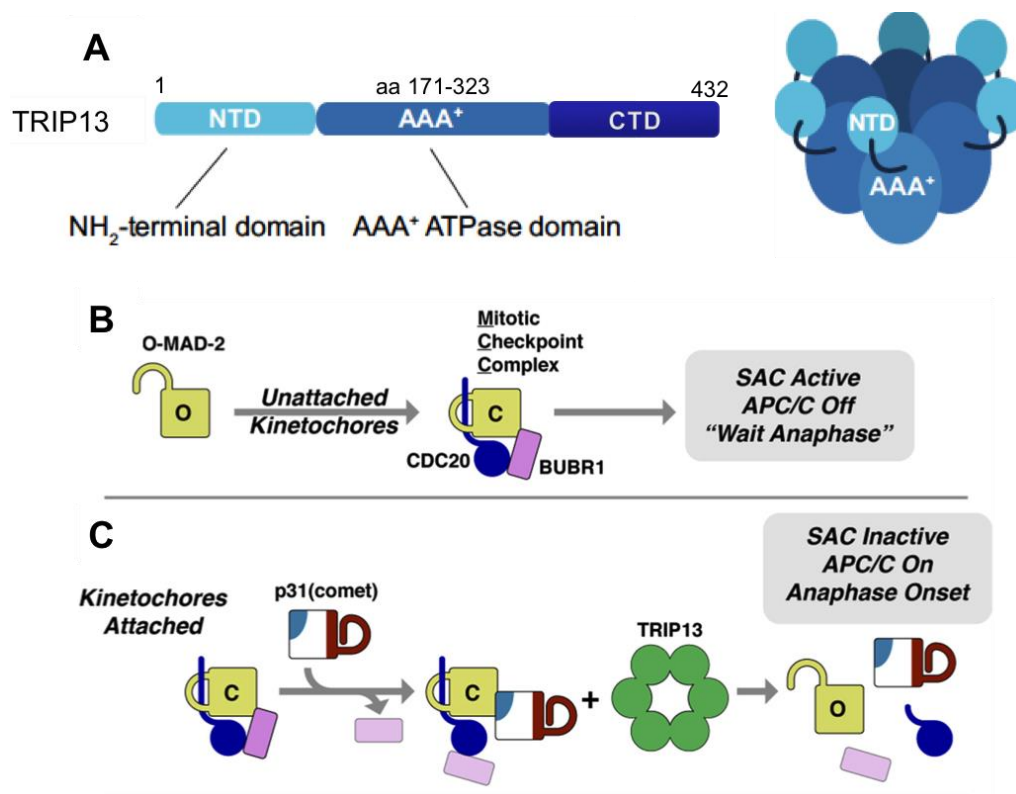


Fig. 1.3 Schematic organization of the human TRIP13 and the proposed model for its role in mitotic checkpoint silencing

(A) TRIP13 contains one AAA⁺-ATPase domain that is located between 171-323 residues of which is preceded by a non-catalytic NTD. Like many other AAA⁺-ATPase proteins, it is suggested that TRIP13 likely assembles itself into a homo-hexameric oligomer. (B) Spindle assembly checkpoint (SAC) and MCC are activated by the presence of unattached kinetochores. The MCC is composed of BubR1 (purple), Bub3 (not shown), CDC20 and closed Mad-2 (C-Mad2) which directly binds and inhibits the anaphase promoting complex/cyclosome (APC/C), inhibiting anaphase onset. (C) Model depicts the role of TRIP13 in disassembling the MCC and promoting mitotic progression. When kinetochores are properly attached, the silencing of the SAC is initiated. p31Comet binds to the existing MCC and displaces BubR1, whilst delivering CDC20:C-Mad2 to TRIP13 for further conformational conversion (to O-Mad2) and disassembly. The release of CDC20 activates the APC/C, which then drives the onset of anaphase. (Figures adapted from [63, 81])

2.2 Upregulated expression of TRIP13 in several human cancers

2.2.1 Genomic instability and aneuploidy in cancer

Chromosomal instability (CIN) and aneuploidy are persistent hallmarks of human solid tumours [38]. Given the essential roles of TRIP13 in regulating chromosomal events during meiosis and mitosis, one of the predicted functions of TRIP13 was to prevent genome instability. This was reflected by many studies that have shown either an amplification of the TRIP13 gene or an overexpression of TRIP13 in several cancers [35, 36, 37, 43, 44]. The CIN signature identifies a set of top-ranked genes that are common upregulated in tumour cells displaying functional aneuploidy. Most of the genes identified to be associated with CIN, for instances TPX2, PRC1, FOXM1 and TRIP13 are critical regulators during DNA replication, SAC signalling, chromosomal segregation and cytokinesis [37]. Net overexpression of this CIN signature was a predictor for poor clinical outcome in 6 different cancer types, namely breast cancer, lung cancer, medulloblastoma, glioma, mesothelioma and lymphoma. Strikingly, the authors also reported the ability to stratify tumour grades from multiple tumour types using the CIN signature, with more aggressive cancer phenotypes typically displaying higher CIN signature expression [37].

Reflecting the findings that a loss of genome stability is an essential step during malignant transformation, TRIP13 was listed amongst multiple breast cancer signatures due to its overexpression in transcriptome profiling across tumour samples from patients associated with poor clinical outcomes [35, 36]. Furthermore, knocking down of TRIP13 inhibited cell proliferation in breast cancer cell lines, highlighting roles of TRIP13 during mitotic progression and cell growth [28].

2.2.2 Chromosomal instability (CIN) in liver cancer

The relevance of CIN and the importance of functional aneuploidy in HCC was left unknown as this cancer type was not included as part of the previous study in defining the CIN signature of cancer patients [37]. Evidence suggesting that CIN similarly plays a role in liver cancer was derived from these early observations. Firstly, the presence of CIN and aneuploidy were correlated with the progression of HCC. Secondly, induction of aneuploidy in HCC cells were associated with elevated levels of telomere shortenings and centromere abnormalities, all of which were indicative of CIN phenotypes [40,41].

Hippo/Yap signalling pathway in inducing CIN in liver cancer

-Function implications of TRIP13 as part of the CIN signature?

Recently in 2017, the authors [39] demonstrated that the CIN signatures as identified previously [37] are similarly detectable in HCC tumour tissues and stratifies a subgroup of HCC patients with poor clinical outcome. The Hippo pathway and its downstream effector

2 INTRODUCTION

yes-associated protein (YAP) are key regulators of tissue and organ size homeostasis where its deregulation was implicated in hepatocarcinogenesis [42]. Overexpression of YAP was sufficient to induce an upregulation of CIN signature genes along with chromosomal aberrations in hepatocytes of transgenic mice (YAP^{S127A}) that were expressing a constitutively active form of YAP [39]. In human HCC tissues, high nuclear expression of YAP correlated with CIN signature expression and aneuploidy. It was then reported that YAP cooperates with FOXM1 in contributing to the expression of CIN gene signatures and chromosomal aberrations during hepatocarcinogenesis [39]. Interestingly, TRIP13 was identified as one of the top 25 ranked CIN signature genes (CIN25) along with FOXM1 and MAD2L1, which were induced by an overexpression of YAP in liver tumour cells from this study. Patients displaying a high CIN25 gene expression were correlated with poor survival and early cancer recurrence. Given the role of YAP in regulating CIN gene expression in HCC, it is plausible that TRIP13 along with several downstream target genes from YAP/FOXM1 contributes towards chromosomal instability in HCC patients displaying CIN25 signatures [39].

2.2.3 Role of TRIP13 in promoting DNA repair and chemoresistance

Squamous cell carcinoma of the head and neck (SCCHN) is an aggressive cancer with high mortality and recurrence rate due to rapid acquiring of treatment resistance by these carcinoma cells [45]. An oncogenic role of TRIP13 was first reported in SCCHN. The upregulated expression of TRIP13 was shown to promote aggressive tumour growth and treatment resistance, supposedly mediated via the roles of TRIP13 in DNA damage repair [45]. TRIP13 copy number and gene expression was found to be upregulated in SCCHN patients when compared against non-tumourous mucosa tissues. The oncogenicity of TRIP13 was established via these key findings: Firstly, overexpressing TRIP13 transformed non-malignant fibroblast cells during a clonogenic assay. Secondly, overexpressing TRIP13 in a SCC cell line expressing low endogenous levels of TRIP13 triggered an increase in cell proliferation, migration and invasiveness as compared to control cells. This was further validated *in vivo* where these TRIP13-overexpressing tumours grew much quicker than control tumours after being implanted into mice. Mice with TRIP13 overexpressing tumours had poorer survival rates than mice with control tumours presumably due to the larger tumour burden in these animals. This tumourigenic effect was reversed when TRIP13 was depleted, as it was demonstrated by doxycycline-induced shTRIP13 KD that significantly arrested tumour growth as compared to doxycycline treated control groups in xenograft models [45].

Adding on to the oncogenic role of TRIP13 in SCCHN, the authors further reported a mechanistic involvement of TRIP13 in promoting treatment resistance via enhanced repair of DNA damage. Using a mass spectrometry screening to identify TRIP13-interacting partners, several non-homologous end joining (NHEJ)/ DNA repair group proteins like KU70, KU80 and DNA PKcs were identified, suggesting a role of TRIP13 in NHEJ. In SCCHN, efficient repair of radiation and chemotherapy-induced double strand breaks (

2 INTRODUCTION

DSBs) was identified as one of the leading causes of chemoresistance and early tumour recurrence. This study provided an important finding that the upregulated expression of TRIP13 confers treatment resistance in SCCHN, emphasizing the importance of targeting NHEJ to overcome treatment failure [45].

2.3 A novel role of TRIP13 in liver regeneration and HCC tumourigenesis

2.3.1 TRIP13 is upregulated in liver cancer

The mortality rates from liver cancer is the second highest worldwide, presumably due to the lack of early presenting signs and symptoms. Patients often present with advanced stage of HCC when first being diagnosed, which further limits their treatment options. Depending on the stage of liver cancer, some common treatment options include surgical resection of the tumour (partial hepatectomy), liver transplantation, radiotherapy, conventional chemotherapy, and more recent targeted and immunotherapy [66]. Vascular endothelial growth factor (VEGF), platelet derived growth factor (PDGF) and fibroblast growth factor (FGF-2) are established proangiogenic factors that play key roles during HCC development. Sorafenib was the first multi kinase inhibitor drug targeting the VEGF/VEGFR to be approved that has demonstrated survival benefits in advanced HCC patients [82, 83]. Despite numerous targeted therapies that made it through to clinical trials, few have been demonstrated to be effective in advanced-stage HCC [66]. Due to the unmet medical needs, novel pathways and cellular mechanisms during hepatocarcinogenesis need to be further explored in order to identify new therapeutic targets or prognostic biomarkers.

In an effort to identify novel regulators in HCC, a former colleague in the lab, Dr. Bettina Meissburger, reviewed publicly available expression data of genes deregulated in HCC (E-GEOD-25097). From these expression data, TRIP13 was found to be strongly upregulated in tumour tissues compared to non-tumour tissues (Fig. 1.4A) in the liver.

A HCC mouse model was set up by injecting Diethylnitrosamine (DEN) to young mice (2 weeks) and to observe for HCC formation at later age of 30 weeks. Trip13 expression was found to be significantly upregulated in liver tumours of DEN-injected mice compared to healthy livers from the control group (Fig. 1.4B). Tissue micro array (TMA) from a cohort of HCC patients revealed similarly an increase in TRIP13 staining exclusively in the hepatocytes (data not shown).

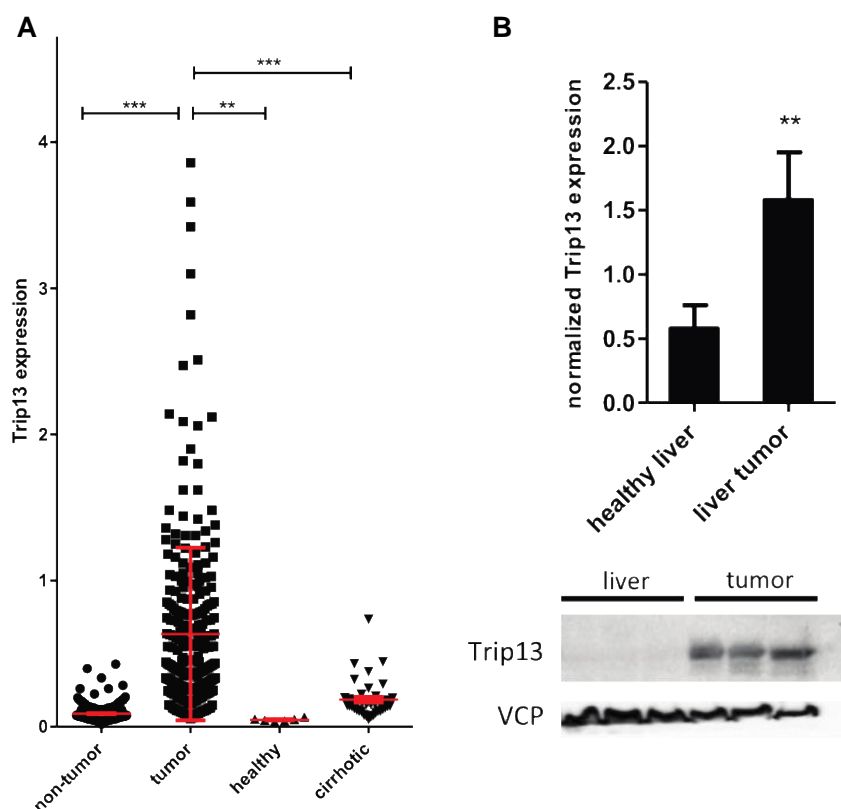


Fig. 1.4 Expression of Trip13 in human HCC and mouse model of DEN-induced HCC

(A) TRIP13 expression in a HCC gene expression profile (accession number: E-GEOD-25097) where TRIP13 is significantly upregulated in tumour tissues compared to non-tumour tissues and healthy liver tissues.

(B) Diethylnitrosamine (DEN)- induced HCC mouse model was established by injecting DEN to young mice at 2 weeks of age and observing for tumour formation by 30 weeks of age. Trip13 expression was significantly upregulated in liver tumours from DEN-injected mice vs healthy liver from control-injected mice.

2.3.2 TRIP13 is induced in partial hepatectomy and fatty liver diseases

The novel role of TRIP13 in hepatocyte regeneration and tumourigenesis was unveiled through various complementary *in vivo* approaches. Interestingly, the expression of TRIP13 was similarly upregulated in various mouse models of fatty liver and steatohepatitis, from ob/ob, db/db mice to high fat diet and methionine-choline deficient diet-induced obesity in animals (Fig. 1.5A). Reflecting the role of TRIP13 during mitotic progression, an induction of TRIP13 was noted at 48 hrs post operation after performing partial hepatectomy (PHX), when cell proliferation was at its peak during liver regeneration (Fig. 1.5B). Subsequently, this PHX procedure was performed again to investigate the regenerative ability of hepatocytes when depleted of Trip13. To knockdown Trip13 specifically in the liver, mice were injected with Adeno-associated virus (AAV) containing miRNA against a non-targeted control (NTC) sequence or Trip13, one-week prior to PHX (Fig. 1.6).

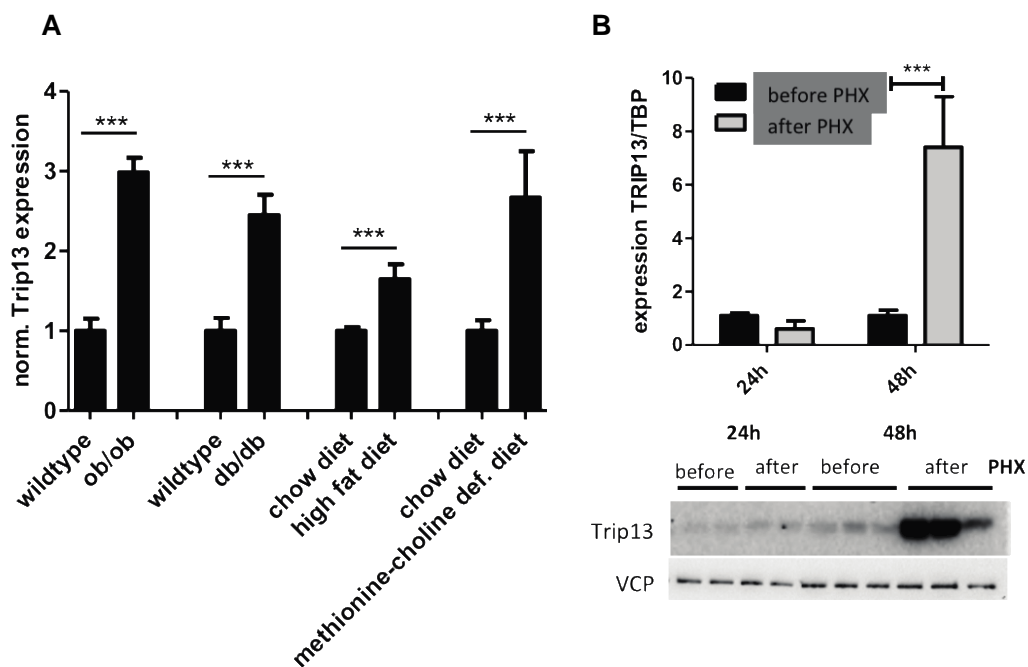


Fig. 1.5 Trip13 is upregulated in mouse models of fatty liver diseases and during liver regeneration

(A) Trip13 expression is upregulated in murine genetic models of insulin resistance as well as diet-induced fatty liver diseases. (B) Partial hepatectomy (PHX) was performed in the liver of mice and liver tissues were harvested 24hrs and 48hrs post PHX. Gene expression of Trip13 was shown to be induced 48 hours post PHX on both mRNA and protein levels.

Expectedly, the number of proliferating cells in the control liver was strongly induced during liver regeneration after the operation. Mice depleted of Trip13 specifically in the liver showed hepatocytes with a decreased ability to regenerate, as seen by a decrease in the expression of a mitotic cell marker, proliferating cell nuclear antigen (PCNA), in liver sections (Fig. 1.6).

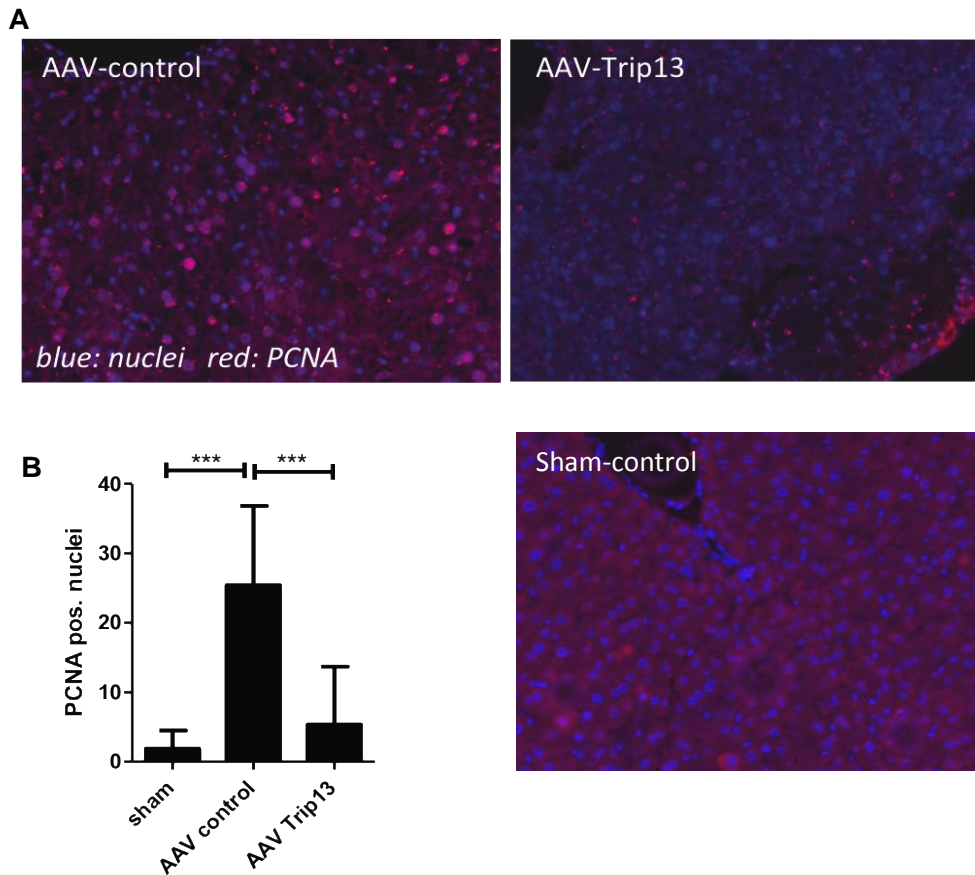


Fig. 1.6 Trip13 is essential during hepatocyte regeneration after partial hepatectomy (PHX) operation in mice

1 week prior to the PHX procedure, mice were injected with Adeno-associated virus (AAV) containing miRNA targeting either a control or a Trip13 sequence. Sham operated mice served as a negative control for the procedure itself. **(A)** 48hrs after the PHX procedure, liver tissues were harvested and processed for histology and microtome sectioning. Liver sections were immunostained with PCNA (proliferating cell nuclear antigen) to detect for cell proliferation. PCNA staining was much weaker in Trip13-depleted liver sections as compared to liver section from control AAV injected mice after PHX. **(B)** The number of proliferating cells (PCNA positive nuclear) was manually counted in each field of view (FOV) and the average from 5 FOV is shown.

2 INTRODUCTION

To examine the oncogenic potential of TRIP13 during tumourigenesis, HCC cells were infected with lentiviral particles harbouring either the shRNA control or the shRNA TRIP13 construct. These HCC cells were then implanted subcutaneously into mice and monitored for tumour growth *in vivo*. In line with the growth-promoting effects of TRIP13 as seen above in Fig. 1.6, tumours developed from TRIP13-depleted HCC cells were much smaller as compared to the control tumours in Fig. 1.7. Furthermore, knockdown of TRIP13 significantly impaired *in vitro* cell growth across all HCC cell lines being investigated as shown in the later results section (Fig. 3.2).

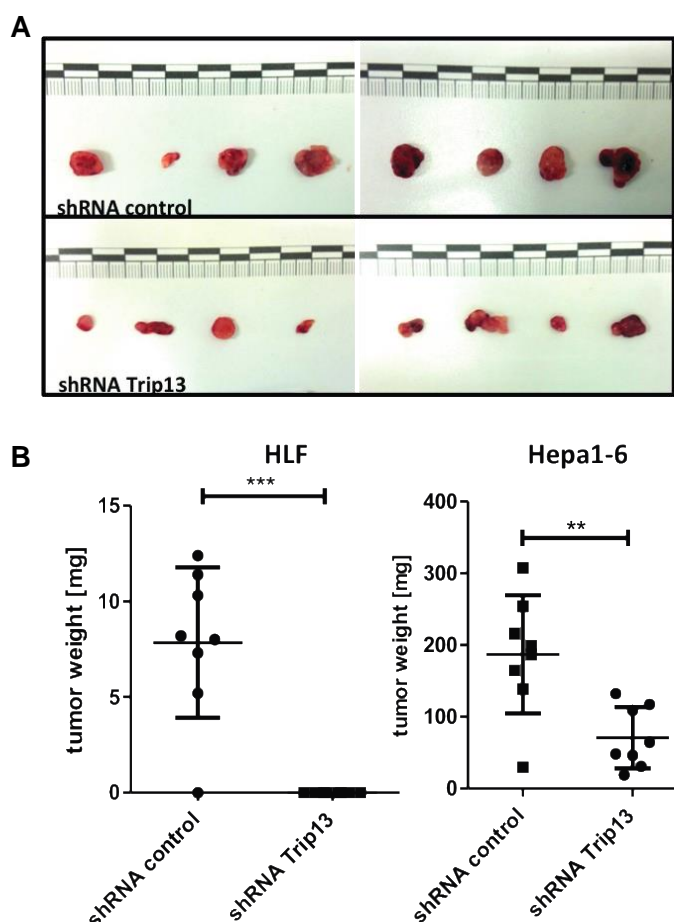


Fig. 1.7 Trip13 depletion inhibits tumour growth in a tumour xenograft model

HLF and Hepa1-6 cells were infected with lentiviruses containing either control shRNA or Trip13-targeting shRNAs. These HCC cells were implanted into the left flank of mice to monitor tumour growth *in vivo*. The experiments were terminated and tumours were harvested when palpable tumour reaches more than a size of 15 mm in any dimensions. (A) Picture shows tumours being harvested from BalbC mice implanted with Hepa1-6 cells from one representative xenograft. Trip13-depleted Hepa1-6 cells resulted in much smaller tumours compared to control Hepa1-6 cells. (B) Weight of tumours derived from animals being injected with Trip13-depleted Hepa1-6 cells were significantly lower compared to control Hepa1-6 cells.

2 INTRODUCTION

Cell invasiveness of HCC cells through transwell chambers were severely impeded post TRIP13 depletion, with HLF cells showing the most dynamic response in this assay (Fig. 1.8B), suggesting an additional role of TRIP13 during HCC cell motility. Cell cycle analysis subsequently revealed that depleting TRIP13 resulted in more cells in the G1 phase for Hepa1-6 and Huh7 whilst more cells accumulated in G2 phase for HLF cells as compared against control cells (Fig. 1.8A) Altogether, the findings above strongly supported a growth regulatory role of TRIP13, both during hepatocyte regeneration and tumourigenesis, where the function of this frequently overexpressed protein has yet to be characterized in liver cancer.

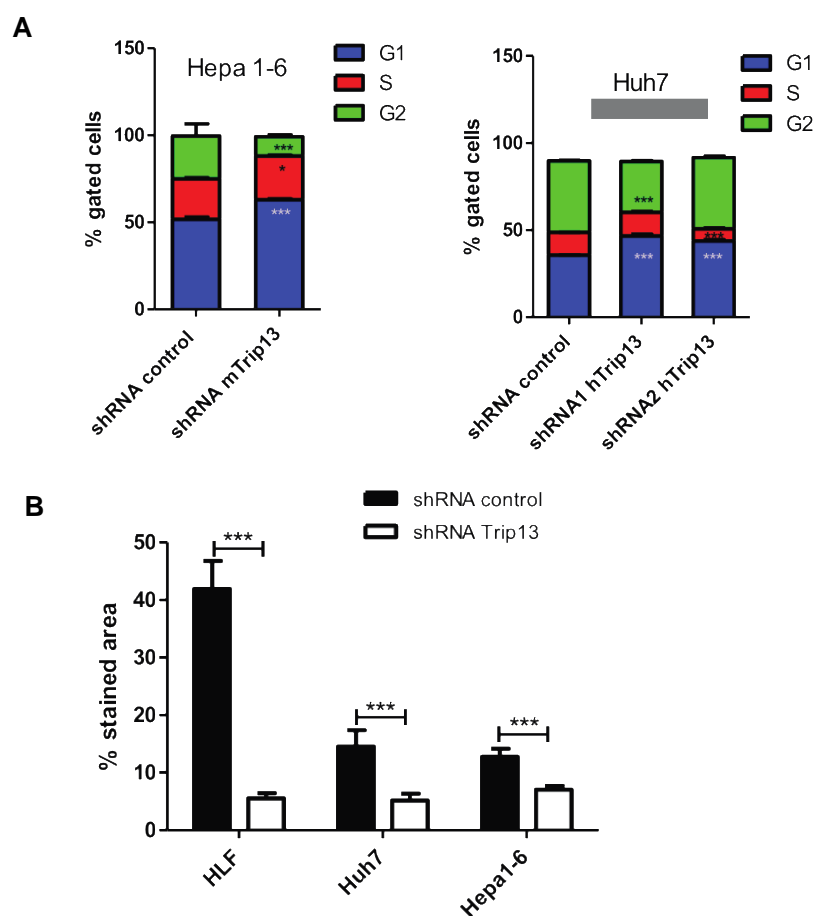


Fig. 1.8 Trip13 depletion in HCC cells affects cell cycle and cell invasiveness through transwell assays

Cell cycle analysis using propidium iodide (PI) staining was performed to compare between control and Trip13 depleted HCC cells. **(A)** Hepa1-6 and Huh7 cells were harvested and fixed in ethanol before being further processed for cell cycle analysis using FACScanto. A shift in cell cycle phases is detected in Trip13-depleted cells, with more cells being accumulated in the G1 phase vs the control cells. **(B)** Cell migration of HCC cells post Trip13 depletion was examined using transwell inserts with 8 μ m pore size. Cells were seeded into transwells containing serum-free media, whilst the lower chambers were filled with media+10% serum. 16 hours post incubation; cells that migrated through the transwell membrane were fixed, stained with 0.1% crystal violet and then imaged. The area of stained cells was analysed with image J.

2.3.3 Involvement of TRIP13 in the mTOR-signalling axis?

Preliminary unpublished data from the lab suggested an oncogenic role of TRIP13 in the mTOR-signalling axis. A decrease in phosphorylation and activation of key mTOR downstream regulators like p-S6K, p-eIF4B and p-4E-BP1 were seen in TRIP13-depleted HCC cells in Fig. 1.9. The EGF signalling axis which acts upstream of the mTOR pathway was similarly impaired, a decrease in receptor activation of EGF along with a decrease in expression levels of this receptor is detected in TRIP13-depleted HCC cells (data not shown). The initial hypothesis is such that TRIP13 could be involved in an oncogenic EGF-mTOR signalling axis during HCC development.

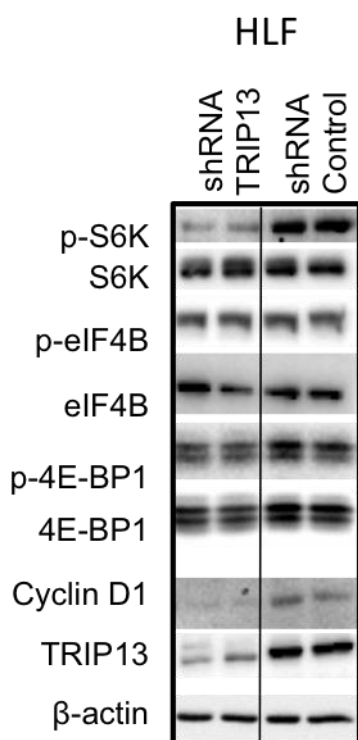


Fig. 1.9 TRIP13 depletion downregulates key regulators in the mTOR-signalling axis
Regulators of the mTOR-signalling pathway were immunoblotted in TRIP13-depleted HCC cells. HLF cells depleted of TRIP13 showed decreased activation/phosphorylation of key factors in the mTOR pathway like S6K, eIF4B, 4E-BP1 and Cyclin D1. β -actin was used as a loading control in this immunoblot.

2.3.4 Identifying novel interaction partners of TRIP13 in HCC

Given the roles of TRIP13 in oncogenic signalling pathways, a mass spectrometry (MS) was performed with aims of identifying TRIP13-interacting partners, which might account for these TRIP13-mediated effects. To this end, endogenous TRIP13 was pulled down from HLF and Huh7 cells and interaction partners were analysed by MS. Out of the proteins that were enriched to be interacting with TRIP13, 39 proteins were identified to be common interacting partners of TRIP13 from both cell lines (Fig. 1.10). Based on KEGG analysis, some of the main pathways identified were involved either in cell cycle regulation, transcriptional co-regulation and DNA damage repair (data not shown). Out of this pool of enriched targets from the MS analysis, candidates with a putative role as transcriptional

2 INTRODUCTION

regulators/co-regulators were picked for further analysis. 2 of this selected targets, SIN3A and SAP130 have been described to form part of the histone deacetylase (HDAC) complex during transcriptional repression [48, 50]. Efforts aimed at characterizing the interactions between TRIP13 and its interaction partners along with the functional relevance of this interaction during tumourigenesis forms the bulk of the work in this thesis.

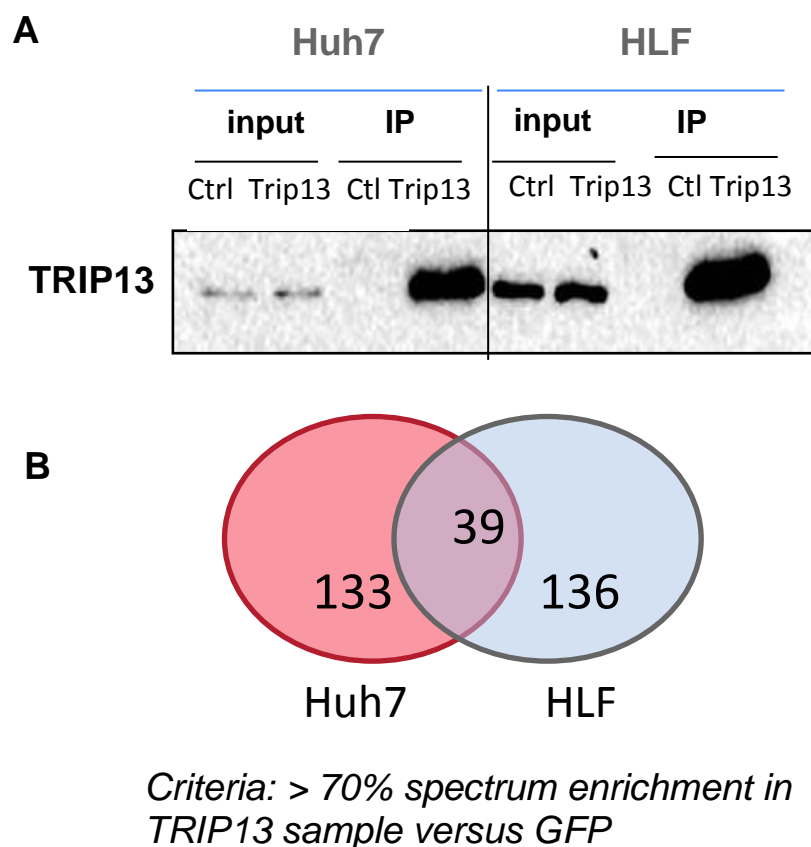


Fig. 1.10 Mass spectrometry-based identification of TRIP13 interaction partners

(A) Representative Western blot of TRIP13-IP in Huh7 and HLF cells. Cells were harvested from a 15 cm dish and cell lysates were subjected to a typical agarose beads protocol for protein pull down. Precleared cell lysates were incubated with equal amounts of either a control GFP antibody or TRIP13 antibody on a rotating wheel at 4°C overnight. Endogenous TRIP13 proteins eluted from the pulldown were verified via western blotting. For analysis of interaction partners by mass spectrometry, eluates were run on a gradient gel, Coomassie stained and submitted for protein analysis. (B) Venn diagram of proteins identified by mass spectrometry. 39 proteins were identified that interacts with TRIP13 in both HLF and Huh7 HCC cell lines.

2.4 SIN3A— role as a transcriptional regulator in the context of cancer?

2.4.1 Structure and function of SIN3A

Sin3 (SWI-independent-3) family was first identified in a genetic screen to study mating-type switching in yeast cells [47]. This protein family is highly conserved from human to yeast, with its roles described as both an enhancer and repressor of gene expression [46]. In mammals, the Sin3 family consist of two isoform members, Sin3A and Sin3B that have both overlapping and distinct functions [48]. Sin3 proteins have 4 paired amphipathic α helices (PAH) that share structural similarities to the helix-loop-helix dimerization domains of the Myc family of transcription factors. The other two conserved domains include the histone interacting domain (HID) and the highly conserved region (HCR) in the c-terminal [48, 49] as illustrated in Fig. 1.11.

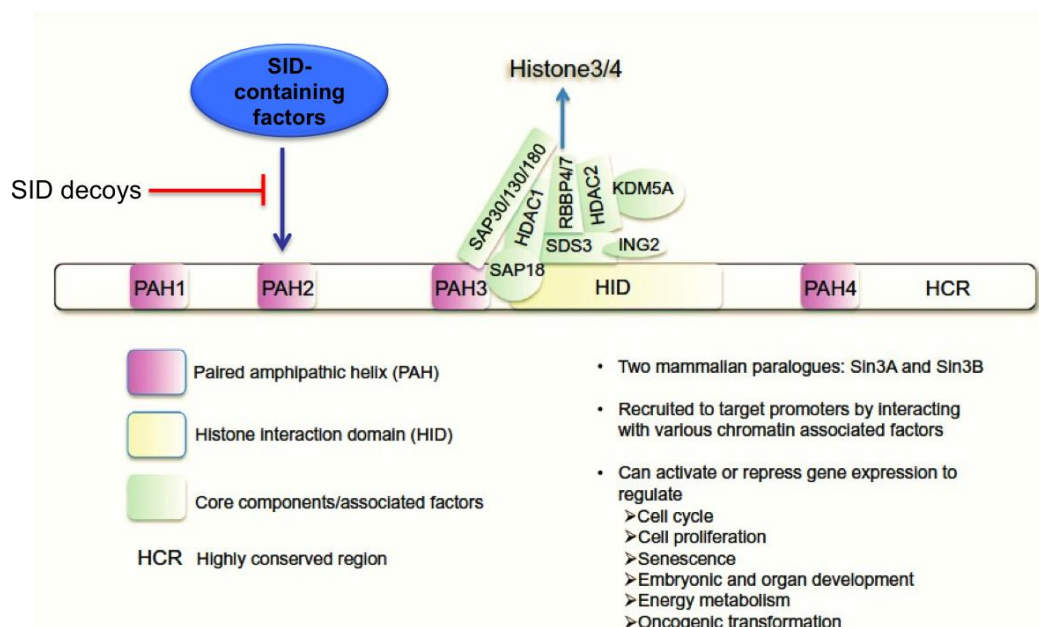


Fig. 1.11 Schematic representation of structural domains in Sin3 protein

Sin3 contains 6 highly conserved domains including 4 PAH domains, along with one HID and one HCR domain at the C-terminal. Cellular functions of Sin3 as both a positive and negative regulator of gene expression is shown above. The Sin3/HDAC complex is a class one HDAC-containing complex consisting of several chromatin-associated factors as shown above in green. The PAH2 domain interacts with a subset of transcription factors containing a conserved sequence called the Sin-interacting domain (SID). In a targeted therapy against Triple-negative breast cancer (TNBC) discussed in section 2.4.3, SID decoys were used to block the interaction between PAH2 domain of Sin3A and its interaction partners. Figure adapted from [49].

2 INTRODUCTION

Sin3 has been described as a master transcriptional regulator due to its ability to act as a molecular scaffold to recruit several chromatin-associated factors like HDAC1/2, RBBP4/7, SDS3, SAP30/130/180, RBP1 to form what is known as the Sin3/HDAC complex. This complex transcriptionally regulates several genes and diverse cellular functions due to an ability to bind to target promoters with or without target specific transcription factors [48, 50].

The Sin3/HDAC complex is commonly referred to as the “co-repressor complex” due the recruitment of HDAC activities being linked to promoter hypoacetylation and gene repression [48, 51]. Recent evidence points to a versatile role of Sin3 in both gene activation and repression. This is best illustrated in the regulation of the pluripotency factor, Nanog, in embryonic stem cells (ESC). The recruitment of Sin3/HDAC by Sox-2 activates the expression of Nanog in proliferating ESC whilst p53-mediated recruitment of the same complex silences Nanog during differentiation [51, 52]. The mechanism of gene activation mediated by Sin3 is not well characterized and this dual mode of gene regulation seems dependent on both the cellular and molecular conditions and upon interactions with different chromatin-associated regulators [48, 51].

2.4.2 SIN3A as a tumour suppressor in cancer

SIN3A was identified as one of the interaction partners for TRIP13 during our MS screening using whole cell lysates from HCC cells (Fig. 1.10). Given that SIN3A acts as a master regulator of several essential genes in critical cellular functions, it is hardly surprising that aberrant gene regulations mediated by this protein complex could have far-reaching consequences during cellular malignancies [49, 54]. Recruitment of Sin3A/3B by the Mad-Max heterodimer was shown to be essential in antagonizing transcriptional activations driven by the proto-oncogene Myc during cell proliferation and transformation [53-55]. Other than Mad-Max dependent negative regulation of c-Myc, Sin3/HDAC complex was shown recently to direct antagonize c-Myc activity via deacetylation and destabilization of the Myc protein [54]. A tumour suppressor role of Sin3A was demonstrated using the *Drosophila* (multiple endocrine neoplasia type 2) MEN2 model [56]. The *drosophila* homologue of human Sin3A, *dsin3*, was identified to be an important regulator of EMT, where the RNAi-mediated depletion of *dsin3* led to strong enhancement of cell migration and mesenchyme phenotypes [56].

2.4.3 SIN3A as a tumour oncogene in promoting tumourigenesis in Triple negative Breast cancer (TNBC)

Triple negative breast cancer (TNBC) is an aggressive and poorly differentiated subtype of breast cancer that is diagnosed one out of five breast cancer patients. Currently, no forms of hormonal/targeted therapies are available due to the absence of the estrogen (ER), progesterone (PR) and EGFR receptors in TBNC tumours [57, 58].

2 INTRODUCTION

SIN3A was demonstrated to mediate oncogenic functions in TNBC via protein-interactions between the PAH domain of SIN3A and specific interaction partners [59]. The PAH2 domain of SIN3A is well characterized and is known to interact specifically with a subset of transcription factors that contain a conserved sequence called the SIN3-interaction domain (SID), see Fig. 1.11. In an attempt to understand the consequences of targeting the PAH2 domain of SIN3A in TNBC, the authors from this study [61] expressed a SID decoy to specifically disrupt PAH2 domains of SIN3A from binding to SID-containing partners. The SID decoy led to epigenetic reprogramming and re-expression of TNBC-associated silenced genes of ER and retinoic acid receptor along with the downregulation of markers for cancer stem cells and epithelial-mesenchymal transition (EMT) [59-61]. The re-expression of these hormone receptors made this previously “undruggable” cancer subtype “druggable” again with hormone-targeted therapies [61]. This study highlighted the discovery of an interaction between SIN3A and a SID-containing adaptor protein, PF1, [59] as essential in the oncogenic maintenance of EMT and CSC phenotype in TNBC.

The decrease in CSC functions of TNBC by SID treatment reflects previous reports of the positive role of Sin3A in promoting pluripotency in proliferating ESC [52]. This finding stands in contrast with the tumour repressor role of Sin3A/HDAC complexes as a c-Myc-antagonist. At this point, the conflicting roles of SIN3A as either a tumour suppressor or an oncogene remains controversial. The dual mode of transcriptional regulation mediated by SIN3A is likely to be context dependent and subjected to the dynamics of its spatial-temporal associations with different factors, as reflected by numerous examples discussed above [49-51].

Aims of the study

In lieu of the unmet medical needs for improving targeted-therapies and diagnostic biomarkers in liver cancer, it was of paramount interest in characterizing novel targets and mechanisms involved that were important during hepatocarcinogenesis.

Previous unpublished work from the lab has shown an oncogenic role of TRIP13 in human and mouse HCC through various experimental mice models of HCC and expression data sets from HCC patients.

The aim of the present study was to further characterize the mechanisms through which TRIP13 exerts its oncogenic effects during liver cancer growth. We hypothesized that TRIP13 could be regulating or be part of a central regulator pathway that determines cellular outcomes in terms of cell survival, growth or death.

To do so, we adopted various complementary in vitro approaches to examine for the oncogenic functions of TRIP13 in several HCC cell lines including HLF, Huh7, HepG2 and Hepa1-6. Cell viability, proliferation and apoptosis upon siRNA-mediated KD of TRIP13 were determined in here. Additionally, we aim to examine the expression levels of key oncogenic signalling factors to identify upstream and downstream pathways through which TRIP13 is involved in. The oncogenic relevance between TRIP13 and its interaction partner of SIN3A, which was identified from a mass-spectrometry analysis, were characterized. In order to determine whether this interaction was functionally relevant for cell growth, we examined for effects on HCC cell lines upon either single siRNA KD of TRIP13, SIN3A or both. Using lentiviral-mediated shRNA KD of SIN3A, we plan to establish a stable HLF cell line (shTRIP13+shSIN3A) for use in subcutaneous tumour implantation studies in order to accurately recapitulate this relationship in vivo.

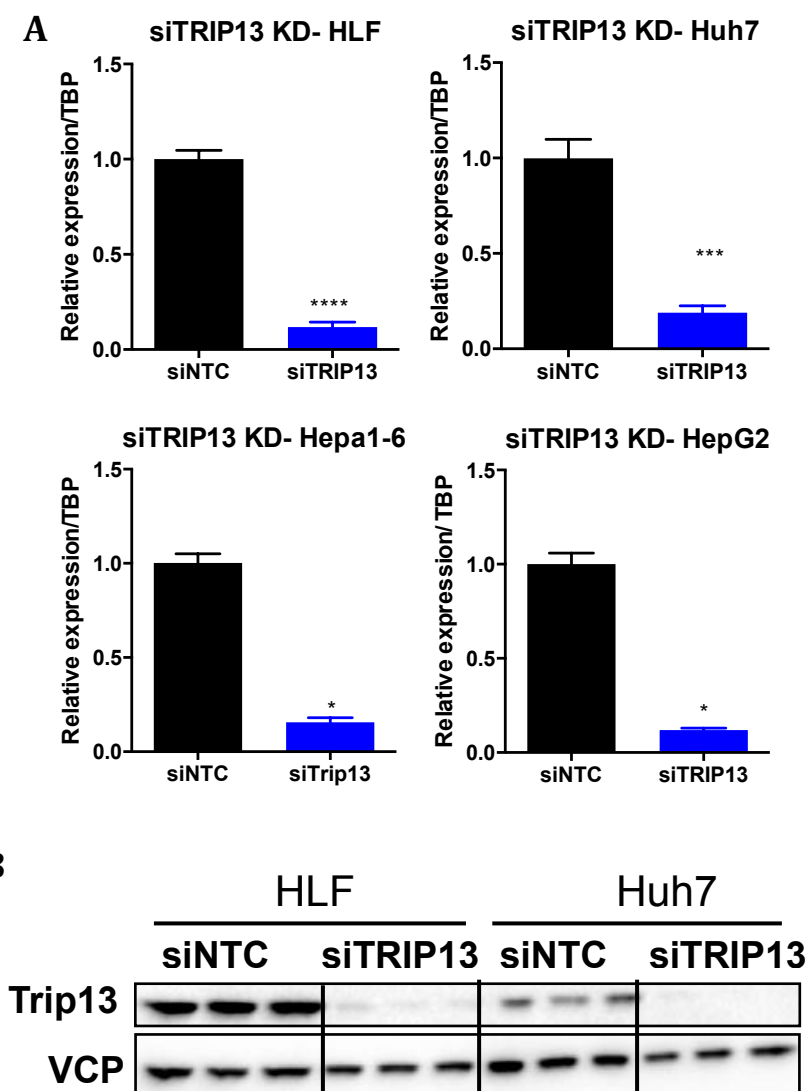
From all the findings above, we aim to dissect the mechanistic framework and provide functional annotations on the oncogenic roles of TRIP13 during hepatocarcinogenesis. This would serve as an interesting basis for developing novel biomarkers during diagnosis or targeted-therapies against HCC.

3 Results

3.1 TRIP13 regulates cell growth and proliferation in HCC cells

We have seen a regulation of TRIP13 during hepatocytes regeneration as well as its central role during HCC in human and mice (Fig.1.5 to Fig.1.8). Given these striking *in vivo* data, we were intrigued to further investigate the importance of TRIP13 as an oncogenic factor in HCC cells.

To this end, we first performed siRNA transfections using human HCC cell lines of HLF, Huh7 and HepG2 as well as mouse cell line of Hepa1-6. These cell lines were transfected either with a non-targeting control (siNTC) or a TRIP13- (human or mouse) specific siRNA (Fig. 3.1) to study cell proliferation (Fig. 3.2). Quantitative analysis of mRNA and protein levels 3 days post transfection showed that a knockdown of more than 75% of endogenous TRIP13 was achieved in all cell lines being utilized (Fig. 3.1).

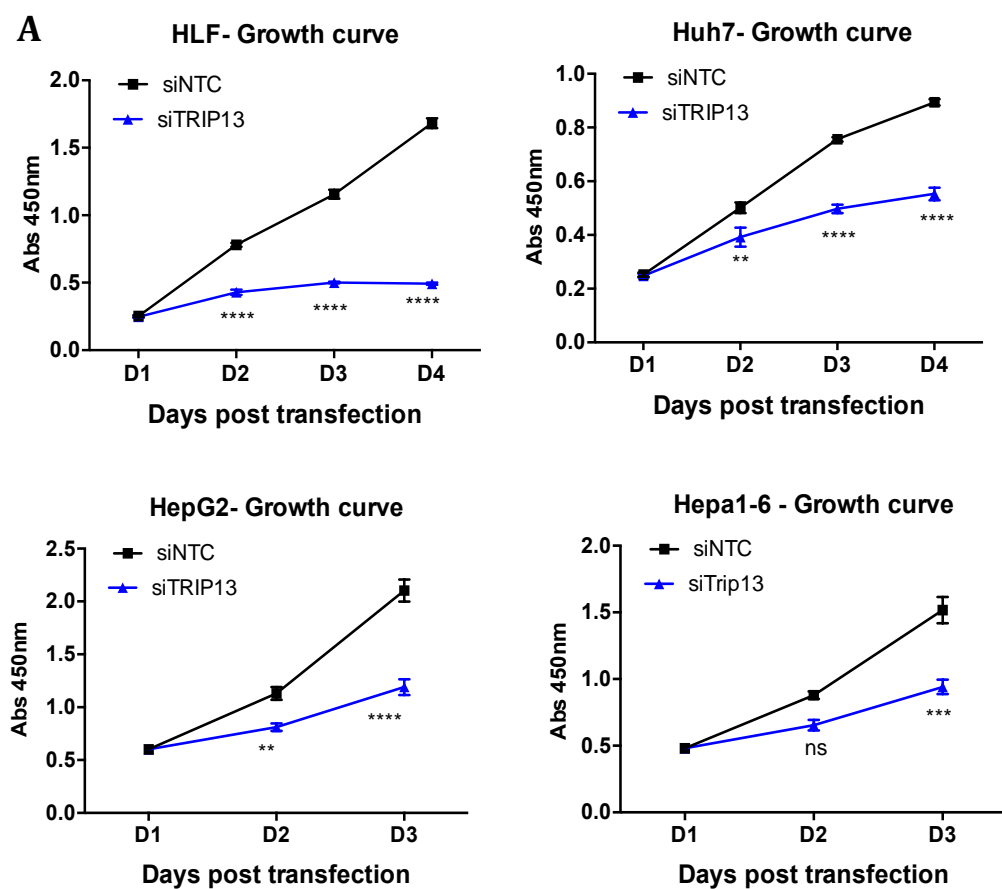


3 RESULTS

Fig. 3.1 Validation of siRNA-mediated knockdown in human and mouse HCC cell lines

The different cell lines were seeded in 12-well plates and siRNA transfections were performed the following day in accordance to protocols in section 4. Samples were harvested for RNA extraction and protein lysis at 72hrs post transfection. **(A)** mRNA expression levels of TRIP13 are relative to TBP and values shown are normalised against the siNTC group. **(B)** Western blot of TRIP13 from HLF and Huh7 cells transfected with siNTC or siTRIP13 siRNAs. VCP: Valosin containing protein (loading control). Data are plotted as mean \pm SEM. **** $p < 0,0001$; *** $p < 0,0002$; * $p < 0,05$; vs siNTC determined by two-tailed welch's t-test

As shown previously in vivo, a depletion of TRIP13 strongly reduced tumour growth in the xenograft models. Similarly in here, the knockdown of TRIP13 resulted in a significant arrest in cell growth 48hrs post transfection. The severities of siTRIP13-induced proliferation arrest in these various cell lines are listed in the order from HLF, Huh7, and HepG2 to Hepa1-6, with HLF cells being the most severely impaired (Fig. 3.2A).



3 RESULTS

As an alternative readout to assess cell proliferation, we have also utilised the BrdU incorporation kit, which determines BrdU incorporation into DNA as a measure for cell proliferation (Fig. 3.2B). Cell proliferations were similarly decreased across all HCC cell lines examined. Our *in vitro* data therefore strongly demonstrates that TRIP13 indeed plays a central role during cell proliferation.

B

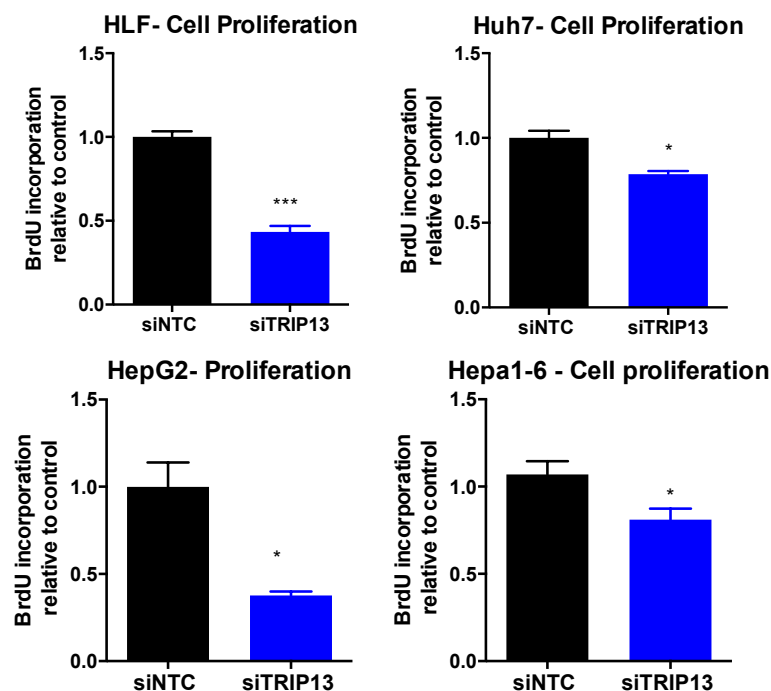


Fig. 3.2 TRIP13 regulates cell proliferation in various HCC cells

24hrs post siRNA transfection, cells are trypsinized and reseeded into 96-well plates with at least 3 repeats per siRNA conditions. (A) Growth rate of cells in 96-well plates D1 to D4 post transfection were measured by using CCK8 (cell counting kit 8). Absorbance at 450nm directly correlates to the number of viable cells in the well. (B) Cell proliferation was measured at D3 post transfection using a BrdU incorporation kit following protocols in section 1. Absorbance at 540nm correlates directly with actively proliferating cells. Values are shown normalized to that of the siNTC conditions

Data are plotted as mean \pm SEM. (A) **** $p \leq 0,0001$; ** $p \leq 0,01$; vs siNTC determined by 2-way Anova. (B) * $p \leq 0,05$; *** $p \leq 0,001$ vs siNTC determined by two-tailed welch's t-test versus siNTC

3.2 TRIP13 as a regulator of EGFR

3.2.1 EGFR expression is dependent on cellular levels of TRIP13

Based on our *in vivo* and *in vitro* data that supported a pro-tumourigenic role of TRIP13 in HCC development, we aimed to further identify and characterize the mechanistic involvement of TRIP13 in this context. From TRIP13 depleted HCC cells, we observed a decreased expression of EGFR, phosphorylation of key factors in the mTOR signalling pathway like E2F, IF4, along with downstream targets like cyclin D (Fig. 1.9).

Indeed, the EGFR signalling system has been implicated as a key player in the reparative and regenerative response of the liver, ranging from early inflammation and hepatocyte proliferation to fibrogenesis and neoplastic transformation [115]. EGFR expression and gene copy number has been found to be hugely upregulated in more than 50% of the HCC patients and tumour samples [116]. This has been accompanied alongside by an elevated expression of the EGFR ligands.

We first hypothesize that the EGFR/mTOR signalling pathway could be involved in here, in which a reduced signalling through this pathway could mediate the marked decrease in proliferation in TRIP13-depleted HCC cells. In order to investigate this mechanistic link, we first determined mRNA and protein expression of EGFR upon TRIP13 knockdown in multiple HCC cells (Fig. 3.3). We observed a significant decrease in both mRNA (Fig. 3.4A) and protein expression of EGFR (Fig. 3.3) across all HCC cell lines investigated (only data from HLF and Huh7 cells are shown in here).

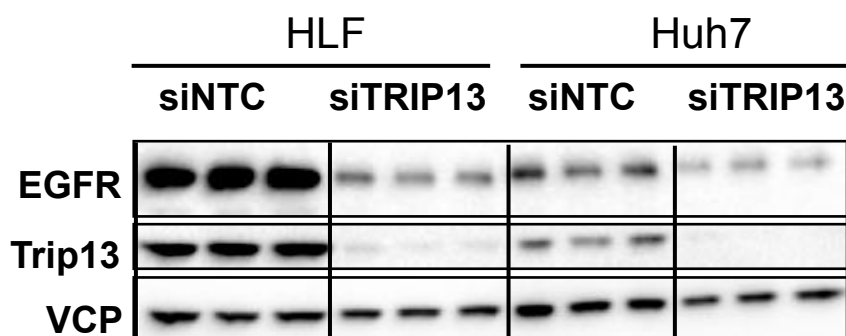


Fig. 3.3 TRIP13 regulates EGFR protein expression in HCC cells
72hrs post siRNA transfection, cell lysates were harvested for western blot. Three repeats per siRNA conditions per cell line were immuno-stained for TRIP13, EGFR and VCP (loading control) as shown.

3 RESULTS

We wanted to address whether manipulating the cellular levels of TRIP13 could affect the mRNA expression of EGFR in either ways. To do so, we examined cells that were either depleted (siTRIP13) or overexpressing TRIP13 (p-TRIP OE).

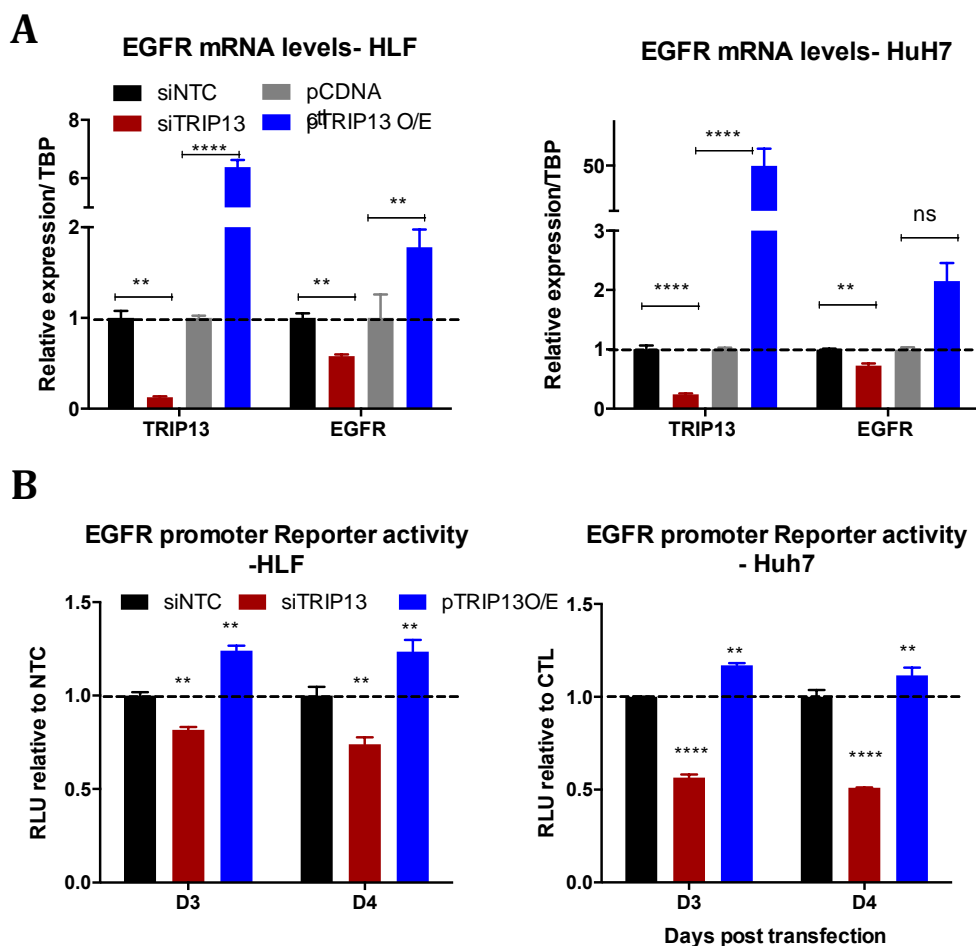


Fig. 3.4 Cellular levels of TRIP13 affect EGFR mRNA and promoter activity in HCC cells

TRIP13 levels were manipulated by either siRNA knockdown or overexpressed via a plasmid vector expressing the full-length sequence of TRIP13 (A) 72 hrs post transfection, cells were harvested for RNA extraction and subsequent qPCR analysis for TRIP13 and EGFR expression levels. Values are normalized against TBP and relative to that of either siNTC or the p-CDNA3.1 (empty vector) group. (B) An EGFR-promoter reporter construct (p-EGFR-HRP) has been co-transfected along with different siRNA or plasmids in here. The cell culture media was collected over D3 and D4 post transfection and the EGFR promoter reporter activity was measured with a Dual luciferase reporter assay. Relative luminescence values (RLU) correlates directly to the EGFR promoter activities. The values shown are relative to that of the control groups of either siNTC or p-CDNA3.1 (not displayed in this graph). Data are plotted as mean \pm SEM. **** $p \leq 0,0001$; ** $p \leq 0,01$; vs siNTC determined by 2-way Anova. NS indicates non significant differences

3 RESULTS

True indeed, EGFR mRNA expression was down regulated in TRIP13 KD cells and upregulated in HCC cells overexpressing the full-length human TRIP13 protein (Fig. 3.4A). To further investigate whether TRIP13 transcriptionally regulates EGFR via its promoter activity, we co transfected HCC cells with a human EGFR promoter reporter construct (p-EGFR-HRP) along with either siTRIP13 or p-TRIP13 OE (Fig. 3.4B). Similar to changes in EGFR levels upon TRIP13 KD or OE, a decrease in EGFR promoter activities were observed for TRIP13 KD cells whilst an increase in promoter levels was seen for TRIP13 OE cells. In conclusion, our data suggests that EGFR could be transcriptionally regulated by TRIP13.

3.2.2 The EGF pathway does not significantly contributes to TRIP13-dependent cell proliferation

In order to test our initial hypothesis that EGF signalling acts as a downstream mediator in conveying TRIP13-dependent effects on cell proliferation, we performed a loss of function analysis on cell growth upon EGFR knockdown. In both HLF and Huh7 cells, a successful knockdown of EGFR could be seen both on the mRNA and protein levels (Fig. 3.5A, B). The knockdown of EGFR resulted only in a minor growth defect in both cell lines (Fig. 3.5C). This was particularly so in HLF cells where proliferation impairment became apparent only at D4 post knockdown (Fig. 3.5C) as compared to an arrested cell proliferation already at D2 post TRIP13 knockdown (Fig. 3.2A). Due to the minor effects on growth as seen during EGFR knockdown, the initial hypothesis that EGF signalling plays a central role in mediating a TRIP13-dependent effect on cell growth could not be confirmed.

Along the same direction in refuting our initial hypothesis, a microarray analysis from a HCC patient cohort in Heidelberg showed that EGFR expression was relatively higher in the non-tumour samples vs the tumour samples (Fig. 3.6A). In line with our findings thus far, TRIP13 expression was shown to be significantly upregulated in the tumour samples vs the non-tumour samples. A spearman correlation analysis was performed between the expression levels of TRIP13 and EGFR (Fig. 3.6B). A negative correlation coefficient value of $r = -0,272$ was derived from this analysis.

In light of the above findings, we came to the conclusion that the EGF signalling pathway does not play a central role in mediating the TRIP13-dependent oncogenic effects as seen during proliferation of HCC cells.

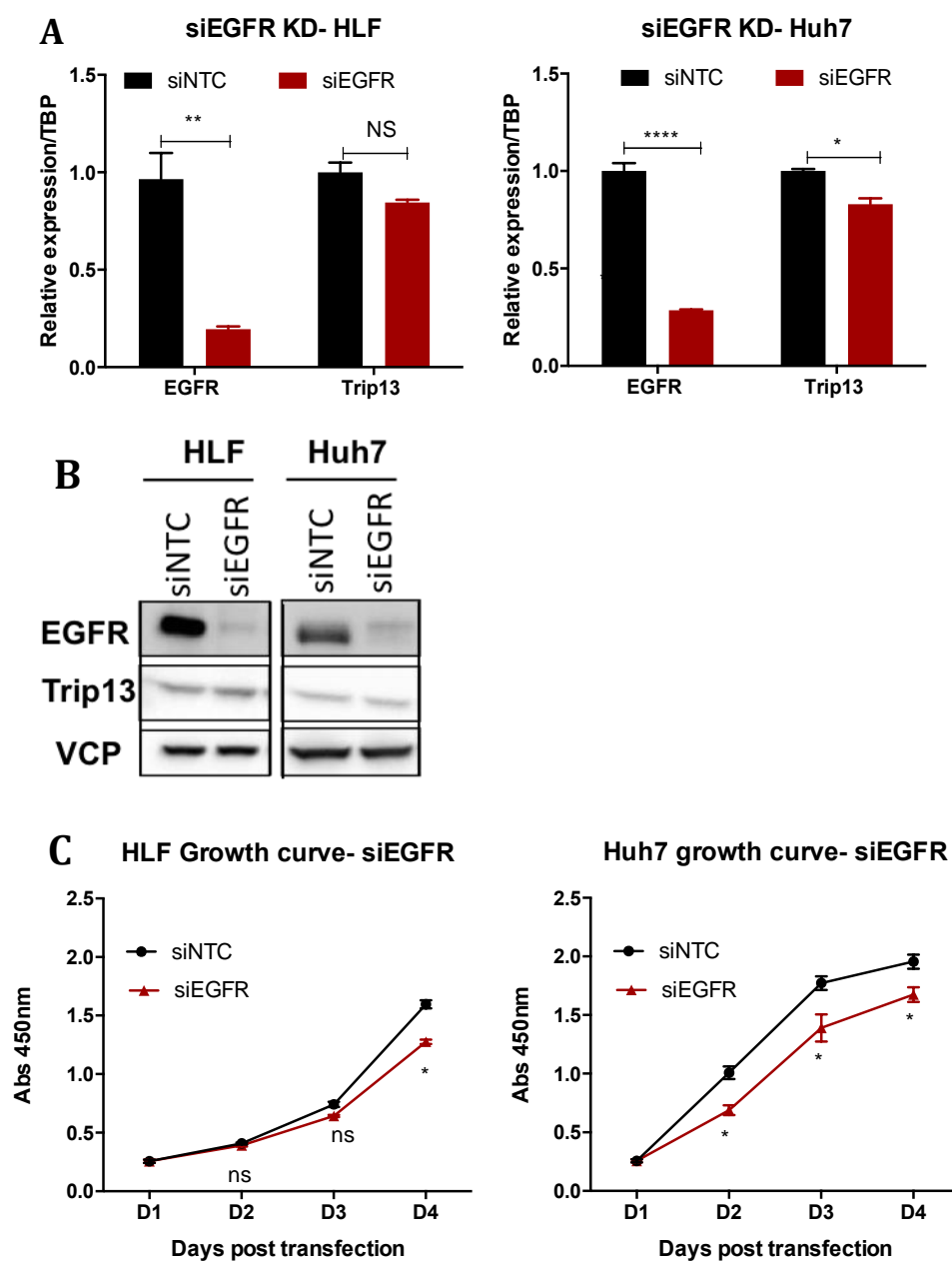


Fig. 3.5 EGFR knockdown only has a minor effect on cell proliferation in HCC cells

Expression levels of EGFR and TRIP13 D3 post transfection in HLF and Huh7 cells. Cell growth was assessed between D1 to D3 post siRNA transfection. (A) mRNA levels of EGFR and TRIP13 are normalized against TBP and shown as relative to the siNTC group. (B) Blotting for EGFR and TRIP13 with VCP as a loading control. (C) Growth rate of cells D1 to D4 post transfection were measured by using CCK8 (cell counting kit 8). Absorbance at 450nm directly correlates to the number of viable cells in the well *Data are plotted as mean \pm SEM. (A) **** $p \leq 0,0001$; ** $p \leq 0,01$; vs siNTC determined by two-tailed welch's t-test. (C) * $p \leq 0,05$; vs siNTC determined by 2-way Anova. NS indicates no significant differences*

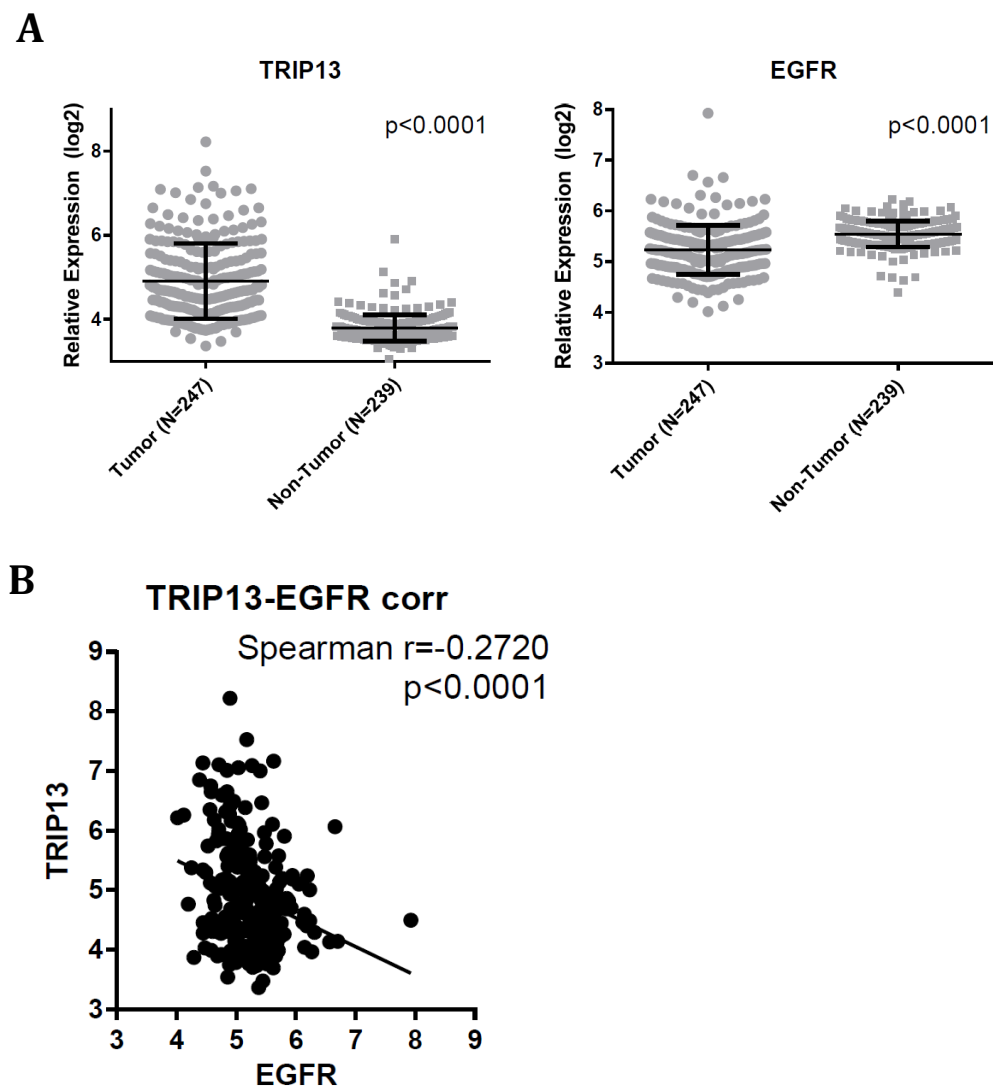


Fig. 3.6 TRIP13 and EGFR expression are not positively correlated in HCC cancer

(A) TRIP13 and EGFR microarray expression data in a HCC patient cohort dataset from Heidelberg (In collaboration with Stephanie Roesler from Heidelberg). TRIP13 and EGFR expression from tumour samples (N=247) vs non-tumour samples (N=239) are compared here. (B) A Spearman correlation analysis was performed between expression levels of TRIP13 and EGFR. The spearman correlation coefficient R is as stated. Data are plotted as mean \pm SEM. (A) **** $p \leq 0,0001$ vs Non tumour group, unpaired t-test.

3.3 Investigating the mechanistic role of TRIP13 in its tumour promoting functions

3.3.1 Identification of TRIP13-interaction partners that could define involved regulatory complexes

In order to decipher the mechanistic framework through which TRIP13 exerts its oncogenic function in HCC, a Mass spectrometry-based screening to identify TRIP13 interaction partners was performed. As outlined in Fig. 1.10, an immunoprecipitation (IP) approach was performed to pull down endogenous TRIP13 protein from both HLF and Huh7 cells. Amongst the co-precipitated proteins that were identified from the MS analysis, 39 proteins were found to be identical between both cell lines. Intriguingly, amongst the most enriched co-purified proteins, we detected SIN3A and SAP130, which have been previously identified to function as transcriptional regulators [48, 50]. Several members from the TRIP family including TRIP13 have been suggested to act as transcriptional co-regulators [85]. In lieu of this, we were interested to see whether TRIP13 along with its interaction partners of SIN3A and SAP130 might shed new light into the mechanistic workings of the tumour promoting function of TRIP13.

To rule out the possibility of false positives arising from enriched hits in our MS analysis, we decided to perform further biochemical analysis to prove that SIN3A and SAP130 are indeed interaction partners of TRIP13. Previous attempts to perform a TRIP13-IP to pull down SIN3A, SAP130 as well as a SIN3A/SAP130-IP to pull down TRIP13 have been unsuccessful (data not shown). We decided to adopt another method called the Proximity ligation assay (PLA), which has been reported to be more sensitive and dynamic in detecting interaction partners vs the traditional co-IP method.

To do this, we first performed an immunofluorescence staining to identify the intracellular localization of TRIP13, SIN3A and SAP130 (Fig. 3.7). We detected TRIP13 expression strongly in the perinuclear zone, ubiquitously in the cytoplasmic and weakly in the nuclei. SIN3A and SAP130 expression were strictly nuclei-localized, in line with published findings from other studies [48, 50].

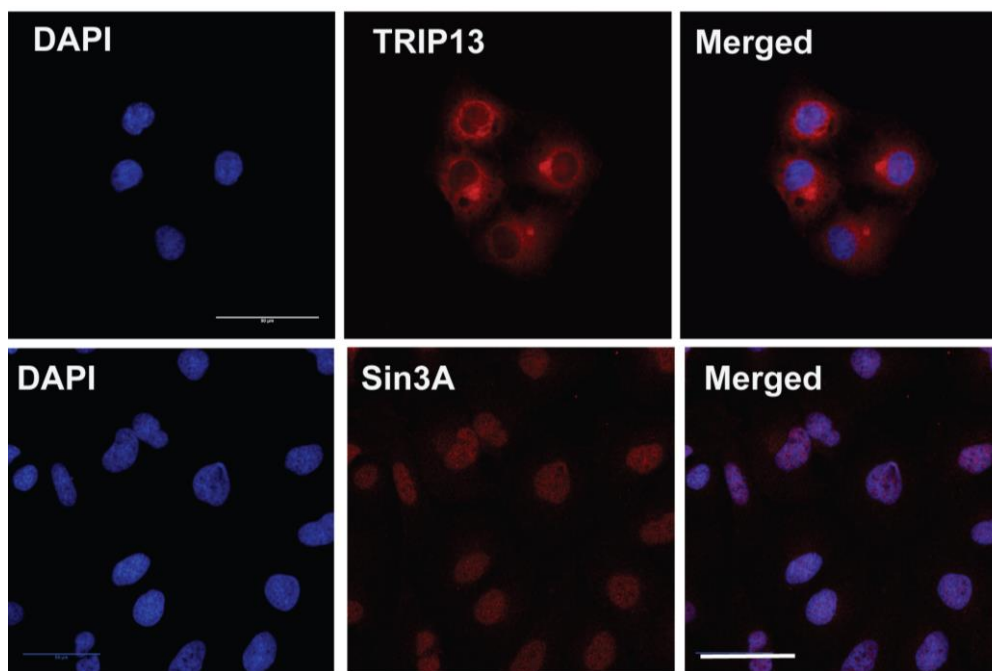


Fig. 3.7 Intracellular localization of TRIP13, SIN3A and SAP130 in HCC cells by confocal imaging

Immunofluorescence staining for TRIP13, SIN3A and SAP130 reveals the cellular localization of these proteins respectively in HLF cell line. DAPI staining marks the cell nucleus. The fixing of cells in chamber slides and subsequent processing for immunofluorescence and confocal imaging is outlined in methods in section 5. Scale bar: 50 μ m

Thereafter, we performed the PLA assay to validate an intracellular interaction between TRIP13 with SIN3A or SAP130 (Fig. 3.8) Antibodies derived from different species are needed in order for this PLA procedure to be able to detect interactions between 2 potential targets. In Fig. 3.8, TRIP13 antibodies derived from rabbit along with either SIN3A or SAP130 derived from goat was used during this assay to probe for potential interactions. Every single red fluorescence spot indicates a close proximity of < 40 μ m of interactions between these two proteins being probed for. For detailed description on this PLA procedure, please refer to methods in section 5.

3 RESULTS

As a positive control for this assay, SIN3A+SAP130 (interacting partners as previously published) have been probed to first verify that this assay is working optimally under the given conditions (top panel in Fig. 3.8). As expected, the red fluorescence dots corresponding to interactions between SIN3A and SAP130 were localized mainly in the nucleus. PLA for TRIP13 and SIN3A interactions showed up mainly in the nucleus, with some faint red dots in the cytoplasm. In the PLA for TRIP13 and SAP130, interactions seem to be localized mainly to the perinuclear and cytoplasm, along with weak staining in the nucleus. Please refer to the discussions in section 4, where a possible shuttling of TRIP, SIN3A is discussed. In the negative controls of this PLA assay, where one of the 2 antibodies in a probed pair has been replaced either with a control rabbit or goat IgG antibody, minimum background staining was seen in the cytoplasm but not in the nucleus. In essence, we have been able to verify that MS-identified TRIP13 partners of SIN3A and SAP130 do indeed interact with TRIP13 in an independent experimental setup.

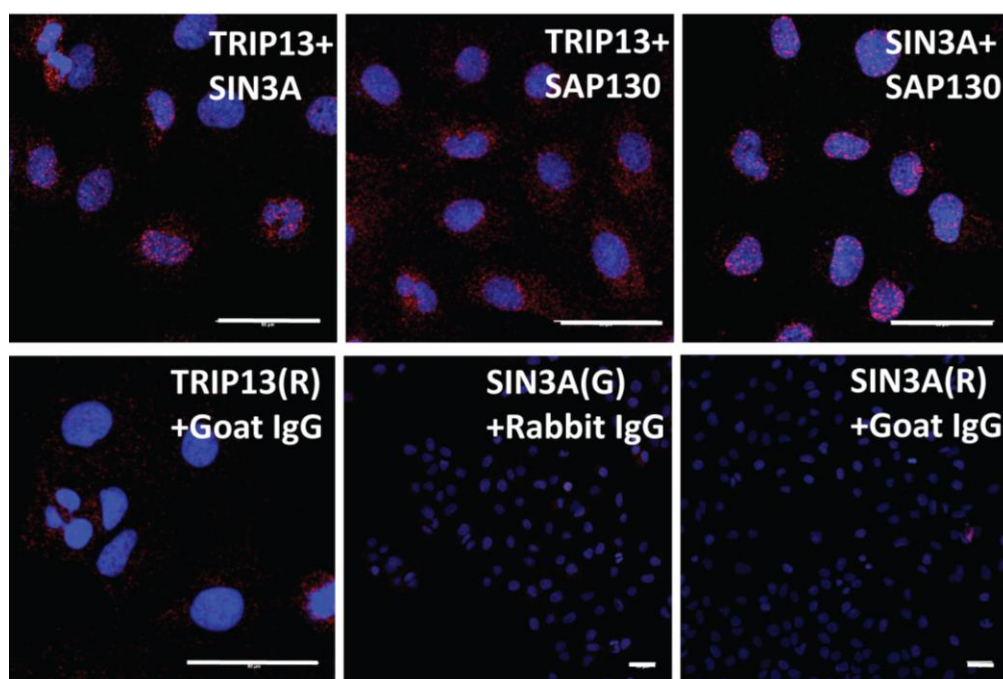


Fig. 3.8 Proximity ligation assay (PLA) to validate an intracellular interaction between TRIP13 with SIN3A or SAP130 that were previously identified via a MS screen.

Confocal imaging has been performed on Huh7 cells being processed for PLA staining. In this PLA protocol, pairs of antibodies of different species have been used to probe for interactions between TRIP13 (Rabbit) and SIN3A (Goat) or TRIP13 (Rabbit) and SAP130 (Goat) with reference to methods section 5. Every red fluorescent spot indicates a close proximity (< 40 μm) interaction between two targets being probed for. PLA staining for SIN3A+SAP130 served as an internal positive control for interacting partners. Negative controls for this PLA staining are shown in the bottom panel where one of the antibodies in a probed pair has been replaced with either an unconjugated Goat IgG or Rabbit IgG antibody. Scale bar: 50 μm

3.3.2 Effects of TRIP13 and interaction partners of SIN3A/SAP130 in HCC cell proliferation

To test the effects of TRIP13 along with SIN3A and SAP130 on HCC cell growth, we performed siRNA transfections whereby different combinations of specific siRNA were used and proliferation was thereafter monitored in Fig. 3.9A. Whilst cell proliferation was impaired in TRIP13 knockdown cells as previously seen, SIN3A or SAP130 knockdown alone had no effects on proliferation. Interestingly, the TRIP13 siRNA proliferation defect was restored upon combinatorial knockdown of either SIN3A or SAP130. Due to the similar growth restoring effect that SIN3A and SAP130 gene depletion both exert in TRIP13 knockdown cells, we decided to focus only on SIN3A in future experiments (given that the functions of SAP130 has been ascribed mainly due to its direct binding to SIN3A as reviewed in introduction).

Concomitantly knockdown of SIN3A reverses growth defect in TRIP13-depleted cells

A separate experiment was thereafter performed to examine only the growth effects of a concomitant knockdown of TRIP13+SIN3A. A similar rescue in growth defect of TRIP13 knock down cells was observed up to D6 post combinatory depletion of TRIP13+SIN3A (Fig. 3.9B). The cell growth results above were further reaffirmed by a BrdU incorporation assay performed (Fig. 3.9C), where a combined knockdown of TRIP13+SIN3A significantly restored cell proliferation from TRIP13-depleted cells.

Thereafter, using the cell lysates from these HLF cells depleted either of TRIP13 or SIN3A or both, we determined apoptotic levels by measuring caspase 3/7 activities in these cells (Fig. 3.9D) The Caspase 3/7 levels as measured in Fig. 3.9D were in accordance to what has been previously observed for TRIP13-depleted cells, in comparison to these cells, TRIP13+SIN3A depleted cells had only half the amount of Caspase 3/7 levels.

Next, we checked for the mRNA and protein expression of genes regulating proliferation by qPCR and western blotting from HLF cell lysates harvested from this experiment (Fig. 3.9). Remarkably, we noticed a significant depletion of a proto-oncogene c-MYC, on both the protein and the mRNA levels upon TRIP13 knockdown (Fig. 3.10A, B). With regards to the well described role of c-Myc as a master regulator during cell proliferation and its frequent overexpression in multiple cancers including HCC, it seems plausible that reduced c-MYC activity could account for an arrested cell growth upon TRIP13 knockdown in HLF cells (Fig. 3.9B, C). In line with this notion and reflecting its corresponding effects on cell proliferation, the depletion of c-MYC in TRIP13 knockdown cells were partially restored when SIN3A was concomitantly depleted (Fig. 3.10). Conversely, SIN3A knockdown alone had no effects on cell growth or c-MYC levels (Fig. 3.10A). In the combined knockdown group, only a marginal decrease in knockdown efficiency of TRIP13 (<5%) was seen as compared to the single TRIP13 siRNA knockdown group. This indicates that a restored cell growth and c-MYC activity after concomitantly depleting TRIP13 and SIN3A cannot be due to a reduced efficiency of TRIP13-depletion induced growth arrest in this case.

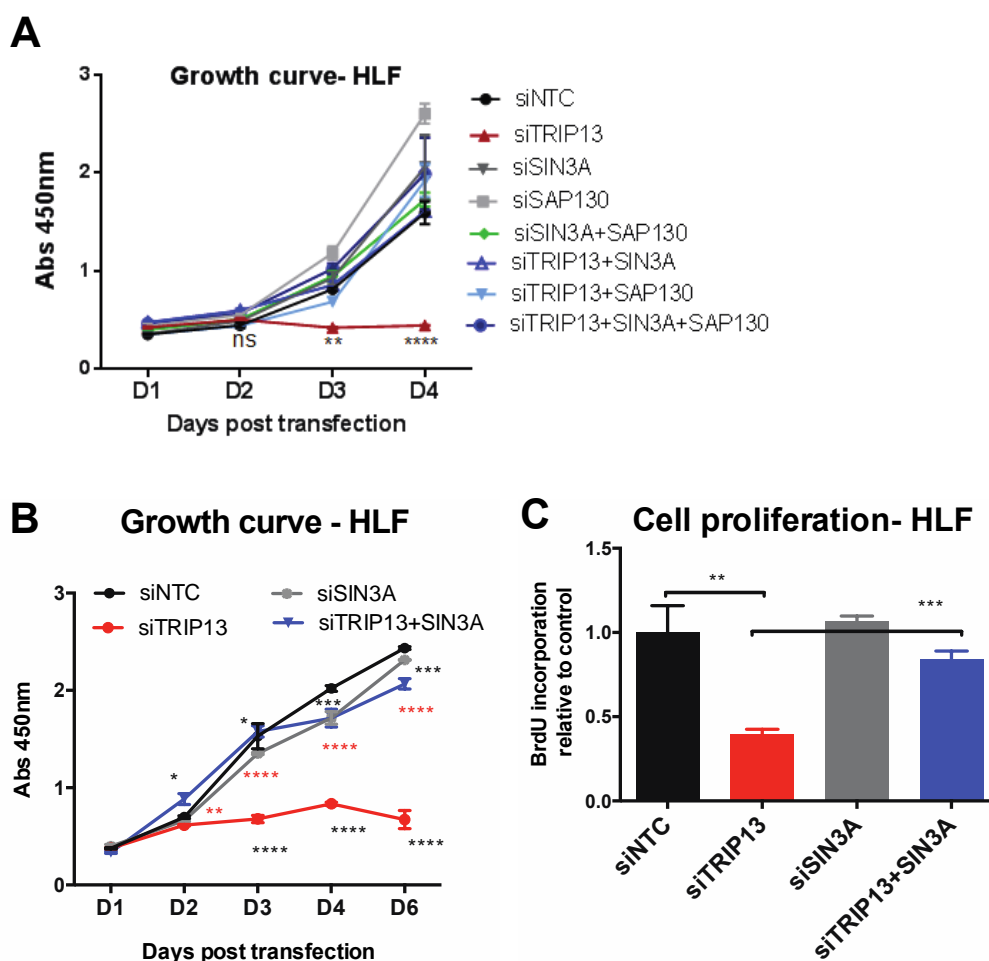


Fig. 3.9A - C Concomitant KD of SIN3A or SAP130 rescues the proliferation defect exerted by TRIP13 depletion in HLF cells

Transfections using siRNAs targeting either TRIP13 or SIN3A or SAP130, or both were performed. Cell proliferation are thereafter monitored up to D6 post transfection. Results from representative experiments were shown. **(A)** Growth rate of cells in 96-well plates D1 to D4 post transfection were measured by using CCK8 (cell counting kit 8), following protocols described in section 5. Absorbance at 450nm directly correlates to the number of viable cells in the well. **(B)** Growth rate of cells comparing siTRIP13 cells vs combined KD of TRIP13+SIN3A up to D6 post transfection. **(C)** Cell proliferation from combined siRNA KD was measured at D3 post transfection using a BrdU incorporation kit following protocols described in section 5. Values are shown normalized to that of the siNTC conditions

Data are plotted as mean \pm SEM. **** $p \leq 0,0001$; *** $p \leq 0,001$; ** $p \leq 0,01$; vs siNTC determined by 2-way Anova. NS indicates not significant.

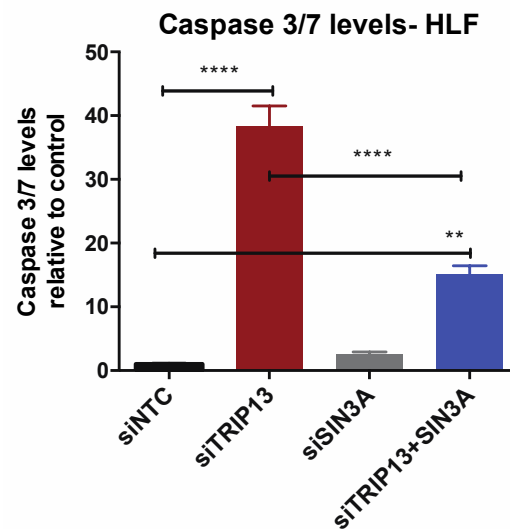


Fig. 3.9D Apoptotic levels in HLF cells depleted either with TRIP13 or SIN3A or both

HLF cells were harvested D3 post transfection and apoptosis were determined by measuring Caspase 3/7 levels from cell lysates using an assay kit: Glo-caspase3/7 homogenous assay, following protocols in section 5. Fluorescence values for the amount of caspases3/7 levels present were plotted relative to the siNTC group. Data are plotted as mean \pm SEM. ** $p \leq 0,01$; **** $p \leq 0,0001$ vs siNTC or siTRIP13 as indicated in the chart and determined by 2-way Anova.

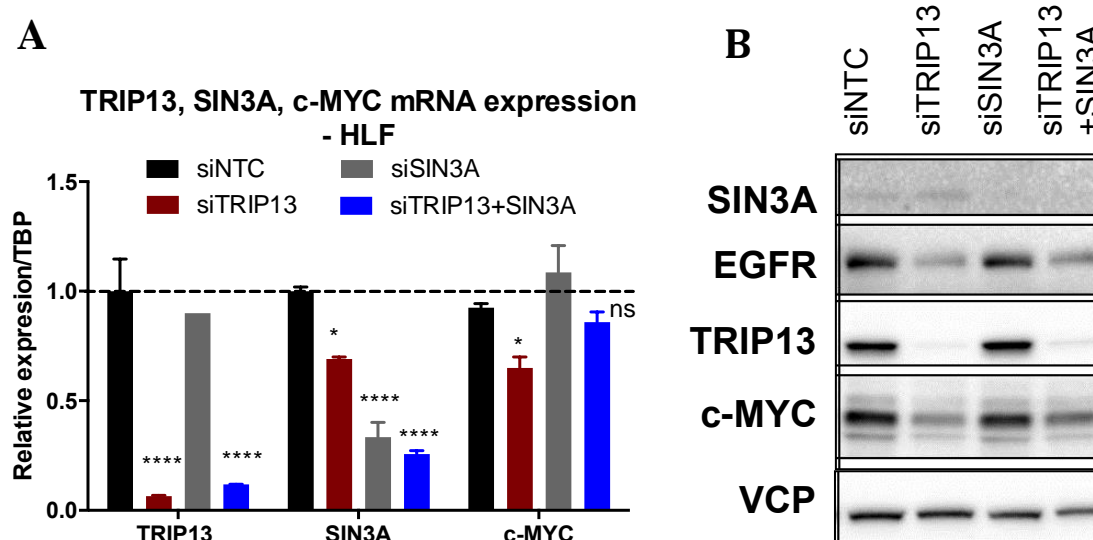


Fig. 3.10 Expression levels of TRIP13, SIN3A and c-MYC after combined siRNA transfection in HLF cells

mRNA and protein expression levels D3 post transfection.

(A) mRNA levels of TRIP13, SIN3A and c-MYC are normalized against TBP and shown as relative to the siNTC group. (B) Blotting for SIN3A, EGFR, TRIP13 and c-MYC with VCP as a loading control. Data are plotted as mean \pm SEM. (A) **** $p \leq 0,0001$; ** $p \leq 0,01$; vs siNTC determined by two-tailed welch's t-test. (C) * $p \leq 0,05$; vs siNTC determined by 2-way Anova. NS indicates not significant difference.

Thereafter, we performed at least four additionally experiments under the experimental set up as before and have always observed a corresponding rescue of TRIP13-depletion dependent growth defect upon simultaneous knockdown of SIN3A in HLF cells (cell growth are similar to Fig. 3.9). A partial restoration of c-MYC and CyclinD1 in TRIP13+SIN3A conditions could similarly be seen from 3 of these independent experiments conducted in Fig. 3.11.

Next, in order to determine whether cellular localization of TRIP13 and SIN3A changes upon single or combined gene knockdown, we performed cellular fractionation on these HLF cells, harvested D3 post transfection. In Fig. 3.12, TRIP13 expression was seen in both the cytoplasmic and nuclear fractions, whereas SIN3A was localized only to the nuclear fraction. No changes were however observed in the cellular localization of SIN3A upon TRIP13 knockdown or vice versa in TRIP13 upon SIN3A knockdown.

In conclusion of the above findings, we have observed a robust restoration of cell proliferation and c-MYC levels during TRIP13-depletion when SIN3A was concomitantly inactivated in HLF cells. It is conceivable that a reduced c-MYC activity accounted for the severe proliferation defect along with a down regulation of growth promoting proteins like EGFR and CyclinD1 in TRIP13 inactivated HLF cells (Fig. 3.10)

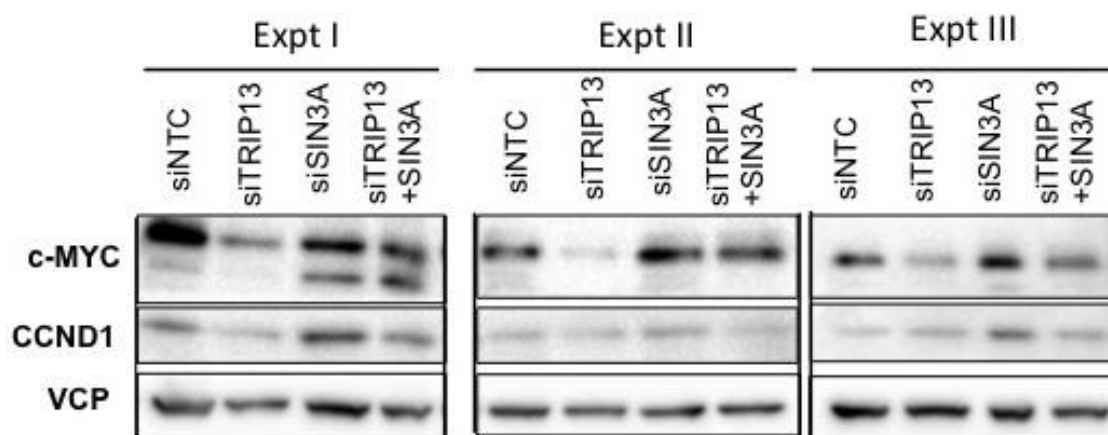


Fig. 3.11 Partial restoration of c-MYC and Cyclin D1 (CCND1) after concomitantly knockdown of TRIP13+SIN3A from 3 independent experiments

Cell lysates were harvested D3 post transfection in HLF cells and blotted for c-MYC and CCND1, with VCP as a loading control. siRNA KD on protein levels for TRIP13 and SIN3A has been separately verified via western blot (data not shown).

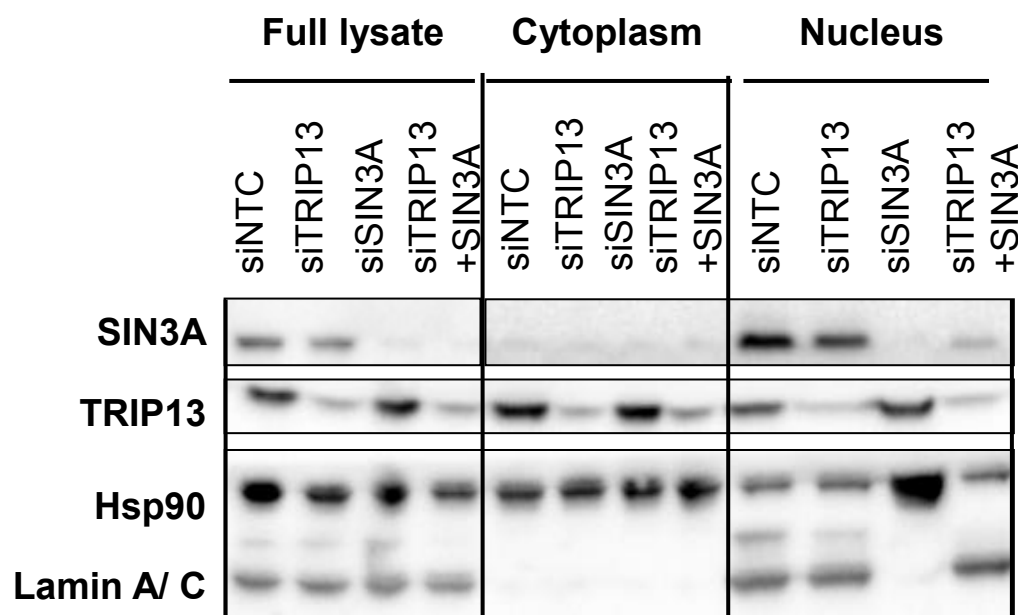


Fig. 3.12 Cellular fractionation to determine cell localization of TRIP13 and SIN3A during single and combined knockdown of these genes
Cell lysates were harvested D3 post transfection in HLF cells and blotted for SIN3A and TRIP13, with HSP90 and LaminA/C as a loading control for cytoplasmic and nuclear fractions respectively. The loadings from the whole cell lysate, cytoplasmic and the nuclear fraction are shown.

3.3.3 SIN3A knockdown reverses the anti-proliferative effects from TRIP13-depletion and is recapitulated in several HCC cell lines

In order to rule out a common experimental pitfall that our findings above were cell line-specific only in HLF cells, we decided to include several other HCC cell lines namely human Huh7, HepG2 and mouse Hepa1-6 cells. In Fig. 3.13, we performed siRNA transfections to knockdown either TRIP13 or SIN3A or both and measured cell proliferation in these various cell lines as shown. In Huh7, HepG2 and Hepa1-6 cells, a concomitant knockdown of SIN3A partially restored cell growth in TRIP13-depleted cells from D3 onwards (Fig. 3.13A, B&C). These results above were also reaffirmed during a BrdU assay in Huh7 (Fig. 3.13D) cells. For Hepa1-6 in Fig. 3.13E, there were no effects on BrdU uptake across all samples as compared to the control group. This was in contrast with our previous results in Fig. 3.2 showing that an impaired cell proliferation during TRIP13-depletion in Hepa1-6 could be captured both via a CCK8 cell counting kit and the BrdU uptake assay. We assumed that a lack of changes in BrdU uptake even in the TRIP13 depleted cells could be due to the suboptimal knockdown efficiencies for Hepa1-6 in this experiment.

Thereafter, we analysed the gene expression of c-MYC from these various cell lines upon single or combined depletion of TRIP13 and Sin3A (Fig. 3.14). A reduction of c-MYC protein levels in Huh7 cells across all samples upon depleting either TRIP13 or SIN3A or both was seen. The corresponding effect in the combined knockdown of TRIP13+SIN3A is unclear. The lower endogenous levels of c-MYC in Huh7 cells made it hard to ascertain whether there was indeed a partial restoration of c-MYC in this case. We observed also a depletion of c-MYC across all samples upon depleting either TRIP13 or SIN3A or both in Hepa1-6 cells. The restoration of c-MYC levels as seen previously in HLF cells (Fig. 3.11) was not seen in Hepa1-6 cells, where the c-MYC levels were lower in the combined knockdown of TRIP13+SIN3A vs the single gene knockdown.

In summary, we were able to reverse the antiproliferative effects of TRIP13-depletion by concomitantly depleting SIN3A in various HCC cell lines of HLF, Huh7, HepG2 and Hepa1-6 cells. The corresponding effect in restoring c-MYC levels during TRIP13-depletion, when SIN3A is concomitantly depleted is established in HLF cells. Due to the absence of a clear rescue of c-MYC levels in other cell lines, this effect could not be conclusively confirmed in other cell lines as tested.

3 RESULTS

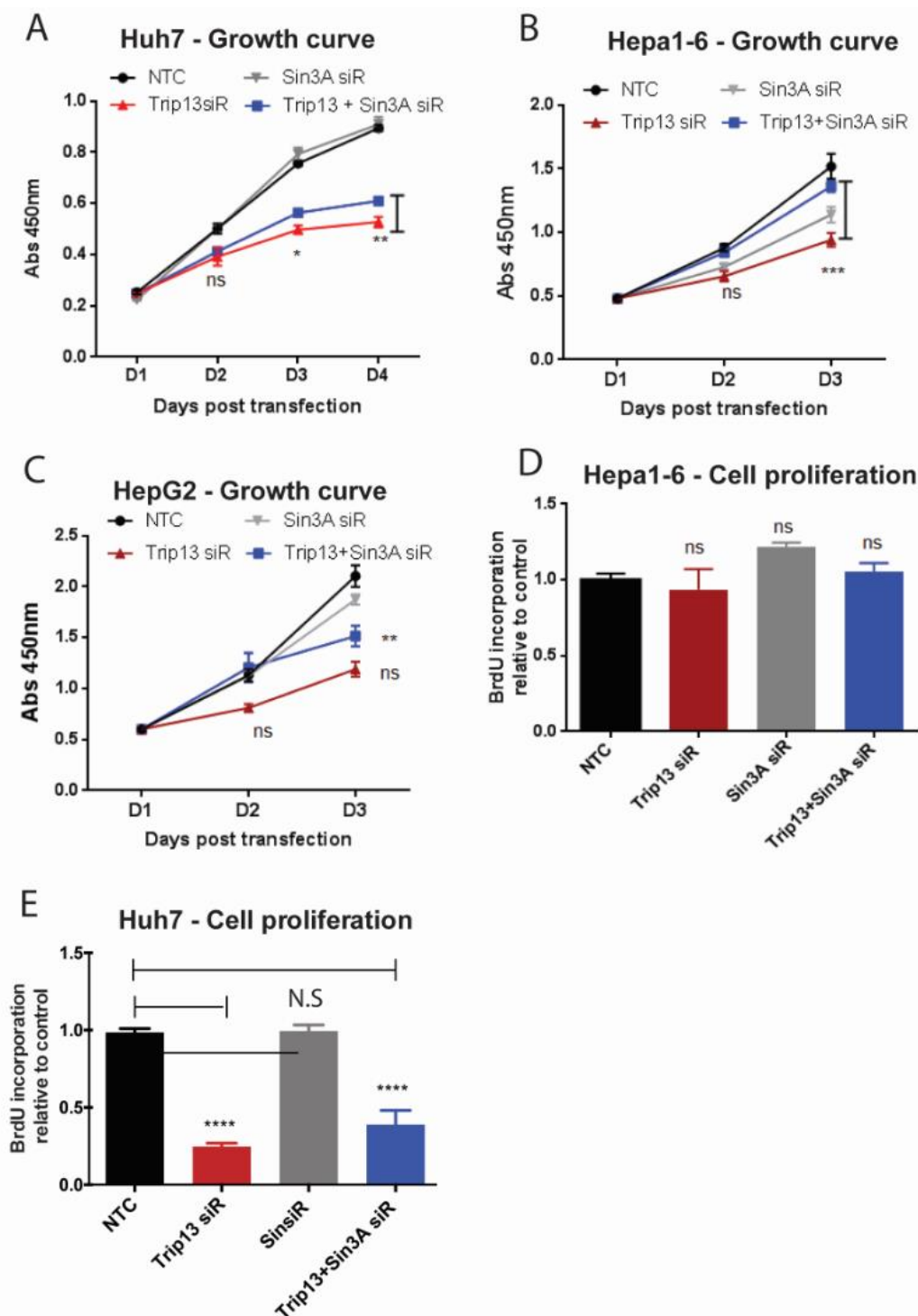


Fig. 3.13 Concomitant KD of SIN3A rescues the growth defect in TRIP13-depleted human Huh7 and HepG2 but not mouse Hepa1-6 cells
 siRNA transfections to knockdown either TRIP13 or SIN3A or both was performed in Huh7, HepG2 and Hepa1-6 cells. Cell proliferation was monitored up to D4 post transfection. (A) Cell proliferation has been measured via a CCK8 kit (B) Cell proliferation has been measured via BrdU incorporation using a BrdU labelling kit Data are plotted as mean \pm SEM. (A) *** $p \leq 0,001$; ** $p \leq 0,01$ * $p \leq 0,05$ vs siTRIP13 determined by two-tailed welch's t-test. (C) **** $p \leq 0,0001$; vs siNTC determined by 2-way Anova. NS indicates non-significant differences

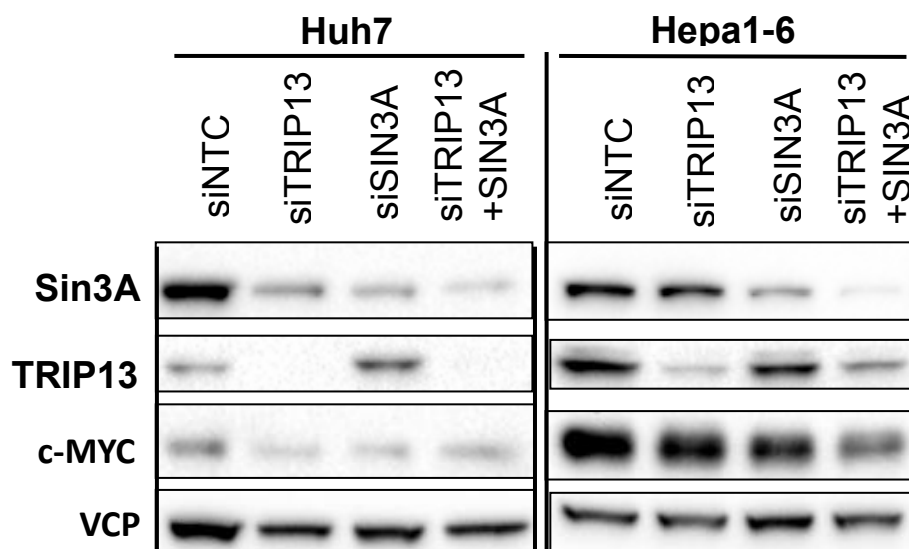


Fig. 3.14 Expression levels of c-MYC after depleting TRIP13 or SIN3A or both in Huh7 and Hepa1-6 cells

Western blot was performed using cell lysates harvested D3 post siRNA transfection. Immunoblotting for SIN3A, TRIP13 and c-MYC was performed with VCP as a loading control.

3.3.4 The oncogenic c-MYC pathway in mediating antiproliferative effects upon TRIP13 depletion in HLF cells

We first observed a marked reduction in c-MYC levels, along with several growth promoting factors like EGFR and cyclinD1 when we knock down TRIP13. In order to decipher the mechanistic framework in the oncogenic functions of TRIP13, we performed a MS analysis to identify interaction partners defining involved regulatory complexes (Fig. 1.10). Due to the initial hypothesis that TRIP13 might transcriptionally regulate EGFR mRNA levels, we decided to focus on this MS-enriched target, SIN3A, with well-characterised functions as a global transcriptional regulator. As shown from Fig. 3.9 to Fig. 3.11 in HLF cells, the decrease in growth and c-MYC levels upon TRIP13 ablation was strikingly reversed upon a concomitant ablation of SIN3A. Indeed, SIN3A forms part of the histone deacetylation complex (HDAC) and represses MYC activities by directly deacetylating and destabilizing c-MYC [48].

In line with this, we wanted to test the idea that a reduction in c-MYC related activities accounted for the growth arrest along with a down regulation of growth promoting factors like EGFR and Cyclin D1 in TRIP13 inactivated cells (Fig. 3.10). To test this hypothesis that c-MYC could be an important mediator in conveying TRIP13-dependent effects on cell growth, we performed a gain of function analysis by overexpressing a full length human c-MYC to observe for effects on cell proliferation thereafter (Fig. 3.15).

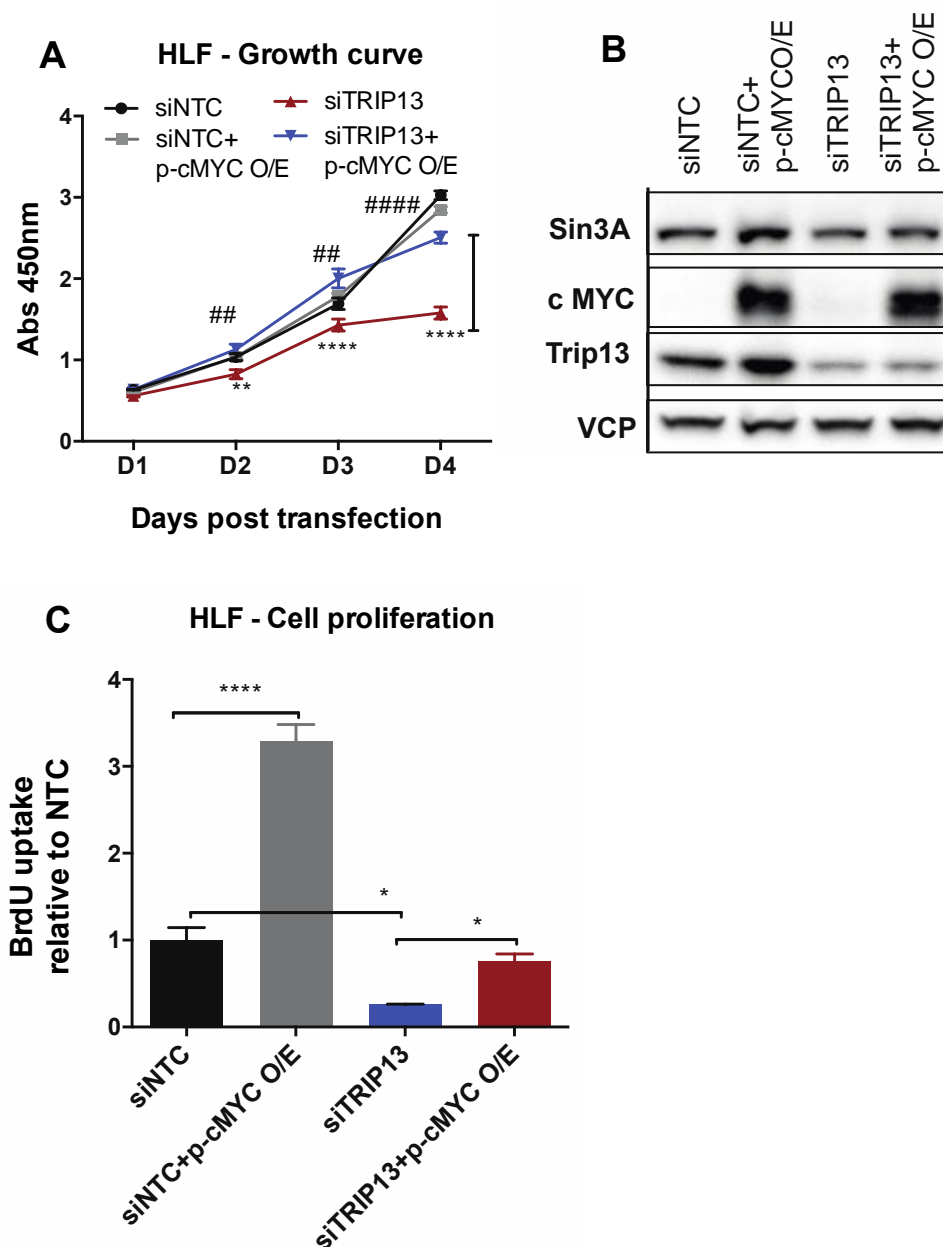


Fig. 3.15 Overexpression of c-MYC rescues the proliferation defect in TRIP13 deficient HLF cells

Co-transfections with siRNAs targeting against TRIP13, +/- a plasmid overexpressing full-length human c-MYC was performed in HLF cells. Cell proliferation and western blot are shown. **(A)** Cell proliferation has been measured via a CCK8 kit using protocol from section 5. Abs at 450nm correlates directly to the number of cells in this assay. **(B)** Cell proliferation has been measured via BrdU incorporation using a BrdU labelling kit. **(C)** Immunoblotting for SIN3A, TRIP13 and c-MYC with VCP as a loading control. Data are plotted as mean \pm SEM. **(A)** **** $p \leq 0,0001$; ** $p \leq 0,01$; vs siTRIP13 determined by two-tailed welch's t-test. ## $p \leq 0,01$; #### $p \leq 0,0001$ vs siNTC **(B)** *** $p \leq 0,001$; * $p \leq 0,01$ vs siNTC determined by 2-way Anova.

3 RESULTS

HLF cells were co-transfected either with a plasmid overexpressing c-MYC (p-cMYC O/E), or an empty vector backbone along with NTC or TRIP13 targeted siRNAs. In Fig. 3.15A, TRIP13-depleted cells were expectedly growth arrested from D2 post gene knockdown. This growth arrest was remarkably reversed when a full-length c-MYC protein was concomitantly overexpressed in these TRIP13-depleted cells, resulting in an almost complete proliferation rescue at D3 and D4. This was similarly recapitulated in the BrdU uptake assay where concomitantly overexpressing c-MYC resulted in 4 times the amount of cell proliferation in TRIP13-depleted cells (Fig. 3.15B), nearly reaching control BrdU levels. On another note, the increase in BrdU uptake upon c-MYC overexpression in the si-Control group was not recapitulated in the growth curve via the CCK8 assay (Fig. 3.15A). Cell lysates from this experiment was subsequently harvested and immunoblotted to verify for TRIP13, c-MYC and SIN3A expression against VCP as the loading control (Fig. 3.15C).

These results above are in line with our hypothesis that reduced c-MYC activities contribute towards the anti-proliferative effects of TRIP13-depleted HCC cells. Reflecting a central role that c-MYC plays in relaying the tumour-promoting function of TRIP13, we observed a complete rescue of growth arrest when c-MYC was simultaneously overexpressed in TRIP13-depleted cells. For further in-depth discussion with regards to this TRIP13-SIN3A-c-MYC axis that we propose, please refer to discussions in section 4. We hypothesize that the ability of SIN3A to exert a destabilizing effect on c-MYC depends on the absence of TRIP13. A SIN3A-dependent depletion of c-MYC is lifted when both TRIP13 and SIN3A were concomitantly depleted, as seen by the partial restoration of c-MYC levels in those cells in Fig. 3.11.

3.3.5 Establishing stable cell lines with concomitant depletion of TRIP13 and SIN3A for in vivo tumour implantation models

We aim to validate our hypothesis of a TRIP13-SIN3A-MYC axis in vivo in a tumour implantation model as outlined in Fig. 3.16A. In this approach, TRIP13 or SIN3A or both will be inactivated either in Human HLF or mouse Hepa1-6 cells using a lentivirus-mediated shRNA incorporation approach. Genetically modified cells would then be implanted either into immune-deficient mice (Human HLF cells) or C57Bl/6 mice (mouse Hepa1-6 cells). Tumour growth would be monitored and cell proliferation markers would thereafter be analysed at the end of the study from these tumour tissues.

Numerous attempts in the past have failed to establish a stable knockdown of TRIP13 in HCC cells, due to a low cell viability post TRIP13 depletion. Using an alternative approach to circumvent this problem, we decided to first establish a stable knockdown of SIN3A in HLF and Hepa1-6 cells since depleting SIN3A conferred no effects on cell growth. One week prior to the tumour implantation study, these SIN3A-depleted stable cell lines would be infected with Lentiviral particles to mediate an shRNA dependent knockdown of TRIP13. After one round of antibiotics selection using blasticidin (SIN3A) and puromycin (TRIP13), these shTRIP13+shSIN3A-depleted cells would be directly implanted into the animals.

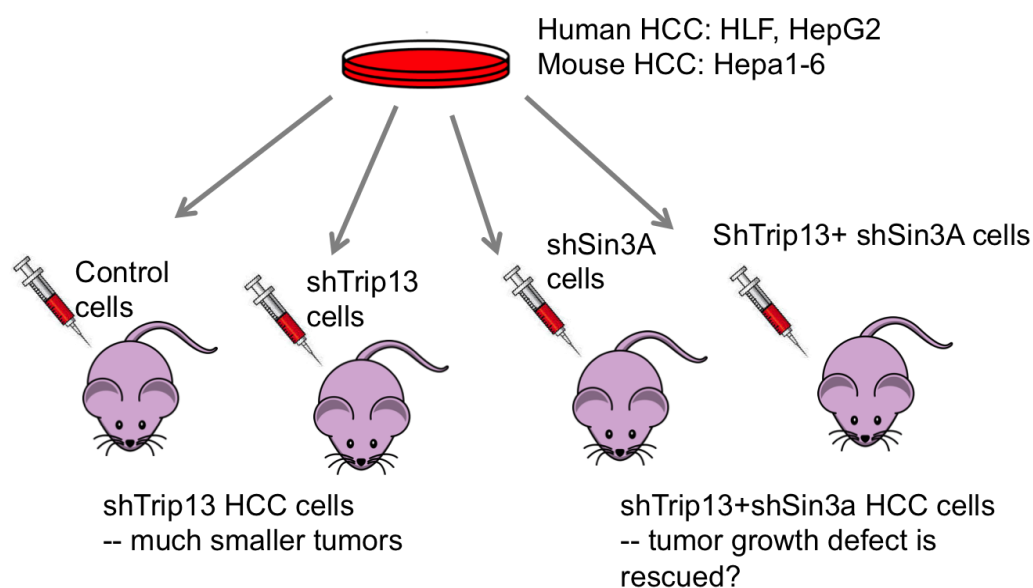


Fig. 3.16A Planned tumour implantation study using shTRIP13+shSIN3A HCC cells

A set of 4 SIN3A-specific shRNA constructs, each containing a unique 29mer specifically targeting SIN3A was ordered from Origene. For the specific vector backbone and shRNA sequences of these 29mer, refer to materials in section 5. As the SIN3A shRNA vectors were available only in a pGFP-C-shLenti plasmid backbone that conferred a puromycin resistance gene (which was similar to that of the antibiotic resistance for TRIP13-shRNA expression vectors that we already have), we had to subclone these SIN3A-shRNA expression cassettes into another vector backbone of pRFP-C-shLenti that confers the blasticidin resistance gene (data not shown).

After the sequences of the subcloned SIN3A-shRNA constructs have been verified via sequencing analysis, we then proceeded to package these constructs into the respective lentiviral particles using HEK293T cells. The efficiencies of each of these lentiviral-mediated knockdowns of SIN3A, 7-days post blasticidin selections in HLF and Hepa1-6 cells are as shown in Fig. 3.16B. Lentiviral particles containing shRNA constructs from shSIN3A_1 and shSIN3A_4 mediated the most efficient knockdowns in HLF and Hepa1-6 and were used subsequently to establish stable SIN3A knockdowns in these cell lines.

Due to the lack of time, the initial aim to perform an in vivo tumour implantation study using shTRIP13+shSIN3A HCC cells could not be realized in time before the thesis was completed.

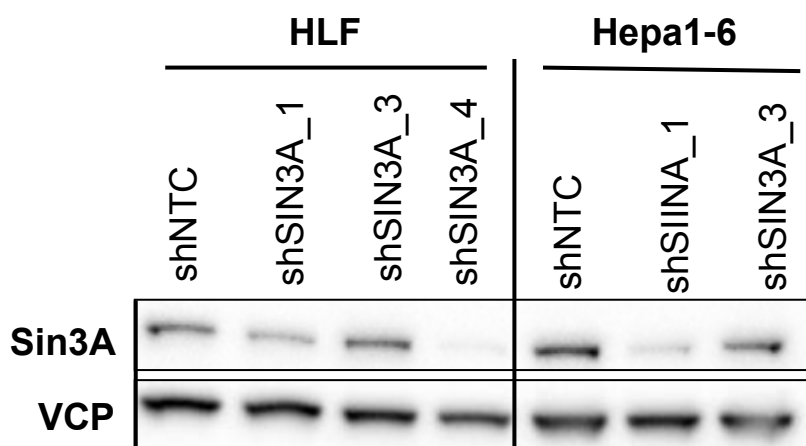


Fig. 3.16B Generating stable HLF and Hepa1-6 cell lines with shR KD of SIN3A using a Lentiviral-mediated system

Lentivirus containing plasmid with different shRNA sequence targeting against SIN3A are denoted as shSIN3A_1, shSIN3A_3 and shSIN3A_4. Lentivirus production and quantification was outlined in methods in section 5. Lentivirus was added to cells at an MOI of 10 along with polybrene (8 mg/ml) to enhance the virus transduction. D5 post-viral transduction, Blasticidin at (2 mg/ml) was added to select for resistant cells that are successfully expressing the pLKO-shRSIN3A plasmids. Western blot shows SIN3A expression in different cell lines D7 post blasticidin selection, using VCP as a loading control.

3.4 Effects of overexpressing Trip13 in non-tumourigenic AML12 liver cells

3.4.1 Overexpressing Trip13 in AML12 cells boosted an increase in cell proliferation

As shown in the Fig. 1.5, Trip13 was upregulated in various fatty liver-related disease conditions in ob/ob, db/db and high fat diet fed mice as well as in a mouse model of non-alcoholic steatohepatitis (NASH) upon methionine-choline deficient diet feeding. Furthermore, numerous reports have shown TRIP13 to be significantly upregulated in various types of cancer including liver cancer (from our own data). We have also provided *in vivo* and *in vitro* data indicating that TRIP13 plays a central role in oncogenic growth of liver cancer cells.

AML12 is a non-transformed mouse liver cell line, derived from a mouse transgenic for human TGF α , allowing it to be continuously passaged in cell culture. We have separately verified that the expression levels of Trip13 in AML12 to be at least 4 times lower than that in HCC cell lines of HLF and Huh7, based on mRNA expression analysis (data not shown). Under this premise, we were interested to investigate if overexpressing Trip13 could contribute to oncogenic transformation of AML12 cells.

Overexpressing a full-length mouse Trip13 in AML12 cells resulted in a significant induction in cell growth, 3 days upon Trip13 overexpression (Fig. 3.17A). This increase in cell growth was similarly reflected in the BrdU uptake assay in Fig. 3.16B, where Trip13 overexpressing cells showed 1,5 fold increase in proliferation vs the control cells. In line with the growth promoting effects, western analysis for different tumourigenic factors like EGFR, c-MYC and p-53 showed all these proteins to be upregulated in the Trip13 overexpressing AML12 vs the control cells (Fig. 3.16C). On a separate note, an overexpression of a full length human TRIP13 in a HepG2 liver cancer cell line did not showed any significant effects on cell growth, BrdU uptake and c-MYC levels (Fig. 3.16D, E, F). We were unsuccessful after numerous attempts to perform the Colony forming assays for AML12 to compare tumourigenicity between Trip13 overexpressing vs control cells. These cells were deemed to be unsuitable for this colony assay in our hands, due to the low cell viability (when AML12 cells were seeded at a low density to perform this assay) and inability to form viable colonies.

In view of the above, we have further highlighted the pro-tumourigenic function of TRIP13 by demonstrating that an overexpression of this gene is sufficient to stimulate cell proliferation in a non-tumourigenic hepatocyte cell line of AML12. This induction in cell proliferation is further reflected by a corresponding upregulation of growth promoting factors like EGFR and c-Myc.

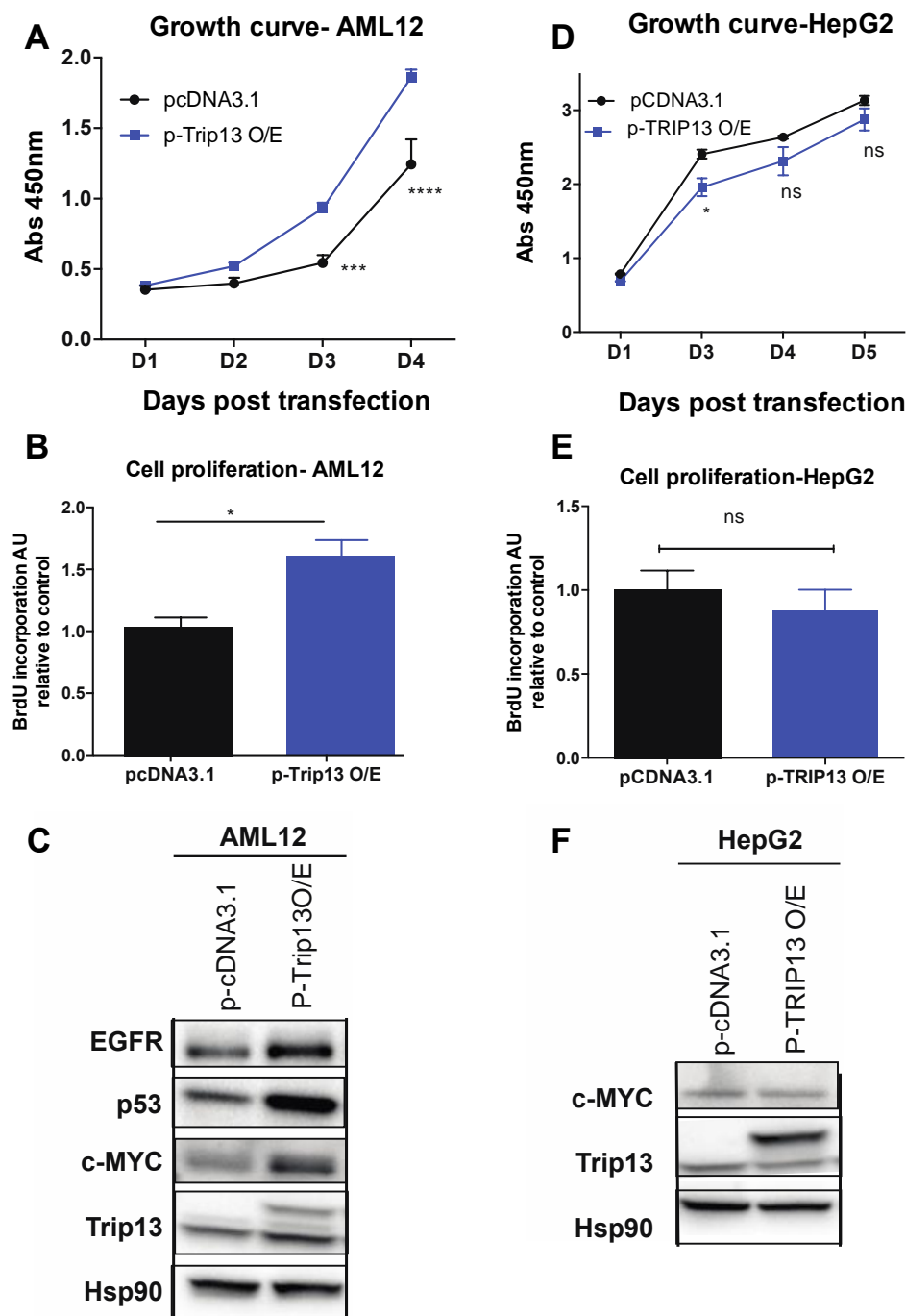


Fig. 3.17 Overexpression of TRIP13 resulted in an increase in cell proliferation in non-tumourigenic AML12 cells but not in HepG2 cells
 Transfections using plasmids overexpressing either a full-length human or mouse TRIP13 was performed in HepG2 or AML12 cells respectively. **(A)** Cell proliferation has been measured via a CCK8 kit. Abs at 450nm correlates directly to the number of cells in this assay. **(B)** Cell proliferation has been measured via BrdU incorporation using a BrdU labelling kit on D3 post transfection. **(C)** Blotting for EGFR, p-53, TRIP13 and c-MYC with HSP90 as a loading control. Data are plotted as mean \pm SEM. **** $p \leq 0,0001$; *** $p \leq 0,001$; * $p \leq 0,01$ vs pcDNA3.1 determined by 2-tailed Welch's t-test. N.S indicates non significant differences

3.5 Role of TRIP13 in the DNA damage repair pathway

3.5.1 Chromosomal instability (CIN) and upstream regulation of TRIP13

Chromosomal instability is a phenomenon commonly seen in tumour cells when chromosomes are improperly segregated in daughter cells due to the loss of proper checkpoint controls. In this regard, a CIN signature refers to a specific set of highly ranked genes that is consistently correlated with chromosomal instability in cancer. The Hippo/YAP signalling was found to be one of the main drivers in regulating the expression of the CIN signature genes in liver cancer, with TRIP13 being found to be one of the 25 top ranking genes (reviewed in section 2.2.2). In a mouse model for HCC, it was found that overexpressing YAP stimulated both invasiveness and growth of tumour cells. Furthermore, liver cancer patients with tumour gene expression pattern associated with the CIN signature were characterized by a poorer prognosis [39].

In this context, it seems possible that YAP could be an upstream regulator of TRIP13, where an upregulation of the hippo/YAP signalling mediates a corresponding increase in TRIP13 as commonly seen in human HCC patients. We picture that knocking down YAP could result in a corresponding decrease in TRIP13 along with its downstream targets in HCC cells.

To test this hypothesis, we performed a loss of function analysis by knocking down YAP1 using target specific siRNA. As shown in Fig. 3.18A & B, a knockdown of YAP1 resulted in a corresponding decrease in expression of TRIP13 along with EGFR, in both HLF and Huh7 cells. This decrease in mRNA expression levels of TRIP13 and EGFR was similarly recapitulated on the protein levels via western blot analysis in Fig. 3.17C. In Huh7 cells (Fig. 3.18B), the knockdown of YAP1 resulted in an almost complete depletion of YAP1, which might account for the marked decrease in a corresponding expression of TRIP13 and EGFR (vs the less dramatic effects in HLF cells). These results seen above suggest that YAP could indeed be an upstream regulator of TRIP13 in HCC cells.

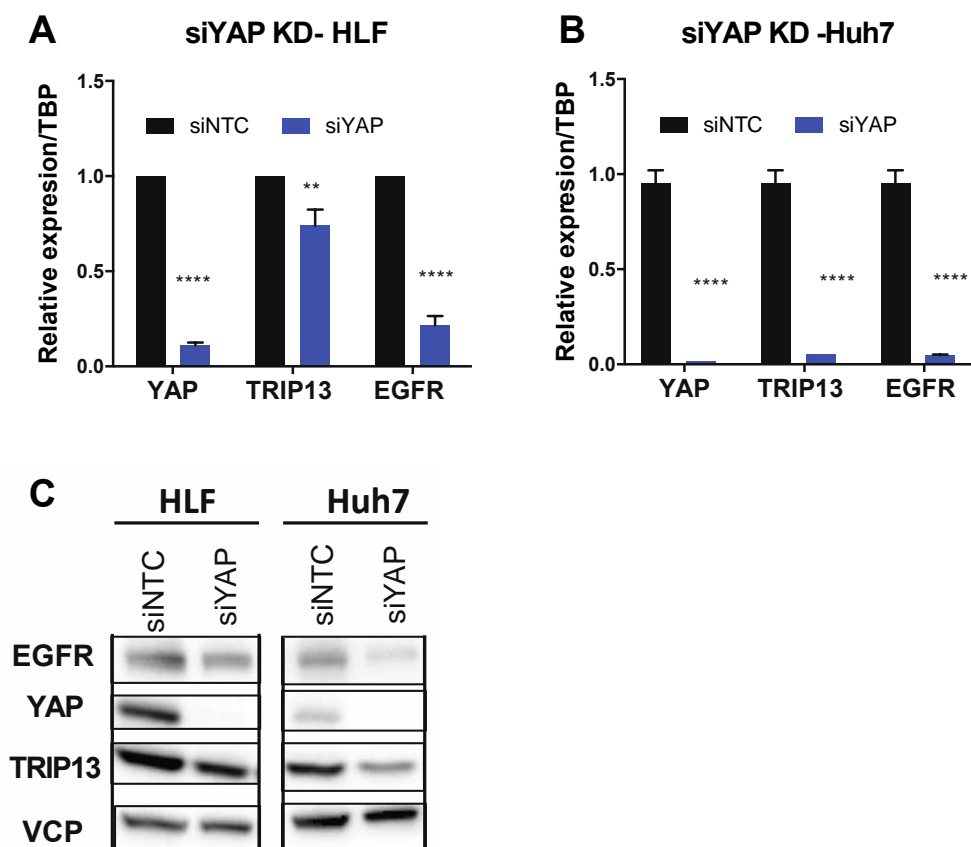


Fig. 3.18 YAP as a plausible upstream regulator of TRIP13

siRNAs targeting against YAP1 was performed in HLF and Huh7 cells. mRNA and protein expression has been performed on cells harvested D3 post transfection. (A) mRNA expression of YAP, TRIP13 and EGFR were normalized against TBP and represented relative to the NTC group. (B) Blotting for EGFR, YAP, and TRIP13 with HSP90 as a loading control. Data are plotted as mean \pm SEM. **** $p \leq 0,0001$; ** $p \leq 0,001$ vs siNTC determined by 2-tailed Welch's test.

3.5.2 TRIP13 in DNA damage repair pathways

TRIP13 has been described in several reports [34, 35, 45] to be indispensable during DNA damage repair and non-homologous end joining (NHEJ). Furthermore, the role of TRIP13 during NHEJ was proposed to be the main oncogenic mechanism in conferring chemoresistances to head and neck tumour cells [45]. Owing to the enhanced DNA repair machinery of these TRIP13-overexpressing tumour cells, these cells acquire resistances against the genotoxins commonly used in chemotherapeutic treatments [45].

We were similarly interested to explore the DNA damage repair role of TRIP13 and more importantly whether this pathway when deregulated attributed to the severe growth defect in TRIP13 depleted HCC cells. D3 post TRIP13 depletion, DNA fragmentation was characterized by grossly abnormal nuclear morphology and nuclear blebbing in Fig. 3.19A.

3 RESULTS

pH2AX γ , which is a marker to detect for DNA damage was also remarkably upregulated in these TRIP13-depleted HLF cells (Fig. 3.19B). Reflecting what was seen above, the caspase 3/7 levels in these TRIP13-depleted cells were 38 folds more than that of the control group in Fig. 3.19C.

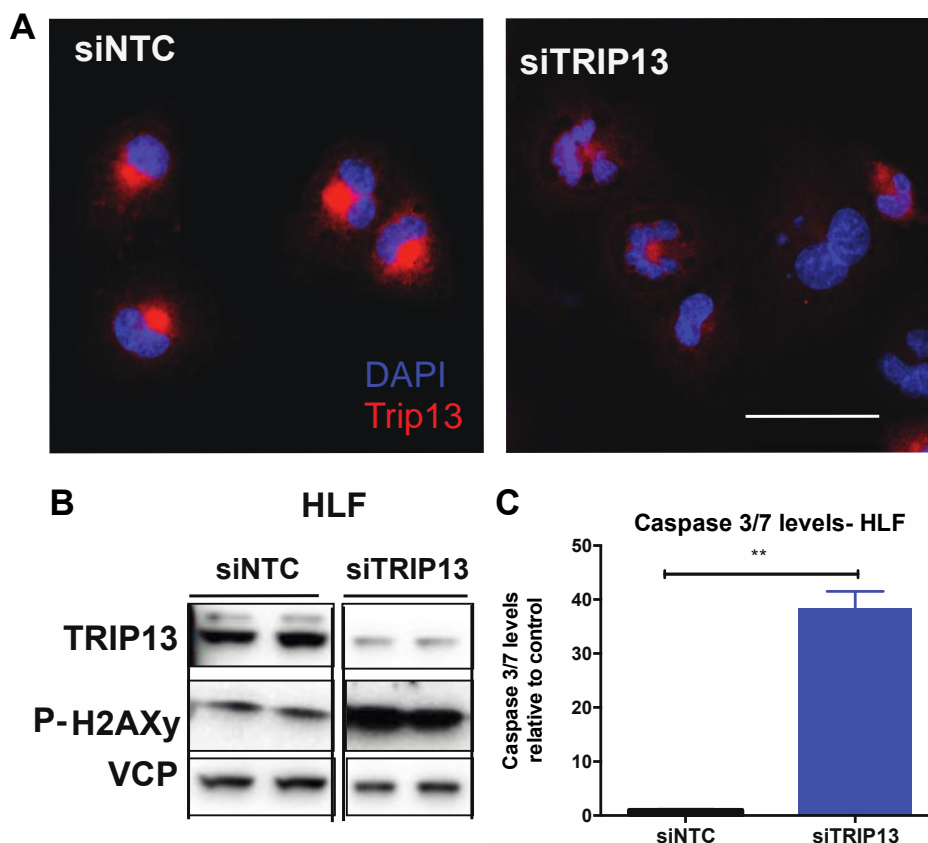


Fig. 3.19 A– C TRIP13 depletion triggered an increase in DNA damage
Confocal images of siNTC vs siTRIP13 HLF cells are shown. Cell lysates were harvested for western blotting and separately measured for caspase 3/7 levels. **(A)** Immunofluorescence staining of DAPI and TRIP13 are compared between siNTC vs siTRIP13 cells. **(B)** Western Blotting for TRIP13 and p-H2AXy with VCP as a loading control. **(C)** Caspase 3/7 levels has been measured from cell lysates using this assay kit: Glo-caspase3/7 homogenous assay, following protocol of section 5. Fluorescence values for the amount of caspases3/7 present were plotted relative to the siNTC group. Scale bar indicates 50um. Data are plotted as mean \pm SEM. ** $p \leq 0,001$ vs siNTC determined by 2-tailed Welch's test.

3 RESULTS

3.5.3 DNA damage signalling pathway does not play a central role in causing proliferation defect in TRIP13-KD cells

Our data thus far suggests that TRIP13 could be part of an oncogenic signalling network, regulating downstream c-MYC activities, which could indeed play a central role in HCC tumourigenesis. In lieu of this hypothesis above, one has to also consider several other aspects of oncogenic regulation that determines the final outcome between cell survival vs cell death. In this respect, we questioned whether the role that TRIP13 plays during DDR could also have a central role in determining the oncogenic growth of HCC cells.

KU60019 is an ATM (Ataxia Telangiectasia Mutated Protein) inhibitor that is used frequently to block the central DNA damage response (DDR) mediated via ATM signalling. In this experiment, we treated HLF cells in a final concentration of 3 μ M of KU60019 to observe for a possible effect on cell growth between the control vs TRIP13-depleted cells in Fig. 3.19D. TRIP13-depleted cells were expectedly growth arrested D2 upon gene depletion. Importantly, we observed that an inhibition of the DDR pathway via ATM signalling (+KU60019) did not reverse the growth defect in these TRIP13-depleted cells. If an accumulation of DNA damage due to TRIP13 depletion were mainly responsible for the growth arrest in TRIP13-depleted HCC cells, then a reversal of this growth defect would have occurred when this DDR pathway was inhibited which was not the case in Fig. 3.19D. In light of the above findings, we argue that the DNA damage repair role of TRIP13 is no doubt an important aspect during tumourigenesis; it was however not a main attributor in inhibiting proliferation as seen upon TRIP13 knockdown in HCC cells.

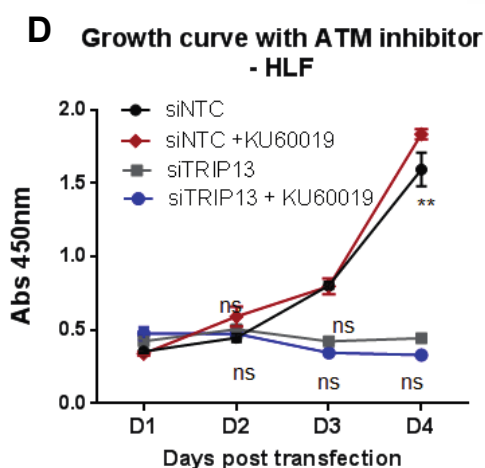


Fig. 3.19D Growth defect in TRIP13-depleted cells are not dependent on the ATM DNA damage pathway

Growth of HLF cells +/- an ATM inhibitor (KU60019) was compared between the siNTC vs siTRIP13 group. One day post siRNA transfections, KU60019 was added at a final concentration of 30 μ M to the respective wells. Fresh media +/- KU60019 was given to cells and cell growth was assessed with the CCK8 kit. The absorbance at 450nm correlates directly to the cell numbers. Data are plotted as mean \pm SEM. $**p \leq 0,001$ vs siNTC determined by 2-tailed Welch's test. NS indicates non-significant difference between siTRIP13 +/- KU60019.

3 RESULTS

3.5.3 DNA damage persist despite a growth rescue during concomitant depletion of TRIP13+SIN3A

As previously seen in Fig. 3.9 and Fig. 3.11, growth arrest in TRIP13-depleted cells could be reversed by concomitantly depleting SIN3A in multiple HCC cell lines. We were curious to examine also the DNA damage levels in these “growth rescued” cells as compared to the TRIP13-depleted cells alone.

In Fig. 3.20A, we observed a marked accumulation of p- γ H2AX in the nucleus of TRIP13-depleted cells as compared to the control cells D3 post gene-depletion. In the bottom panel of Fig. 3.20A, despite an apparent growth rescue of cells by a concomitant depletion of TRIP13+SIN3A, these cells continue to accumulate high levels of p- γ H2AX. As a side note, as images were captured on a random field of view, the number of cells in the images are non-representative of the true total amount of cells in that sample. Similar to what was observed on the immunofluorescence (IF) staining for p- γ H2AX, we observed an upregulation of this DNA damage marker in both TRIP13 depleted and TRIP13+SIN3A depleted cells in Fig. 3.20B. No changes in the level of p- γ H2AX in SIN3A-depleted cells were observed (data not shown).

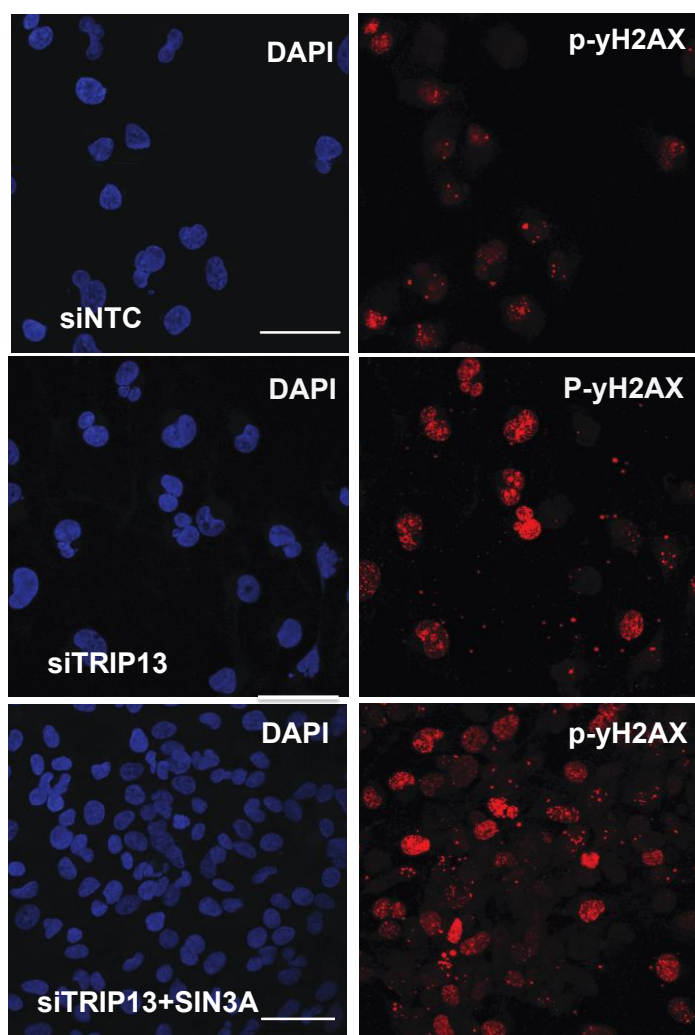


Fig. 3.20A Accumulation of DNA damage in combined siTRIP13+SIN3A persisted in spite of a growth rescue

HLF cells were transfected with siNTC, siTRIP13 or siTRIP13+SIN3A, using siNTC for titrations to an equal final amount during transfection. D1 post siRNA transfections, cells were seeded into chamber slides for further incubation before being harvested for immunofluorescences (IF) staining D3 post transfection. IF was performed in reference to methods in section 5. Confocal images shows IF staining for DAPI and p-γH2AX from the different siRNA conditions. Scale bar indicates 50 μm.

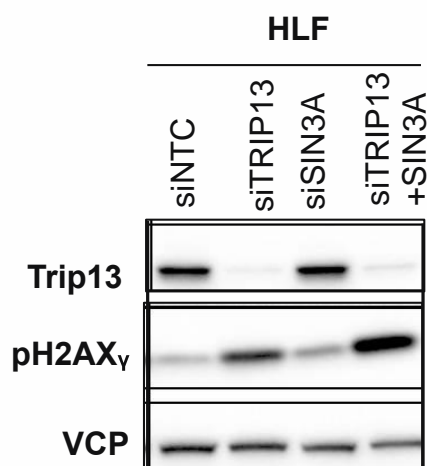


Fig. 3.20B Detection of DNA-damage markers in HLF cells depleted either with TRIP13 or SIN3A or both

HLF cells were harvested D3 post transfection for western blotting to deter for DNA damage. Immunoblotting was performed for TRIP13 and p- γ H2AX with VCP as a loading control.

As a summary to conclude what has been observed thus far, a reversal of growth arrest is seen in TRIP13-depleted cells upon concomitant knockdown of SIN3A. Interestingly, proliferation in these cells was apparently not impaired by an accumulation of DNA fragmentation as seen via an upregulation of p- γ H2AX unlike the corresponding growth arrest in TRIP13-depleted cells. In lieu of the above findings, it is unlikely that an accumulation of DNA damage could have accounted for the severe growth arrest in TRIP13-depleted cells. This proliferation impairment could have been caused by a deregulated oncogenic signalling pathway, in this case the c-MYC proto-oncogene, which when overexpressed was able to reverse the growth arrest in TRIP13-depleted HLF cells.

4 Discussions

4.1 TRIP13 as an oncogenic regulator of tumour growth

4.1.1 TRIP13 in cell cycle checkpoint and cancer

TRIP13 was first identified as a novel transcriptional co-regulator that binds to the Thyroid hormone receptor (TR), both in the presence or absence of Thyroid hormones (TH) [85]. Early studies of the conserved mammalian orthologue of Trip13 in budding yeast cell; *C-elegans* and *Drosophila* have discovered an essential role of this factor in regulating chromosomal events during meiosis and mitotic progression [25, 26]. Functional roles of Trip3 in meiotic recombination dates back to its activating roles in double strand-break (DSB) checkpoint responses and in establishing inter-homologous recombination (HR) during chromosome synapsis [27, 87]. Mammalian Trip13 was found to be involved in both the activation and silencing of the spindle assembly checkpoint (SAC) during mitotic progression [34].

Intriguingly, TRIP13 was observed to be upregulated in a variety of human cancers, ranging from breast cancer, squamous cell carcinoma of head and neck (SCCHN), prostate cancer, non-small cell lung cancer and leukaemia [28, 37, 43, 45, 84]. The oncogenic properties of TRIP13 were recently investigated in breast cancer and SCCHN, where the upregulated expression of TRIP13 stimulated growth and cell invasiveness of these tumour cells [45, 28]. Furthermore, the ability of treatment-resistant SCC cells to escape cell death was proposed to be due to the enhanced ability of such high-TRIP13 expressing cells in repairing DNA damage induced during chemotherapy [45]. Besides this aforementioned DNA-repairing role of TRIP13 in conferring surviving advantages to tumour cells during genotoxic assaults, the underlying molecular and cellular mechanisms of TRIP13 in mediating a pro-proliferative effect during tumourigenesis is largely unclear.

4 DISCUSSION

4.1.2 A proliferation-promoting role of TRIP13 in liver cancer

The present study is the first to have confirmed an oncogenic role of TRIP13 in hepatocellular carcinoma (HCC). Through various *in vivo* tumour xenograft models and established *in vitro* systems of HCC cell lines, we have established the following findings: Firstly, TRIP13 is essential during hepatocyte regeneration and HCC cell proliferation, without which, cell proliferation is impaired. Secondly, we identified novel interaction partners of TRIP13 via a MS screening, which has shed new light into the proliferative roles of TRIP13 in section 3.3. Thirdly, we demonstrated that the proliferation impairment during TRIP13-depletion was not attributable to an upregulation of the DNA-damage response (DDR) pathway in section 3.5. Lastly, we have data to suggest the mechanistic regulations, both upstream and downstream of TRIP13 in section 3.2, 3.3 and 3.5. Our findings confirm previous aforementioned publications regarding the oncogenic role TRIP13 whilst providing a functional annotation and unveiling the mechanistic involvements of TRIP13 during tumourigenesis.

We have previously shown that overexpressing Trip13 in a non-transformed liver cell line, AML12, stimulated cell proliferation in those cells (Fig. 3.16). Further along this line, an upregulation of oncogenic factors like C-MYC, EGFR was observed (Fig. 3.16). Interestingly, overexpressing TRIP13 in several human HCC cell lines did not produce this pro-proliferative effect as seen in AML12 cells. We speculate that these HCC cells could have been non-responsive to a further increase in TRIP13 levels, due to already high endogenous levels of TRIP13. Under this pre-text of a high TRIP13-driven proliferative growth in these HCC cells, simply increasing TRIP13 independently of other oncogenic factors would not further stimulate proliferation in these tumour cells. Conversely in AML12 cells, where the endogenous Trip13 levels are much lower compared to HCC cells, overexpressing Trip13 could stimulate proliferation via activation of growth-promoting pathways which is synonymous with what we have observed. It remains to be seen whether overexpressing TRIP13 in a HCC cell line with low endogenous levels of TRIP13 would similarly stimulate cell proliferation as in AML12 cells.

4.2 The functional implications of an interaction between TRIP13 and its interaction partner, SIN3A

4.2.1 Validating an interaction between TRIP13 and interaction partners

TRIP13 is a member of the highly conserved family of AAA⁺ATPases that are known to mediate diverse cellular activities. Through its ability to mediate protein-protein and protein-DNA complex assembly and disassembly, members from this ATPase family have been implicated in regulating diverse functions including cell signalling and cell cycling [24]. In order to investigate the mechanism through which TRIP13 exerts an oncogenic effect in liver cancer, we decided to perform a mass spectrometry screening to identify novel

4 DISCUSSION

interacting partners of TRIP13 (Fig. 1.10). Endogenous TRIP13 was immunoprecipitated from both HLF and Huh7 cells using TRIP13-specific antibodies. Based on KEGG pathway analysis, some of enriched pathways identified were cell cycle regulation, transcriptional co-regulation and DNA damage repair pathways.

TRIP13 could act as a transcriptional co-regulator in binding to TR as suggested by early studies [85] and from our own observations; TRIP13 seems to regulate the expression of EGFR. Based on these early hypotheses that TRIP13 might function as a transcriptional co-regulator, we decided to focus on 2 candidates that were enriched from the MS screen, SIN3A and SAP130. These proteins have been well characterized as transcriptional regulators in forming part of the histone deacetylase complex (HDAC) during transcriptional repression [48, 50].

We sought to independently perform co-IP to re-confirm a protein interaction between TRIP13 and its MS-identified interaction partners. Despite numerous attempts and optimizing Co-IP protocols, a pull down of Sin3A and SAP130 could not be captured from TRIP13-IP from HCC cells lines. There could be several biological and technical reasons as to why a co-IP did not work in here. One feasible biological theory could be that a transient interaction between TRIP13+SIN3A/ SAP130 could be taking place at a specific cell cycle phase for instance in the M –phase where assembly and disassembly of mitotic complexes have been known to mediate this tightly orchestrated process. In light of this hypothesis, by synchronizing cells in specific cell cycle phases, we might be able to capture this transient interaction between TRIP13+SIN3A/ SAP130. As an evidence to back up this theory, we have seen an enrichment of interactions between TRIP13 and SIN3A or SAP130 in the nucleus and in mitotic cells undergoing various phases in the M-phase during PLA (Fig. 3.8). At a higher magnification of the PLA images, these interaction signals seem to be localized around the chromosomes in mitotic cells. Using fluorescent immunocytochemistry, we have verified that TRIP13 is predominantly localized in the cytoplasm and around the perinuclear region, whilst SIN3A and SAP130 are strictly nucleus- bound (Fig. 3.7). Although we were not able to confirm a transcriptional co-regulatory function of TRIP13, our above findings seem to suggest a checkpoint-related function resulting from an interaction between TRIP13 and SIN3A/SAP130.

In one study looking at the recovery of renal epithelial cells following acute kidney injury, the authors showed that TRIP13 played a fundamental role in the recovery phase of these damaged cells by modulating p53 activity via its interaction with a p53 cofactor, Tetratricopeptide domain 5 (TTCP5) [88]. Under normal basal conditions, TTCP5 was predominantly in the nucleus whilst TRIP13 was mainly in the cytoplasm. Under sublethal dose of H₂O₂, TRIP13 was detected also in the nucleus via an importin α/β -independent pathway. Furthermore, an overexpression of TRIP13 with TTCP5 resulted in a redistribution of TRIP13 into the nucleus along with a decrease of p53 induction in the nucleus [88]. The shuttling of TRIP13 into the nucleus during an interaction with SIN3A/SAP130 might be in agreement with our PLA results in Fig. 3.8. It would be interesting to test whether there is indeed a shuttling of TRIP13 between the cytoplasm and nucleus in response to the following scenarios: an acute hepatic stress injury (eg. Partial Hepatectomy), chronic stress like the

4 DISCUSSION

administration of hepatotoxins (eg. Tetrachloride CCL₄, which does not induce genotoxic) or in response to an overexpression of interactions partners of SIN3A/SAP130.

4.2.2 Depleting of SIN3A reverses the growth impairment of TRIP13-depleted cells

TRIP13 expression is upregulated in several different kinds of cancers; however the functional annotations of its pro-proliferative roles are still unclear. The cancer related roles of SIN3A are similarly controversial due to its role as an oncogene in breast cancer whilst being separately reported to act as an antagonist against the proto-oncogene c-MYC [53-56]. We were curious to investigate the biological relevance of an interaction between TRIP13 and its interaction partners of SIN3A and SAP130 in the context of liver cancer. Much to our surprise, we observed a stark rescue in the proliferation defect of siTRIP13 KD cells when we concomitantly depleted SIN3A or SAP130 (Fig. 3.9). Due to the overlapping functions of SAP130 ascribed mainly via its binding to SIN3A, we decided to focus on SIN3A in order to reduce the complexities during further experiments. What was remarkable in these cells that were depleted of both TRIP13 and SIN3A was that the DNA damage marker, p- γ H2AX remained high (marginally less than TRIP13-KD cells), whilst these cells appeared phenotypically normal with almost no signs of DNA fragmentation when counter-stained with DAPI (Fig. 3.20). This was in stark contrast against the DNA-damage response consistently observed during TRIP13 depletion, not only in our context of liver cancer but also in other cellular systems for instance in head and neck cancer, breast cancer and during ischemia injury of the kidney [88, 45, 28].

In this scenario, we imagine an antagonistic interaction between TRIP13 and SIN3A on an unknown master regulator that plays a central role in signalling output. Under this regulator, cells are either committed for recovery or to progress towards cell death in response to severe DNA damage. A downregulation of growth promoting factors like c-MYC, EGFR and downstream targets of the mTOR-signalling pathway (Fig. 1.9; Fig. 3.10) in TRIP13-depleted cells was reversed when both TRIP13 and SIN3A were concomitantly depleted. The relevance of these pathways in accounting for the reversal of proliferation defect in double KD of TRIP13+SIN3A are being discussed in the next sections below.

Recently, fundamental questions regarding how TRIP13 recognizes and remodels its target-substrate/complexes has been unveiled in some studies. Through X-crystallography, it was demonstrated that the N-terminal domain (NTD) of TRIP13 is responsible for the binding of substrates or adaptors, for instance p31^{comet}, which acts together with TRIP13 in silencing the mitotic checkpoint complex (MCC) [63]. In head and neck cancer, the ATPase domain of TRIP13 has been demonstrated to be vital in conferring its oncogenic properties during tumour growth [45]. In lieu of these findings, it would be of interest to use site-directed mutagenesis to generate mutants in the NTD and/or ATPase domain of TRIP13 to probe for domain-interactions with SIN3A and downstream targets or pathways that would be altered. These results would be informative in providing more mechanistic basis for the interactions between TRIP13 and SIN3A and how this in turn translates to our observation of growth revival of HCC cells upon depletion of both factors.

4.3 Role of the oncogene c-Myc in liver cancer

The proto-oncogene c-MYC is a ubiquitous transcription factor that regulates important aspects of biological functions including cell cycle progression, DNA replication, cell proliferation, growth, differentiation and apoptosis [97-99]. c-MYC is frequently upregulated not only throughout the progression of liver carcinogenesis but recently also implicated with chronic liver disease like alcoholic liver diseases, viral hepatitis and liver fibrosis/cirrhosis [100]. Through the use of various experimental murine models of HCC including transgenic mouse models overexpressing c-MYC, this proto-oncogene has been demonstrated to be essential in HCC development [reviewed in 100]. Studies with c-MYC are of great clinical interest as high c-MYC levels along with p53 inactivation are an indicator for poor prognosis and early cancer recurrence in HCC patients [74,101].

4.3.1 Possible cross talk between TRIP13 and c-MYC signalling pathways?

Given the importance of c-MYC during liver regeneration and HCC tumourigenesis, we were intrigued by the possibility that c-MYC inactivation might account for the proliferative arrest and massive cell apoptosis upon TRIP13-depletion (Fig. 3.10). The decrease in c-MYC expression and its downstream target Cyclin D1 (CCND1) were consistently decreased in HLF and Huh7 cells upon TRIP13 KD. Interestingly, there was a partial restoration of the c-MYC levels, which coincided with the revival of cell proliferation when being depleted of both TRIP13 and SIN3A (Fig. 3.10).

In order to test for the relevance of the c-MYC oncogene in here, we overexpressed (OE) a full-length human c-MYC protein and observed a partial rescue of growth defect and decrease in cell death in TRIP13-depleted cells (Fig. 3.15). Given that TRIP13-depleted cells were arrested in G2 phase of cell cycle, it would be informative to study the cell cycle profile of these TRIP13 KD cells that are growth revived upon OE of c-MYC. These findings support the hypothesis that a deregulation of c-MYC and its target genes might have resulted in changes in important cellular outcomes in terms of cell viability and proliferation as seen in cells depleted of TRIP13 or SIN3A or both.

c-MYC has been described to be essential during hepatocyte regeneration after partial hepatectomy (PHX), it would be interesting to explore a possible interaction or cross talk between c-MYC and TRIP13 during proliferation under this context. As shown previously, TRIP13-depleted livers were significantly impaired during hepatocyte regeneration after PHX (Fig. 1.6). Further experiments to investigate if overexpressing c-MYC could rescue the regenerative defect of TRIP13-depleted livers after PHX will allow us to examine for a possible cross talk between TRIP13 and c-MYC. Concurrently, an overexpression of TRIP13 with or without the co-expression of c-MYC during PHX and in mice models for HCC would be definitely insightful to probe for this possible cross talk.

Due to the central role that c-MYC plays in regulating various aspects of cellular functions and in cancer, it is hardly surprising that an altered expression of this oncogene leads to deregulation of a large number of target genes that are consequently essential during

4 DISCUSSION

tumour growth. In order to look for novel Myc target genes during lymphomagenesis, Marinkovic, D.*et al* [89] used murine B and T lymphoma cells line that has been transformed with a conditional Myc-allele [89]. True indeed, the list of Myc target genes as identified via microarray analysis revealed essential functions ranging from cell proliferation, differentiation, signalling, metabolism, and protein synthesis to DNA repair [89]. Trip13 was found to be one of the 88 Myc-target genes in this list and was being categorized under the function of cell signalling [89]. We have separately verified from a “Champion ChIP transcription factor search portal” that TRIP13 contains 2 c-MYC binding sites (E-boxes sequences) in its 5’UTR promoter region. Recently in 2017, TRIP13 was identified to be an oncogenic factor in human chronic lymphocytic leukemia (CLL) [84]. The authors further proposed that c-MYC promotes TRIP13 expression by directly upregulating its transcriptional activities in CLL cells [84].

4.3.2 A possible TRIP13- c-MYC-SIN3A axis in HCC?

Coming back to our findings in the context of HCC, we do not exclude the possibility that the relationship between TRIP13 and c-MYC could indeed be acting bidirectional. In terms of transcriptional regulation, an overexpression of c-MYC commonly seen in liver tumours could well result in a transcriptional activation and upregulation of TRIP13 in tumour cells. On the other hand, the depletion of c-MYC consistently seen in TRIP13-depleted HCC cells suggests that TRIP13 could similarly act in a feed-forward loop in here to maintain c-MYC expression in oncogenic cells. In addition to the above, there exist also the possibilities that the relationship/interaction between TRIP13 and c-MYC is mediated indirectly via other interacting factors or complex assembly. It is well appreciated that Myc possess a large interactome, where Myc can be recruited through protein-protein interactions to the promoters of specific gene targets [90] whilst the recruitment of different effectors has been shown to affect the protein stability of Myc itself [90, 91]. Chromatin-immunoprecipitation (ChIP) and dual luciferase reporter assays should be performed in order to test for this possible transcriptional regulatory relation between TRIP13 and c-MYC.

SIN3A has been originally identified to be a co-repressor, associated to Myc-antagonist of Mad-Max heterodimer in inhibiting Myc target activities [53-55]. The recruitment of the Sin3A/HDAC complex was shown to directly antagonize c-Myc activity via deacetylation and destabilization of the c-Myc protein [54, 92]. In light of we have observed, where there is a partial restoration of c-MYC and cell proliferation of TRIP13-depleted cells upon simultaneous deletion of SIN3A, it seems plausible that TRIP13 and SIN3A exert opposing effects on c-MYC activity. SIN3A depletion alone results in no observable decrease in cell proliferation or c-MYC levels, suggesting that the ability of SIN3A to exert its destabilizing effects on c-MYC depends on the absence of TRIP13. In this model, we speculate that the interaction between TRIP13-SIN3A prevents SIN3A from complex formation with HDAC associated co-factors and subsequent deacetylation and degradation of c-MYC. TRIP13 depletion releases SIN3A to exert its repressive effects on c-MYC, resulting in inhibition of c-MYC activities like cell growth, proliferation and

4 DISCUSSION

expression of growth related factors like EGFR and Cyclin D1. Further studies to investigate whether an overexpression of SIN3A in the presence/absence of TRIP13 would affect the de-acetylation levels and stability of c-MYC; along with promoter assay of c-MYC or c-MYC target genes would be necessary to reveal this functional relevance of a cross talk between TRIP13-SIN3A and c-MYC. Alternatively, overexpressing a c-MYC mutant (expressing a mimic of constitutive-acetylation for instance by replacing lysine with glutamine) would also allow us to test the functional relationship between TRIP13 and SIN3A and the consequent effects on c-MYC activities.

4.4 The relevance of EGFR signalling pathway during liver homeostasis and tumourigenesis

Several loss of function studies have highlighted the important role of EGFR during liver regeneration after partial hepatectomy (PHX). In these studies using mice with hepatocyte-specific knockout or expression of a dominant negative mutant version of EGFR, an impairment of hepatocyte proliferation upon acute liver injury or after PHX were consistently reported [93, 94, 95]. In human HCC, overexpression of EGFR occurs in more than 68% of patients being detected with aggressive tumours, metastasis, and poor clinical outcomes [102-104].

We first observed a remarkable decrease in EGF receptor and receptor activation (EGF stimulation) across all HCC cells lines being investigated during TRIP13 depletion (Fig. 3.3). Concomitantly, a decrease in activation/phosphorylation of key factors along the mTOR-signalling pathway with the likes of S6K, eIF4B, 4E-BP1, cyclin D1 was seen. EGFR dual luciferase reporter assay further suggested that EGFR expressions could have been regulated by TRIP13 (Fig. 3.4). The preliminary conclusion that we first drawn were that the decrease in EGF-mTOR signalling could have been responsible for the proliferation defect seen during TRIP13-depletion. To investigate this, we decided to first test for the functional relevance of EGFR in HCC cells. Much to our dismay, a siRNA-mediated depletion of EGFR resulted only in a minor proliferation defect in HCC cells (Fig. 3.5). These minimal effects question the hypothesis that the EGFR signalling pathway plays a central role in regulating cell proliferation under our framework with TRIP13. Further pointing us away from this direction was the fact that EGFR expression was not upregulated in an expression array from a cohort of HCC patients in Heidelberg (Fig. 3.6). The overexpression of TRIP13 was nonetheless detected across all samples from CLD and HCC patients where we then saw a negative correlation between TRIP13 and EGFR expression (Fig. 3.6).

EGFR inhibitors such as gefitinib, erlotinib or lapatinib, which also inhibits ErbB2, have been successful in the treatment of HCC in animal models and in other human tumours such as non-small cell lung carcinoma. Surprisingly, the use of EGFR inhibitors has shown only limited success in HCC patients during clinical trials [105, 106, 107]. Furthermore, it was shown that EGFR plays distinct roles in hepatocytes vs Kupffer cells during HCC development [94]. A hepatocyte specific depletion of EGFR was shown to promote tumour growth whereas a deletion of EGFR in the kupffer/macrophages in the liver reduced HCC

4 DISCUSSION

growth in mice [94]. Interestingly, the authors further propose that EGFR positive macrophages (in the tumours) and not EGFR positive HCC cells provided prognostic values for overall survival in patients [94].

In light of the above findings, it might not come as a surprise that we observed minimal effects on HCC cell proliferation upon depletion of EGFR alone. Many other growth factors or their receptors are similarly deregulated in HCC and could directly or indirectly influence EGFR signaling. A compensatory increase in hepatic growth factor/c-MET signaling has been demonstrated during EGFR inhibition, possibly to compensate for the impaired hepatocyte proliferation [95]. It seems that simultaneous targeting of several growth factor pathways was necessary in here in order to exclude possibilities of functional redundancies amongst signals involved during hepatocyte regeneration and carcinogenesis. In order to further verify the relevancy of EGFR signaling in our context, it would be notable to molecularly dissect and characterize the various HCC cell lines (the different oncogene gene mutations, EMT status etc.) before deciding on the appropriate combinations of receptor tyrosine kinases (RTK) inhibiting-strategies to study during hepatocarcinogenesis.

As we do not have evidence to prove a direct interaction or promoter binding between TRIP13 and EGFR, the decrease in EGFR levels upon TRIP13 depletion could well have been secondary effects on gene expression upon DNA damage checkpoint inductions. It has been well described that changes in global gene expression in response to checkpoint inductions may derive either directly from gene transcriptional regulation or indirectly due to effects secondary from cell synchronization (resulting from growth arrest) [111-113]. In this case, it would be important to distinguish whether TRIP13 indeed exerts a direct effect on EGFR levels or these are simply unspecific changes secondary to growth arrest.

4.5 The role of TRIP13 in DNA damage repair pathway and the implications in liver diseases and tumourigenesis

4.5.1 YAP as a regulator of TRIP13 in CIN signatures

Chromosomal instability (CIN) represents a persistent hallmark of human solid tumours [37, 38]. Genetic alterations and genomic instability have long been recognised as a common feature between human chronic liver disease (CLD) and liver cancer [41, 66]. It was not until recently in 2017 that the molecular mechanisms linking this progression from increased hepatocyte regeneration (in CLD) to eventual liver tumourigenesis has been revealed [20, 39]. The authors proposed that Caspase 8 mechanistically links the increase of hepatocyte apoptosis during compensatory proliferation in CLD to later HCC development [20]. In the second study, the authors reported that a collective gene signature, termed the CIN25, stratified HCC patients with poor survival and early cancer recurrence [39]. The YAP protein, which forms part of the Hippo signalling pathway was found to be essential in regulating the expression of this CIN25 signature in HCC.

4 DISCUSSION

As introduced in section 2.2, TRIP13 was identified as one of the top 25 ranked CIN signature genes (CIN25) along with FOXM1 and MAD2L1, which were induced by an overexpression of YAP in liver tumour cells [39]. Indeed, we have seen a corresponding decrease in TRIP13 and EGFR levels upon YAP depletion in HCC cells (Fig. 3.18) It is feasible that the YAP/FOXM1 is regulating downstream target genes including TRIP13 in accounting for chromosomal instability seen in HCC patients displaying CIN25 signatures [39].

4.5.2 TRIP13 in DNA damage and repair pathway

In SCCHN, high expression of TRIP13 was shown to be the main mechanism through which chemoresistance develops as these tumour cells have an enhanced ability to repair DNA damages acquired during the genotoxic assaults [45].

Our observations are in line with what has been reported of TRIP13 as a regulator during DNA damage repair [45, 88]. Firstly, we noted a remarkable upregulation and an essential role of Trip13 during hepatocyte regeneration post PH. Secondly; TRIP13 depletion resulted in severe proliferation defect and DNA damage in HCC cells. The plausible relevance of Trip13 under this chronic cycle of inflammation-necrosis-regeneration was further demonstrated by its upregulation in mouse and human CLD and across all etiologies of human HCC from our data. What these previous papers [45, 88] did not address however was the oncogenic pro-proliferative aspect that TRIP13 exerts. Besides indirectly recapitulating the regulatory role of TRIP13 during DNA repair in CLD and HCC, we have observations that suggest a DNA repair-independent role of TRIP13 during cell proliferation. A decrease in c-MYC along with growth promoting factors like EGFR and Cyclin D1 suggest that TRIP13 could be directly or indirectly involved in signalling pathways that determine cell proliferation. Furthermore, there was no rescue of proliferation defect in TRIP13-depleted cells when the major DNA damage response (DDR) and DNA repair pathway mediated by ATM was blocked in Fig. 3.19D. In the same direction, a remarkable reversal of proliferation defect in TRIP13-depleted cells upon concomitantly depleting SIN3A was observed, albeit the persistence in high levels of DNA damage markers of p- γ H2AX and cleaved-PARP (lower level than TRIP13KD alone).

On a separate note as mentioned in section 4.4, we discussed the possibility of changes in gene expression, which could be mediated directly via transcriptional regulation or indirectly due to checkpoint activation in response to DNA damages [111-113]. Performing global transcriptome profiling on HCC cells arrested in different cell cycle phases would be necessary to distinguish whether the changes in gene expression of c-Myc, EGFR, etc. that has been observed upon TRIP13 depletion are indeed specific effects or secondary effects to growth arrest in specific cell cycle phase (for instance in G2).

Nonetheless, our current findings suggest that the increase in DNA damage during TRIP13 depletion alone was not sufficient to explain the severe proliferation impairment in HCC cells. It is likely that a continuous activation of signalling cascades associating with cell

4 DISCUSSION

proliferation and survival is pivotal during tumourigenesis, where the reversal of malignant phenotypes occurs when these central pathways are targeted.

In this scenario, we imagine a possible cross talk between c-MYC, p53 and TRIP13. A high expression of TRIP13 and c-MYC commonly observed in human cancer increases cell proliferation by accelerating mitotic progression, leading to increased frequencies of mutations, replication errors and subsequent genomic instability in these cells [114]. Most cells entering cell cycle with DNA damage are expected to die due to arrest responses orchestrated by p53. Interestingly, TRIP13 was shown as an antagonist against p53-induced cell death activities during the recovery phase of damaged renal epithelial cells [88]. Upregulated expressions of c-MYC coupled with inactivation of p53 are indicators for poor prognosis and early cancer recurrence in HCC patients [74,101]. In this instance, a random mutational inactivation of p53 or an antagonist against p53 (for instance TRIP13) might just create a highly tolerable environment whereby cells overexpressing c-MYC and TRIP13 can both drive mitotic progression and cell proliferation in spite of gross chromosomal abnormalities.

4.6 Concluding remarks and outlook

A role of TRIP13 during liver regeneration and liver cancer has not been previously described and would serve as an interesting basis to further understand the link btw CLD and subsequent HCC development. This brings us to the next question as to why an upregulation of TRIP13 during CLD and HCC seems essential under this hyper-proliferative state. From a functional point of view, the induced expression of TRIP13 might be a compensatory mechanism acquired by the cells in an attempt to maintain genomic stability by repairing DNA damages from an aftermath of rapid proliferation. As shown in head and neck cancer, TRIP13 preferentially adopts a non-homologous end-joining (NHEJ) pathway during DNA repair, which is a form of repair requiring less DNA fidelity (no DNA template required) and results in frequent DNA mismatches [45]. Together with the proliferation-promoting oncogenic role of TRIP13, which has been illustrated throughout our findings, these two TRIP13-dependent roles could set the fertile ground for eventual cellular transformation to occur in hepatocarcinogenesis and other cancers.

The interesting observation from SIN3A, identified as a TRIP13-interaction partner, when concomitantly depleted reverses the proliferation defect in TRIP13-depleted cells is exciting as it reveals a potential aspect of regulation between HDAC co-factors and oncogenes. These finding needs to be further validated in *in vivo* settings during HCC tumourigenesis in order to accurately reflect the functional relevance of an interaction between TRIP13 and SIN3A. It would be interesting to observe whether these proliferation rescued cells (TRIP13+SIN3A depleted) are still able to sustain cell proliferation in spite of an accumulation of massive DNA damage or whether these DNA damages could be eventually resolved over time.

4 DISCUSSION

To further probe for a novel cross talk between TRIP13 and c-MYC, it would be critical to first determine whether this cross talk occurs on a transcriptional level or post-transcriptionally. A dual luciferase reporter assay couple with ChIP and protein stability/half life test would be one of the few ways to test this out. Once this mechanistic interaction has been figured out, it would be noteworthy to bring this further onto *in vivo* studies. A plethora of studies have been conducted using various transgenic mice models overexpressing c-MYC to study HCC. A mice model with an inducible-overexpression of c-MYC specifically in hepatocytes [108, 109] would be extremely valuable to enable us to test this hypothesis of a signalling/interaction axis of TRIP13-c-MYC-SIN3A. In an orthotopic HCC implantation study, the ability of c-MYC overexpression to reverse the proliferation impairment of TRIP13-depleted HCC cells could be examined both spatially and temporally.

Given that TRIP13 forms part of the CIN25 signature during HCC, it would serve as a good biomarker during early screening of patients especially those from a high-risk group (with cirrhosis or present with a history of CLD background) as a preventive measure against HCC.

Furthermore, the expression of TRIP13 along with a predefined set of biomarkers for instance the CIN25 signatures, c-MYC; p-53, etc. might serve to better stratify patients for treatment options and prognostic outcomes. c-MYC currently represents an undruggable target as transcription factors do not harbour enzymatic activities or domains that could be pharmacologically targeted with small molecule inhibitors. TRIP13 might represent an alternative druggable target in here to disrupt cross talks with c-MYC or to deplete c-MYC levels, resulting in loss of function of relevant downstream target genes. A potent and selective small molecule inhibitor against p97, a member of the AAA⁺-ATPase family has been recently demonstrated to display antitumour activities across a broad range of solid tumour models [110]. TRIP13, being a member of the same family could similarly represent a novel and unique druggable target for HCC and other cancer entities.

5 Material and Methods

5.1 Methods

5.1.1 Cell culture

5.1.2 Cell lines

Human hepatocellular carcinoma (HCC) cell lines of HLF, Huh7, HepG2 and Mouse HCC cell lines of Hepa1-6 were used. A non-transformed Mouse liver cell line of AML12 was used to test for oncogenic properties of Trip13. The cell line identities have been separately verified to ensure that no cross contaminations between different cell lines have occurred. HLF cells were a kind gift from Dr. Iryna Ikavets; Huh7, HepG2 and AML12 were obtained from ATCC.

5.1.2 Cultivation of cells

All cells were cultured in 10 cm-plates in 10 ml of high-glucose DMEM supplemented with 10% heat-inactivated FBS and 1% of penicillin/streptomycin all from Gibco in a humidified incubator at 37°C with 5% CO₂. For normal cell line maintenance, fresh media was given to cells 2 times per week and cells were subcultured once per week when cell confluency reaches between 80%-90%.

For subculturing, cells were first washed with 5 ml of DPBS (Gibco) to remove residual culture media and serum before being detached from the cell culture plate using 1 ml of 0,05% Trypsin (Gibco) between 3-5 mins incubation in the 37°C incubator. The trypsinization step was stop by resuspending cells in 10 ml of full DMEM media + FBS. The resuspended cells were centrifuged for 3 mins at 500 x g, resuspended in 10 ml of fresh culture media and 1 ml of this cell suspension was reseeded into a 10 cm dish. Cell morphology was assessed in an inverted light microscope (Olympus).

To seed cells into different cell culture dish formats for experiments, 10 µl of cell suspension was taken from the last step of the cell resuspension and mixed with 10 µl of trypan blue solution. Cells were then counted manually using either a Neubauer cell counting chamber or using the Countess™ automated cell counter. The cell concentrations were determined and the appropriate numbers of cells were seeded according to the surface area of the dishes and the purpose of the experiments.

5.1.3 Freezing and thawing of cells

Cells were trypsinized as described in the section above. After cells were counted and cell concentrations were determined, cell densities were adjusted to 2×10^6 cells /ml by dilution with an appropriate volume of cell media. Thereafter, a freezing media mixture consisting of a final concentration of 40% FBS, 10% DMSO and 50% full DMEM media containing 1×10^6 cells were aliquot in a volume of 1 ml into cryogenic vials. These vials were then put into a Mr Frosty™ freezing container (ThermoFischer Scientific) overnight in -80°C to allow cells to gradually cool down to freezing temperatures.

5 MATERIAL & METHODS

The following day, one cryovial of cells were taken out from -80°C to be thawed to test for cell viability after freezing before this batch of frozen cells are transferred to the liquid nitrogen tanks. During this cell thawing process, one frozen cryovial is thawed in the 37°C water bath for 1-2 minutes before being transferred into a falcon tube containing 9 ml of full DMEM media. The cell suspension is centrifuged for 3 mins at 500 xg to remove the DMSO freezing media before being resuspended in 10 ml of full DMEM media for plating in a 10 cm dish.

5.1.4 siRNA and plasmid transfections

An overview of all the plasmids and Target-on pooled siRNA oligos (Dharmafect) used throughout the thesis is outlined in the material section. One day prior to cell transfection at D0, cells were trypsinized and seeded into either 6-well or 12-well plates as described in 5.1.2. Cells were resuspended and plated in antibiotic-free full DMEM media to reach a confluence of 60-70% the next day for transfection.

Target-ON plus siRNAs (Dharmafect) ordered in the format of lyophilized salt are reconstituted using 1x siRNA buffer (Dharmafect) into a stock concentration of $50\mu\text{M}$. The siRNA oligo tubes were spin briefly before being resuspended in an appropriate volume of buffer, placed on a shaker at 300rpm for 30 mins at RT before being aliquoted into 10 μl volumes for long term storage in -20°C or -80°C .

siRNAs were then further diluted in 1x siRNA buffers into working stocks of $5\mu\text{M}$ before being used at a final concentration of 25nM during transfections. During double siRNA transfections, the final amount of siRNAs used was titrated with the NTC siRNA to ensure that all groups received an equal amount of siRNAs. The set up of a transfection reagent mix using siRNAs is shown for a 12-well culture dish in table 1 , which was similarly applied to a 6-well culture dish by multiplying every volume by a ratio of 2. Components in tube A and B were assembled separately and incubated for 5 mins at RT. The two tubes were then combined and incubated at RT for 20 mins before being added drop wise to the culture media. For every transfection set up, one well of cells would be transfected with a NTC siRNA that has been coupled with a GFP tag to assess for RNAi transfection efficiency in this particular experiment. After an incubation of at least 7 hours at 37°C , the transfection reagent was removed from the cells and replaced with fresh antibiotic-free full DMEM media for overnight incubation. Cells were either trypsinized the next day and reseeded in 96-well plates for cell-based assays or further cultured for 72 hours for RNA and protein extractions

Transfections with plasmids were performed following the same set up as shown in the below table, except where plasmids are used in a final amount of 500ng and lipofectamine 2000 (Invitrogen) was used instead of RNAi max (Invitrogen) reagent. As a control for DNA transfection efficiency, one well of cells was transfected with an enhanced-GFP empty plasmid vector.

Table 1: Set up of siRNA transfection reagents for cells seeded in a 12 –well dish

	Tube A		Tube B	
Reagents	siRNA (5 μ M)	Opti-MEM	RNAi max reagent	Opti-MEM
1 x	5 μ l	95 μ l	4 μ l	96 μ l

5.2 Cell-based assays

5.2.1 Cell counting kit-8 (CCK8)

Cell numbers and cell viability was assessed using a CCK8 reagent from Sigma-Aldrich. This is a highly sensitive enzyme-based colorimetric assay, which makes use of water-soluble tetrazolium salts called WST-8 to assesses cell viability during proliferation and cytotoxicity assays. WST-8 is bio-reduced into an orange-coloured formazan dye by cellular dehydrogenases; therefore the amount of formazan produced is directly proportional to the number of viable cells.

During the initial optimization of assay conditions for using the CCK8, a serial cell dilution process was performed and it was determined that 5000 cells/well during seeding was the optimum cell seeding number for all HCC cell lines over a course of 4 days of growth assay. Due to the slower growth rate of AML12 cells, 8000 cells to be seeded per well was necessary in order to achieve a good correlation between absorption readings and viable cell numbers. One day after transfection, cells were trypsinized and 5000 cells in 100 μ l volumes/well were seeded into 96-wells for different cell-based assays. At least 4 repeats were seeded per experimental conditions and cells were pre-incubated overnight to regain cell viability prior to the CCK8 assay the next day. 10 μ l of CCK8 was added to each 96-well (cells incubated in 100 μ l of cell media) and incubated for colour development at 37°C with 5% CO₂. HLF, Huh7 and Hepa1-6 cells were incubated for 2.5 hours whilst AML12 and HepG2 were incubated for 3 hours for colour development before the readings for absorbance were taken at 450nm.

Due to the low cytotoxicity of the CCK8 reagent, the same cell wells can be used repeatedly for cell proliferation measurements over the entire course of the experiment. The existing CCK8 reagents are removed from the wells, washed once in 1x PBS before 100 μ l of fresh cell media is added to each well for repeated cell number measurements over the next days.

5.2.2 BrdU cell proliferation assay

Cell proliferation was measured using the BrdU cell proliferation ELISA kit from cell signalling. This assay kit detects the amount of the base analog, 5-bromo-2'-deoxyuridine (BrdU) that is being incorporated into the cellular DNA during cell proliferation by using an anti-BrdU antibody, therefore providing a direct indication of cell proliferation.

5 MATERIAL & METHODS

At D3 post transfection, the BrdU labelling reagent from the kit is added at a dilution of 1:1000 (10 μ M) to cells previously seeded in 96-well plates and cells are returned to the incubator for 4 hours at 37°C with 5% CO₂. After removing the BrdU labelling medium, the cells are fixed and DNA denatured at 30 mins RT using 100 μ l/well of the fixing/denaturing solution as provided. The Mouse BrdU detection antibody is then diluted 1:100 in the antibody diluent provided and 100 μ l/well is added and incubated for 1 hr at RT. The cells were then washed 3 times with 1x of wash buffer as provided before being incubated for 30 mins at RT with the anti-Mouse HRP conjugated Mouse antibody (diluted 1:100 in antibody diluent). Finally, cells were washed for 3 times with 1x wash buffer and 100 μ l/well of HRP substrate TMB is then added for colour development for 30mins at RT in the dark. The colour development is stop by adding 100 μ l/well of STOP solution. The absorbance is read at 450 nm where the magnitude of the absorbance provides a direct indication of cell proliferation in each well.

5.2.3 Apoptosis detection assay

The Apo-ONE[®] Homogeneous Caspase-3/7 Assay from Promega was used to measure the amount of active caspase-3/7 present in cells being subjected to different experimental treatments. This assay includes a profluorescent caspase-3/7 consensus substrate, Z-DEVD-R110, which upon cleavage of the C-terminal Aspartate residue of this peptide sequence by caspase-3/7 produces a fluorescent product that is indicative of the active caspase levels in the sample.

The Apo-ONE[®] Caspase-3/7 reagent was prepared by diluting the provided substrate 1:100 with the buffer to obtain a volume of 50 μ l/well in a 96-well plate. To obtain a 1:1 ratio of substrate reagent to sample volume, 50 μ l of the culture medium was removed from each 96-well cell culture sample. 50 μ l of the prepared Caspase-3/7 reagent was then added to each well containing 50 μ l of cells in culture and cells were lysed and homogenized on a shaker at 400 rpm for 15 mins. The samples were then further incubated for 4 hrs at RT in the dark to allow for the Caspase 3/7-enzymatic reaction to proceed. Once the incubation period was over, the Caspase 3/7 activities from each well were measured at a fluorescence excitation wavelength of 495nm and emission wavelength of 525nm. The results from the assays were plotted as relative fluorescence units (RFU) to indicate the activity levels of caspase3/7 in that sample condition.

5.2.4 Immunohistochemistry (IHC) fluorescence staining

Intracellular localization of different protein targets was verified using the IHC fluorescence staining protocol as outlined below. HLF, Huh7 and HepG2 cells were first trypsinized and seeded at a density of 2×10^4 cells/well in a 8-chamber Labtech Microscopy Slide and incubated overnight at 37°C with 5% CO₂. The following day, cell medium was removed and cells were washed once with cold PBS before being fixed with 4% formaldehyde/PBS for 10 mins at RT. Cells were then permeabilized with 4% formaldehyde/0,1% Triton-X in PBS for 5 mins on ice. Thereafter, cells were washed 4 times for 2 mins each in PBS before being blocked in 5% BSA/10% FBS/PBS for 1 hr, shaking at RT. After the blocking step, primary

5 MATERIAL & METHODS

antibodies that have been diluted in blocking solution are added to cells and incubated in a humidity chamber overnight at 4°C. 200 µl/well of reagents were used for every step except when 100 µl/well was used during the primary antibody incubation step. The next day, the primary antibodies were removed and cells were washed 3 times with PBS for 5 mins each. The corresponding secondary antibodies coupled with either Alexa-Fluor® 488 or 555 were added to cells for 1 hr at RT protected from light. Finally, cells were washed thrice for 5 mins with PBS before being mounted in DAPI-VectaSheid with microscope coverslip and the edges of the slides are then sealed with nail vanish. Microscopic slides were store at 4°C in the dark before being imaged using the Olympus confocal microscope FV1000 under the GFP, FITC and DAPI channel. Cells were imaged at a thickness of 5 µM either with a 20x air or a 40x oil-immersion objective. Using the Olympus fluoview software, the maximum projection Z-stacks were merged thereafter for image analyse.

5.2.5 *In situ* Proximity ligation assay (PLA)

Duolink™ *in situ* reagents from Sigma Aldrich was used in order to perform the *in situ* PLA to verify for intracellular interactions between TRIP13 and its MS-identified interaction targets of SIN3A and SAP130 in fixed HCC cell culture samples. The interaction between 2 proteins is detected using 2 corresponding antibodies raised in different species. Species-specific secondary antibodies (species-specific PLA probes that are conjugated with a unique short sequence of DNA) then bind to the primary antibodies. When the two (plus and minus) PLA probes are in close proximity (< 40nm), these DNA strands can interact through a subsequent addition of 2 circle-forming DNA oligonucleotides. A fluorescent signal is then generated during the incorporation of fluorophore-labelled complementary oligonucleotide probes during further amplifications of the DNA circle. Therefore each fluorescent spot represents a single interaction that can be quantified and assigned to a specific cellular localization during confocal imaging.

A brief outline of the PLA protocol optimized for HLF/HUH7 is as follows:

1. Seeding and processing of cells in chamber slides

The process from seeding of cells into chamber slides (8-well) overnight; fixing, permeabilizing and blocking for 1 hr at RT are exactly as what was performed during immunofluorescence staining in section 5.2.4.

2. Adding Primary antibodies for use in PLA

These antibodies for use in PLA must be raised in different species. For this reason the following combinations of antibodies were used: TRIP13 (Rabbit)+SIN3A (goat); TRIP13(R)+SAP130 (G) and SIN3A(R)+SAP130 (G) to detect for interactions between these proteins under investigations. IgG from the same isotypes and antibodies from the same species were used for negative controls. TRIP13 was diluted 1:100, Sin3A 1:50 and SAP130 1:100 in blocking solution. 50 µl of antibodies diluted in blocking solution was added to each of these chamber wells and the wells were sealed with a parafilm before being incubated overnight at 4°C in a humidity chamber.

5 MATERIAL & METHODS

3. Adding PLA plus and minus probes

All washes are done at RT with gentle shaking unless otherwise specified. The next day, the primary antibodies were removed and cells were washed for 3 x 5 mins in PBS. Rabbit PLA plus and Goat PLA minus probes are used in here. The two PLA probes are diluted 1:500 in the PLA diluent as provided, added at a volume of 50 µl per well and incubated for 1 hr at 37°C in a humidity chamber.

4. The chamber gaskets that are separating the wells from each other in the chamber slides can now be removed. A PAP pen is used to mark around each cell-well area and all subsequent washes are done in Coplin jars. Slides are then washed 2 x 5 mins in PBS to remove the residual PLA probes.

5. **Ligation step** (For ligase to add DNA nucleotides to the two PLA probes that will join into a circle if these pairs are in close proximity)

The ligation stock is diluted 1:5 in water to make the ligation solution. Ligase provided is diluted 1:40 in this solution and added at 40 µl/well and incubated for 30 mins at 37°C for the ligation process to take place.

6. Rolling circle DNA amplification

The ligation mix is removed and slides were washed 2 x 5 mins in PBS. The amplification stock was diluted 1:5 in water and DNA polymerase was diluted 1:80 in this solution. 40 µl /well of this amplification mix was added and incubated for 100 mins at 37°C.

7. Final washing and mounting of slides

The amplification mix was tapped off and slides were washed 2 x 5 mins again in PBS before being air dried in the dark for 2-3 mins. Slides were mounted with a coverslip using DAPI vectashield and stored at -20°C until imaging.

8. Detection of red fluorescent amplification signals

Confocal imaging to detect for amplification signals were performed using at least 20x magnification objective and using the FITC filter. DNA were stained with DAPI and imaged under the ultraviolet excitation/emission filter.

5.2.6 Dual luminescence assay

The GLuc-ONTM human EGFR promoter reporter construct (EGFR-HRP pEZX-G04) from Genecopoeia was used in experiments to detect for changes in EGFR promoter activities. This dual reporter system uses the secreted Gaussia luciferase (GLuc) as the promoter reporter and the secreted alkaline phosphatase (SEAP) as an internal control to enable transfection normalization across samples. GLuc and SEAP are both secreted into the cell media and can be detected by the secrete-pairTM dual luminescence assay kit without cell lysis. This EGFR HRP dual-reporter vector is co-transfected with siRNAs in HCC cells using lipofectamine 2000 following transfection protocols in section 5.1.2. Cell culture media were collected at 48 hrs and 72 hrs after transfection and stored in -20°C before samples were analysed. A 1x assay working solution was constituted with the GLuc substrate, coelenterazine, as provided. The assay was set up in a 96-well all-round white opaque plate. 4 repeats (10 µl) was pipetted from each experimental condition and 100 µl of the 1x working assay solution was added and luminescence reading was taken within the first 5 mins of the

5 MATERIAL & METHODS

reaction with the bioluminescent filter of the plate reader. The results are subsequently plotted as relative light units (RLU).

5.3 Virus work

5.3.1 Lentivirus shRNA vector constructs

A set of Lentiviral pLKO.1 vectors containing 4 unique 29-mer shRNA constructs against human SIN3A was purchased from Origene in the form of dried plasmids (TL301698). The scrambled negative control (TR30021) shRNA cassette in the same pLKO.1 plasmid backbone was obtained from Origene. These dried plasmids were subsequently reconstituted with H₂O into a final concentration of 100 µg/µl and transformed into DH5α bacterial cells for plasmid amplification. Lentiviral packaging vectors of psPAX2 (Cat. No. 12259) and pMDG.2 (Cat. No. 12260) were available in the lab plasmid database that were originally obtained from Addgene with the catalogue numbers as stated.

5.3.2 shRNA transfections to pre-select constructs with a good Knockdown

HEK293T cells were seeded into 6-well plates at $2,5 \times 10^6$ cells/well. The next day, transfections with the four different SIN3A specific shRNA constructs were performed using lipofectamine 2000 following the transfection protocol in section 5.1.4. At D3-post transfection, protein lysates were harvested from cells and immunoblotted to select 2 of the shRNA constructs that gave the best SIN3A knockdown. These shRNA plasmid constructs were used for subsequent lentivirus production. Prior to lentivirus production, these 2 selected shRNA constructs were subcloned into another pLKO.1 plasmid vector backbone containing Blastocidin resistance also from Origene (TL30032), details are in the molecular cloning in section 5.7.

5.3.3 Lentivirus production

HEK293T cells were seeded into 10 cm plate at an amount of 3.8×10^6 cells/plate. The following day, the selected PLKO.1 vectors and packaging plasmids were transfected into cells in the following way:

9 µg of pLKO.1 vector, 9 µg of psPAX2 and 0,9 µg of pMD2.g were diluted into 800 µl of Opti-Mem in a 1,5 ml tube for each 10 cm plate. In the second tube, 15 µl of lipofectamine 2000 was diluted into 800 µl of Opti-Mem. These 2 tubes were separately incubated for 5 mins at RT before being mixed and further incubated for 25 mins. The plasmid-lipofectamine mixture (1600 µl) was then added dropwise to the cells. The next day, fresh media containing BSA was given to the cells (Full DMEM+ 10% FBS+ 1.1% BSA) and further incubated at 37°C in the incubator. 48 hrs after transfection, the cell media (containing packaged viruses) was harvested. Media was first centrifuged at 1250 rpm for 5 mins and passed through a 0,45 µM filter fitted syringe to remove cell debris before being stored at -80°C. Fresh media containing BSA was again given to cells to repeat for media harvesting the following day

5 MATERIAL & METHODS

following the exact protocol. Virus supernatant from 48 hrs and 72 hrs post virus packaging are pooled and virus titer of supernatant was determined via qPCR to quantify for expression of HIV p24 antigen.

5.3.4 Lentivirus titer calculations

ABM's Lentiviral qPCR Titer Kit (LV900) was used to determine the virus titer from cell supernatant collected from above. 2 µl of the cell supernatant was lysed with 18 µl of the virus lysis buffer as provided and incubated for 3 mins at RT. The C_t value of this viral lysate is used for subsequent calculations to determine the viral titer of the supernatant. A single step RT-qPCR reactions are set up in triplicates as follow: 12,5 µl of 2X SYBR green qPCR mastermix and 10 µl of reagent-mix are added to 2,5 µl of viral lysate. The qPCR reactions for the lentivirus standard 1 (STD1) and lentivirus standard 2 (STD2) are set up in the same way by adding 2,5 µl of STD1 or STD2 instead of the viral lysate. The reagent mix provided by the kit already contains primers and reagents for reverse transcription of the RNA template. The RT-qPCR program is set up like a usual PCR program with the exception of an additional RT step at the start. The reactions were ran in the (Thermo Fisher) QuantStudio 6 Flex Real time PCR system using this program: reverse transcription for 20 mins at 42°C; enzyme inactivation for 10 mins at 95°C; 30 cycles of template denaturation for 15s at 95°C and primer annealing/extension step for 1 min at 60°C. The virus titer (IU/ml) was calculated using this formula:

$$\text{Titer of viral lysate} = 5 \times 10^7 / 2^{3(C_{tx}-C_{t1})/(C_{t2}-C_{t1})}$$

C_{tx} = Average of 3 C_t values of the unknown viral lysate

C_{t1} = Average of 3 C_t values of STD1

C_{t2} = Average of 3 C_t values of STD2

5.3.5 Lentivirus transduction and establishing stable cell lines

HLF cells were seeded at 2×10^5 cells/well in a 6-well plate with antibiotics-free full DMEM media. The next day, 1 ml of fresh antibiotic free media with 8 µg/ml of polybrene was given to each well. 1 ml of opti-MEM with 8 µg/ml polybrene plus lentivirus was added at an MOI of 5 -20. The next day, cells were given fresh antibiotics-free media and further incubated. After 3-4 days post virus transduction, cells are trypsinized and subcultured into 6 well plates for antibiotic selection with blasticidin (2 µg/ml). Cells were further expanded in 10 cm plates under constant antibiotic selection process over 2 weeks. In the meantime, a small amount of cell lysates are harvested and tested for protein knockdown of SIN3A before the cell line is considered to be a stable cell line for SIN3A KD. These stable cells lines containing either the control shRNA construct or the SIN3A-targeted shRNA construct are frozen and kept subsequently in the liquid N₂ tank for long-term storage.

5.5 RNA methods

5.5.1 RNA extraction from cell culture samples

Cells were washed once with cold PBS before being lysed directly on the wells for RNA extraction following the typical TRIzol (Sigma) phenol-chloroform extraction method. RNA was precipitated from the extracted aqueous organic phase by adding 700 μ l of isopropanol to every 1 ml of TRIzol added, vortexed vigorously and centrifuged at 13 000 rpm for 30 mins at 4°C. The RNA pellet was washed once with 75% ethanol before being air-dried on the heat block at 55°C for 5 mins until all residual ethanol has evaporated. The RNA pellet was reconstituted into 50 μ l of RNase free H₂O and placed onto the heat block again at 55°C for 10 mins. The final RNA concentration, 260/280 and 260/230 ratios were determined using the NanoDrop spectrophotometry. RNA was then stored in -20°C for short term and -80°C for long-term storage.

5.5.2 Reverse transcription of RNA to form cDNA

QuantiTect Reverse Transcription kit from Qiagen was used for synthesizing cDNA (complementary DNA) from RNA extracted. 1 μ g of RNA was diluted into 12 μ l of nuclease free water. Genomic DNA (gDNA) was first removed by adding 2 μ l of gDNA wipe out buffer and incubating for 2 mins at 42°C on the Thermo Heat block and back on ice. The reaction mix is set up by adding 4 μ l of QuantiTect reverse transcriptase (RT) buffer, 1 μ l of RT primer and 1 μ l of RT to each RNA sample. The reverse transcription reaction is incubated for 30 mins at 42°C before the reaction was stop by increasing the temperature to 95°C for 2 mins. 80 μ l of nuclease free water are added to the resulting cDNA solutions and these diluted cDNA (equivalent to 10 ng/ μ l of initial RNA) are used for later qPCR reactions.

5.5.3 TaqMan qPCR to quantify for gene expression

qPCR reactions were set up in 10 μ l per well in MicroAmp optical 384-well reaction plates with triplicates /sample as follow:

qPCR set up using TaqMan ®probes	Volume per sample (ul)
10 ng/ μ l cDNA	2,5
TaqMan probe	0,25
TaqMan ® Gene expression Master Mix	5
Nuclease free water	2,25

The plate was sealed with MicroAmp optical Adhesive film; briefly centrifuged for 2 mins at 2000 rpm and amplification was performed in the Thermo Fischer Quantstudio 6 Flex instrument, 384-well block. The temperature profile for the PCR cycle used was: 2 mins at 50°C, 10 mins at 95°C then 40 cycles of 15 secs at 95°C followed by 1 mins at 60°C. The

5 MATERIAL & METHODS

ΔC_T values are obtained by subtracting the C_T value for gene of interest from C_T value of the housekeeping gene TBP of the same sample. This ΔC_T is then converted to relative gene expression to TBP using this formula for relative expression: $2^{-\Delta C_T}$.

5.6 Protein methods

5.6.1 Protein extraction from cell culture

Cells were washed once in cold PBS on ice before being lysed in RIPA buffer supplemented with protease and phosphatase inhibitors (Sigma). All steps were performed on ice or at 4°C unless specified. To a 6-well plate, 400 μ l of RIPA buffer was added per well and cells were lysed for 30 mins on ice. Thereafter, the cell lysates were collected and transferred into 1,5 ml tubes. Depending on the viscosity of the cell lysates, sonications were also performed using the Bioruptor Plus Sonicator for 3 cycles of 10 secs at low intensity for viscous lysates. 20 μ l of the cell lysates are put aside for subsequent determination of protein concentration whilst the rest of the lysates are stored at -20°C or -80°C until further use.

5.6.2 Determination of protein concentrations

Protein concentrations were determined using the Pierce BCA assay kit on 96-well microtiter plates. BSA standards in a range of 0,025– 2 mg/ml were prepared beforehand by serial dilution of the BSA stock (2 mg/ml) in water. 10 μ l of the protein sample or of the BSA standards were pipetted in duplicates with 200 μ l of assay reagent per well. BCA assay was incubated for 30 mins at 37°C for purple coloration to develop and absorbance values were measured in the plate reader at 560 nm. Protein concentration of samples was extrapolated and calculated from BSA standard curve generated during the assay.

5.6.3 SDS-polyacrylamide gel electrophoresis

20-40 μ g of proteins were diluted in H₂O and 5x SDS loading dye to a final volume of 40 μ l, then denatured for 7 mins at 95°C, shaking on the heat block. Samples are cooled briefly on ice before being loaded onto 8-12% gradient SDS- polyacrylamide gels that has been placed into gel chambers filled with 1x SDS running buffer. Electrophoresis was performed at 90-120 V for 1,5- 2 hrs with powerpac from Biorad. 5 μ l of Precision Dual stain protein ladders from Biorad was used as a size standard.

5.6.4 Protein transfer and immunoblotting

Protein transfer was performed using a wet blot system. After gel separation, gels were removed from the gel cassettes and submerged briefly in the SDS transfer buffer. A sandwich array was assembled in the transfer cassette in the following order: a sponge pad, 1 gel-sized Whatman filterpaper, 1 gel-sized 0,45 μ M nitrocellulose membrane, gel, whatman filterpaper and sponge pad (all components previously soaked in transfer buffer). Protein transfer was performed in Tris-glycine-SDS transfer buffer for 1,5 hrs at 90 v at 4°C using a Mini trans-

5 MATERIAL & METHODS

blot cell. After the transfer, the membrane was removed and stained briefly in Poncea-S solution to access the quality of transfer. Staining was removed by a few washes under running water until no stain remained. Membranes were blocked for 1 hr in 5% milk/TBS-T (0.1% Tween) before being incubated with primary antibodies overnight at 4°C. The next day, blots were washed for 3 x 5 mins in TBS-T before being incubated with HRP-conjugated secondary antibodies (refer to antibodies section) for 1 hr at RT. Blots were washed for 3 x 5 mins in TBS-T. ECL (enhanced chemiluminescence) western blotting detection reagent mix was applied to the membrane, incubated for 1 min and chemiluminescence was imaged with the Bio-rad ChemiDoc system with Image lab software.

5.7 Molecular Cloning

5.7.1 Transformation of bacteria *E.coli* cells

DH5 α chemically competent *E.coli* cells were transformed by using the heat shock method. One aliquot of bacteria cells (50 μ l) is taken out from -80°C and thawed on ice. 10ul of plasmid DNA in an amount ranging from 0.1 μ g to 1 μ g is then mixed with the cells and incubated for 30 mins on ice. Thereafter, cells are subjected to a heat shock at 42°C for 40 secs in a prewarmed waterbath. These cells were given 250 μ l of S.O.C medium and then incubated at 37°C for 1 hr on the shaker at 225 x g. Thereafter, 100 μ l of these cells were spread onto an LB agar containing the appropriate selective antibiotics and incubated overnight at 37°C.

5.7.2 Growing bacteria colonies for plasmid amplification

The next day, single colonies are picked with a 20 μ l pipette tip and inoculated into a starter culture containing 4 ml of LB media with the appropriate selective antibiotics. Culture was incubated for approximately 8 hrs at 37°C shaking at 300 x g. This starter culture is further inoculated into a larger culture volume of 200 ml of selective LB medium and allowed to grow overnight for 12-16 hrs, shaking at 300 x g at 37°C.

5.7.3 Plasmid DNA purification

The next day, the bacterial cells were harvested into centrifuge bottles and centrifuged at 5000 x g for 20 mins at 4°C. All traces of the medium were removed by draining the bottles. The bacteria pellets were frozen in -20°C until further plasmid purification step. All subsequent steps were performed in accordance to the manufacturer's protocol for the HispeedPlasmid Maxi kit (Qiagen). After the plasmid DNA has been finally eluted in 500 μ l of TE buffer, the DNA yield is measured with the Nanodrop at 260nm. Depending on the downstream applications, the DNA is either used for direct transfection into cells or needs to be further digested with appropriate RE to check for correct orientation of the inserts. In the latter case, the RE-digested Plasmids are then analysed by agarose gel electrophoresis.

5.8 Nomenclature of genes and proteins

All Mouse proteins and genes are assigned with a capitalized first letter (e.g. Trip13, Sin3a) whilst human proteins and genes are assigned entirely with block letters (E.g. TRIP13, SIN3A)

5.9 Material

5.9.1 Equipments

Product name	Company
Aspiration adaptor, 8-channel	Neolab
Bacterial Incubator	ThermoFisher Scientific
Bacterial shaking incubator	Infors HT
Balance, Analytical, Entris, 2200g	Sartorius
Balance, Cubis, MSE623S-100DE	Sartorius
Benchtop Microfuge 20 1	Beckman Coulter
Bioruptor® _Plus Sonicator	Diagenode
Bunsen Burner	Campingaz
C-4040 zoom Digital Camera	Olympus
ChemiDoc TMI XRS+ Molecular Imager®	Biorad
Ckx41 Inverted Light Microscope	Olympus
Comfort Thermomixer	Eppendorf
Fluoview FV1000 Confocal microscope	Olympus
Countess II Cell counter, automated	Life Technologies
Laminair Model 1.2	Holtern
Magnetic Stirrer Rsm-10hs	Phoenix Instruments
Micropipette, 8-channel, 0.5-10 ml	Eppendorf
Micropipette, 8-channel, 10-100 ml	Eppendorf
Mini Trans-Blot Electrophoretic Transfer Cell	Biorad
Mr Frosty Freezing Container	ThermoFisher Scientific
Multimode Microplate reader, Varioscan LUX	ThermoFisher Scientific
Multipette® _M4 Multistep pipette	Eppendorf

5 MATERIAL & METHODS

Product	Company
Multipette® _plus Multistep pipette	Eppendorf
Mutistep pipette	Eppendorf
Nanodrop Nd-1000	Thermo Fischer
Neubauer Counting chamber	Brand (Wertheim, Germany)
Ot340 Hotplate	Medite
pH meter Qph 70	GHM Messtech
PowerPac Basic TM gel electrophoresis	Biorad
Rotating Wheel	Neolab
TissueLyser MixerMill	Retsch
Titer plate shaker	ThermoFischer scientific
Trans-Blot cell	Biorad
Trans-Blot, Turbo Blotting System	Biorad
Vortex Genie 2 G560E	Scientific Industries, Inc
Western Blot Tank Blotting System Mini	Biorad

5.10 Consumables

Product	Company	Cat. No.
0.1 -10 µl pipette tips	Eppendorf	0030 072.006
0.2 mL Combitips advanced®	Eppendorf	0030 089.413
0.5 mL Combitips advanced®	Eppendorf	0030 089.421
0.5-20 µl pipette tips	Eppendorf	0030 072.014
1 mL syringe, Soft-Ject® _Tuberkulin	Henke Sass Wolf	5010-200V0
1-200 µl pipette tips	Eppendorf	0030 072.022
10 mL Combitips advanced®	Eppendorf	0030 089.464
1.5 mL safe-lock tube	Eppendorf	0030 120.086

5 MATERIAL & METHODS

Product	Company	Cat. No.
10 cm tissue culture plate	BD Falcon™	353003
10 mL serological pipettes	BD Falcon™	357551
15 cm tissue culture plate	BD Falcon™	353025
2 mL cryogenic vials	StarLab	E31110-6122
2 mL safe-lock tube	Eppendorf	0030 120.094
20 mL syringe	BD Falcon™	300629
25 mL serological pipettes	BD Falcon™	357525
5 mL Combitips advanced®	Eppendorf	0030 089.456
5 mL safe-lock tube	Eppendorf	0030 119.460
5 mL serological pipettes	BD Falcon™	357543
5 mL syringe	BD Falcon™	309050
50 mL serological pipettes	BD Falcon™	357550
50 mL syringe	BD Falcon™	300865
50-1000 µl pipette tips	Eppendorf	0030 072.030
Cell scraper	Corning	3010
Corning® 96 Well Solid Polystyrene Microplate (White)	Corning	CLS3912
Corning™ Falcon™ 15mL Conical Centrifuge Tubes	ThermoFischer Corning, Inc	352096
Corning™ Falcon™ 50mL Conical Centrifuge Tubes	ThermoFischer Corning, Inc	352070
Countess™ cell counting chamber slides	Life Technologies, Invitrogen	C10283
Cover slips 24X60 mm #1	Menzel	BBAD02400600
Cover slips 24X60 mm #1,5	Menzel	BBAD02400600
Imaging plate, 96-well clear bottom black wall	BD Falcon	353219
Lab-Tek II CC2 Glass Chamber Slides 4-well	ThermoFisher Scientific	154526
Lab-Tek II CC2 Glass Chamber Slides 8-well	ThermoFisher Scientific	154941

5 MATERIAL & METHODS

Product	Company	Cat. No.
Microtiter plate, 96-well	ThermoFisher Scientific	260836
Nitrocellulose membrane, Protran® BA85, 0.45 µm pore size	GE Healthcare	10401196
Parafilm® _M	Bemis®	BR701650
PCR tube lids, flat, 8 strip	Greiner Bio-one	373250
PCR Tubes, 8 strips, 0.2 mL	Greiner Bio-one	673210
Petri dish for Agar plates	Greiner Bio-one	632180
Stainless steel beads, 5 mm	Qiagen	69989
Tissue-culture treated plate, 12-well	BD Falcon™	353043
Tissue-culture treated plate, 24-well	BD Falcon™	353047
Tissue-culture treated plate, 6-well	BD Falcon™	353046
Tissue-culture treated plate, 96-well	BD Falcon™	353916
Whatman™ paper	GE Healthcare	3030 917
Novex™ 8-16% Tris-Glycine Mini Gels, WedgeWell™ format, 12-well	Invitrogen	XP08162BOX
Novex™ 4-20% Tris-Glycine Mini Gels, WedgeWell™ format, 12-well	Invitrogen	XP04202BOX

5.11 Kits

Product	Company	Cat. No.
Apo-ONE® Homogeneous Caspase-3/7 Assay	Promega	G7792
BrdU Cell proliferation kit	Cell Signaling Technology	6813S
Cell Counting kit 8 (CCK-8)	Sigma-Aldrich	96992
Duolink detection reagentsRed	Sigma-Aldrich	DUO92008
Duolink in situ PLA probe Anti-Goat Minus	Sigma-Aldrich	DUO92006
Duolink in situ PLA probe Anti-Rabbit Plus	Sigma-Aldrich	DUO92002
ECL Prime Western Blotting Detection Reagent	Amersham Biosciences	RPN2232

5 MATERIAL & METHODS

Product	Company	Cat. No.
Glucose (HK) assay kit	Sigma-Aldrich	GAHK20-1KT
QuantiTect Rev. Transcription Kit	Qiagen	205313
Secrete-Pair Dual Luminescence Assay Kit	Genecopoeia	LF032
Serum Triglyceride determination kit	Sigma-Aldrich	TR0100
qPCR Lentiviral titration Kit	abm Good	LV900
Lenti-X GoStix, 20 tests	Takara Bio Clontech	631243

5.12 Enzymes

Product	Company	Cat. No.
Calf Intestinal Alkaline Phosphatase 1 U/ μ L	Sigma-Aldrich	18009027
FastDigest EcoRI	Fermentas	FD0274
FastDigest KpnI	Fermentas	FD0274
FastDigest XhoI	Fermentas	FD0694
Proteinase K	ThermoFisher Scientific	EO0491
RNase A 10 mg/mL	ThermoFisher Scientific	EN0531
T4 DNA Ligase	Invitrogen	15224017

5.13 Plasmids

Vector name	Company	Cat. No.
pENTR-shRNA-hTRIP13 (TRCN0000022063)	Sigma-Aldrich	SHCLND-NM_004237
pENTR-shRNA-mTrip13 (TRCN0000319690)	Sigma-Aldrich	SHCLND-XM_127444
pGFP-C-shRNA-NTC	Origene	TL30021
pGFP-C-shRNA-SIN3A_1	Origene	TL301698A
pGFP-C-shRNA-SIN3A_4	Origene	TL301698D
pRFP-CB-shRNA-NTC	Origene	TL30032

5 MATERIAL & METHODS

pRFP-CB-shRNA-SIN3A_1	Origene	subcloned from Origene vector
pRFP-CB-shRNA-SIN3A_4	Origene	subcloned from Origene vector
psPAX2	Addgene	12260
pMD2.G	Addgene	12259
pLKO.1-shRNA-scrambled	Addgene	1864
pEZX-PG04-HRP-EGFR	Genecopoeia	HPRM21493-LvPG04

5.14 Chemicals

Product	Company	Cat. No.
Acetic acid	Sigma-Aldrich	45731
Agarose	Carl Roth	3810
Ampicillin sodium salt	Sigma-Aldrich	A9518
Antifade Mounting Medium with DAPI	Vectashield	H-1200
APS (Ammonium persulfate)	Carl Roth	9592
β -mercaptoethanol	Sigma-Aldrich	M7154
CaCl ₂ (Calcium Chloride)	Carl Roth	CN93
Chloroform (CHCl ₃)	Carl Roth	3313
D-Glucose anhydrous	Applchem	A0883
DEPC (Diethylpyrocarbonate)	Sigma-Aldrich	D5758
DH5 α chemically Competent Cells	Invitrogen	18265017
DTT (Dithiothreitol)	Applchem	A2948
Ethanol, absolute	Sigma-Aldrich	32205
Formaldehyde solution 37%	Carl Roth	7398,4
6x DNA Loading Dye	Fermentas	R0611

5 MATERIAL & METHODS

Product	Company	Cat. No.
GeneRuler 1 kb Plus DNA Ladder	Fermentas	SM1334
GeneRuler 100 bp Plus DNA Ladder	Fermentas	SM0323
Glycerol	Sigma-Aldrich	15523
Glycine	Sigma-Aldrich	33226
H ₂ O ₂ (Hydrogen peroxide) solution, 30% (W/V) in H ₂ O	Sigma-Aldrich	H1009
HCl (Hydrochloric acid) 37%	Sigma-Aldrich	30721
KCl (Potassium chloride)	Carl Roth	A137
KH ₂ PO ₄ (Potassium dihydrogen phosphate)	Carl Roth	3904
LB-Agar (Luria/Miller)	Carl Roth	X969
LB-Medium (Luria/Miller)	Carl Roth	X968
Na ₃ VO ₄ (sodium orthovanadate)	Sigma-Aldrich	S6508
NaCl (sodium chloride)	Sigma-Aldrich	31434
NaF (sodium flouride)	Sigma-Aldrich	S1504
NaOH (sodium hydroxide)	Sigma-Aldrich	30620
PhosSTOP™ Phosphatase Inhibitor tablets	Roche	49068450 01
Ponceau S solution 0.1% in 5% acetic acid	Sigma-Aldrich	P7170
Precision Plus Protein™ Dual Color Standards	Biorad	1610374
Protease inhibitor cocktail	Sigma-Aldrich	P8340
Protease inhibitor cOmplete, EDTA free	Roche	11873580 001
Restore Plus Western Blot Striping Buffer	ThermoScientific	46430
Roti®-Histofix 4% acetic acid free (pH 7.0)	Carl Roth	P087
S.O.C. Medium	Invitrogen	15544034
SDS (sodium dodecyl sulfate)	Sigma-Aldrich	D6750
Skim Milk Powder	Sigma-Aldrich	70166
Sodium Azide	Sigma-Aldrich	S2002

5 MATERIAL & METHODS

Product	Company	Cat. No.
Sodium deoxycholate	Sigma-Aldrich	D6750
Sucrose	Sigma-Aldrich	S1888
Triton® X-100	Appllichem	A1388
TRIzol™ Reagent	Invitrogen	15596026
Tween® _20	Sigma-Aldrich	P9416
16% Formaldehyde (w/v), Methanol-free	ThermoScientific Pierce	28908

5.15 Cell culture reagents

Product	Company	Cat. No.
DMEM High Glucose Pyruvate (+ L-glutamine)	Life Technologies™ Gibco	41966-029
DMEM Low Glucose Pyruvate (+ L-glutamine)	Life Technologies™ Gibco	31885-023
RPMI 1640 Medium	Life Technologies™ Gibco	11875093
DMEM/F-12, HEPES	Life Technologies™ Gibco	11330057
Hoechst 33342, trihydrochloride trihydrate, 10 mg/mL	Life Technologies™ Gibco	H3570
Lipofectamine™ 2000 Transfection Reagent	Invitrogen	11668019
Lipofectamine™ 3000 Transfection Reagent	Invitrogen	L3000015
Lipofectamine™ RNAiMAX Transfection Reagent	Invitrogen	13778150
Opti-MEM® I Reduced Serum Medium	Life Technologies™ Gibco	31985-047
Polybrene (hexadimethrine bromide)	Sigma-Aldrich	H9268
Pyruvate 100mM, 100x	Life Technologies™ Gibco	11360-039
Puromycin	Sigma-Aldrich	P8833
Blasticidin S HCL 10 mg/mL	Life Technologies™ Gibco	A1113903
0.25% Trypsin-EDTA (1x), Phenol red	Life Technologies™ Gibco	25200-056
DPBS, no CaCl ₂ , no MgCl ₂	Life Technologies™ Gibco	14190-094

5 MATERIAL & METHODS

Product	Company	Cat. No.
Fetal bovine serum (FBS)	Life Technologies™ Gibco	26400-036
HEPES Buffer solution, 1M	Life Technologies™ Gibco	15630-056
Penicillin-streptomycin, liquid, 100x	Life Technologies™ Gibco	15140-122
Tryphan blue solution, 0.4%	Life Technologies™ Gibco	T10282
Water, nuclease free	Life Technologies™ Gibco	10977-035
BSA for cell culture: Albumin solution from bovine serum, 30% DPBS, sterile-filtered	Sigma-Aldrich	A9576
DMSO (Dimethylsulfoxide) sterile for cell culture	Sigma-Aldrich	D2650

5.16 Antibodies

Primary Antibodies	Company	Cat. No.	Origin
AKT	Cell Signaling	9272	Rabbit
c-MYC	Cell Signaling	9402	Rabbit
Cleaved Caspase-3	Cell Signaling	9664S	Rabbit
Cleaved PARP	Cell Signaling	9544S	Mouse
CyclinD1	Cell Signaling	2926	Mouse
EGFR	Cell Signaling	4267	Rabbit
phospho-EGFR	Cell Signaling	3777	Rabbit
HSP90	Abcam	ab13492	Mouse
Lamin A/C	Abcam	ab8984	Mouse
p53	Cell Signaling	2524S	Mouse
p70S6K	Cell Signaling	2708	Rabbit
Phospho-p70S6K	Cell Signaling	9234	Rabbit
Phospho-AKT	Cell Signaling	9271	Rabbit
Phospho-Histone H2A.X	Cell Signaling	9718	Rabbit
phospho-SAPK/JNK (Thr183/Tyr185) (G9)	Cell Signaling	9255	Mouse
SAP130	Proteintech	12130-1-AP	Rabbit
SAP130	Novusbio	NB100-1077	Goat
SIN3A	Novusbio	AF6115-SP	Goat
m-SIN3A	Santa Cruz biotechnology	sc-994	Rabbit

5 MATERIAL & METHODS

TRIP13	Proteintech	19602-1-AP	Rabbit
Ubiquitin	Sigma-Aldrich	U0508	Mouse
VCP	Abcam	Ab11433	Mouse
β actin	Sigma	A5441	Mouse

Secondary Antibodies	Company	Cat. No.
Anti-Rabbit IgG-HRP	Bio-Rad	170-6516
Anti-Mouse IgG-HRP	Bio-Rad	172-1019
Normal goat IgG isotype control	Santa Cruz	sc-2028
Normal Rabbit IgG isotype control	Santa Cruz	sc-2027
Alexa Fluor 488 - Phalloidin	Invitrogen	A12379
Alexa Fluor 488 donkey anti-Rabbit IgG (H+L)	Invitrogen	A21206
Alexa Fluor 488 donkey anti-goat IgG (H+L)	Invitrogen	A11055
Alexa Fluor 555 donkey anti-Rabbit IgG (H+L)	Invitrogen	A-21428
Alexa Fluor 555 donkey anti-goat IgG (H+L)	Invitrogen	A-21432

5.17 Software

Product	Company/Source
Graphpad Prism 6	GraphPad Software
Illustrator	Adobe system
ImageJ	https://imagej.nih.gov/ij/
ImageLab	Biorad
Microsoft Office	Microsoft
ND-1000	Nanodrop
Photoshop	Adobe System

5 MATERIAL & METHODS

UCSC Genome Browser	http://genome.ucsc.edu
Papers version 3	Mekentosj B.V
Primer-Blast	https://www.ncbi.nlm.nih.gov/tools/primer-blast/
Olympus Fluoview	Olympus

5.18 Commercial probes for TaqMan quantitative PCR

Gene	Species	Entrez Gene ID	TaqMan Assay ID
TRIP13	Human	9319	Hs01020073_m1
Trip13	Mouse	69716	Mm01352446_m1
EGFR	Human	1956	Hs01076090_m1
Egfr	Mouse	13649	Mm01187858_m1
SIN3A	Human	25942	Hs00411592_m1
Sin3A	Mouse	20466	Mm00488255_m1
SAP130	Human	79595	Hs01089391_m1
Sap130	Mouse	269003	Mm00556995_m1
MYC	Human	4609	Hs00153408_m1
Cyclin D1	Human	595	Hs00765553_m1
cyclin D1	Mouse	12443	Mm00432359_m1
TBP	Human	6908	Hs00427620_m1
Tbp	Mouse	21374	Mm01277042_m1

5 MATERIAL & METHODS

5.19 Solutions and Buffers

All stock solutions and buffers were prepared in filtered water unless otherwise stated

Blocking Buffer (5% Milk/TBST)

1x TBS, 0.1% Tween 20, 5% Milk powder

Blocking Buffer (5% BSA/TBST) to block when probing with anti-phosphoantibodies

1x TBS, 0.1% Tween 20, 5% BSA Fraction V

RIPA Buffer

50 mM Tris pH 8.0, 150 mM NaCl, 1% NP40, 0.5% SDS, 0.1% Sodium deoxycholate
1 tablet each of PhoSTOP and protease inhibitor is dissolved in 10 ml of RIPA buffer before use.

LB agar plate

40g/L LB agar (Carl Roth) is dissolved in water by warming up the mixture in the microwave. Mixture is cooled down before adding appropriate selective antibiotics and 20 ml of molten agar was poured per petri dish and allowed to cool down before storing at 4 C for up to 1 month

TBST

1x TBS with 0.1% Tween 20

SDS running buffer (10x)

0.25 M Tris, 1.9 M Glycine, 1% SDS

TBE Buffer (10x)

100 mM Tris, 1 mM EDTA, 90 mM Boric acid, pH 8.0

TE Buffer

1 mM EDTS, 10 mM Tris HCl, pH 8.0

Transfer Buffer

25 mM Tris, 190 mM Glycine, 20% Methanol, 0.1% SDS

10X TBS stock

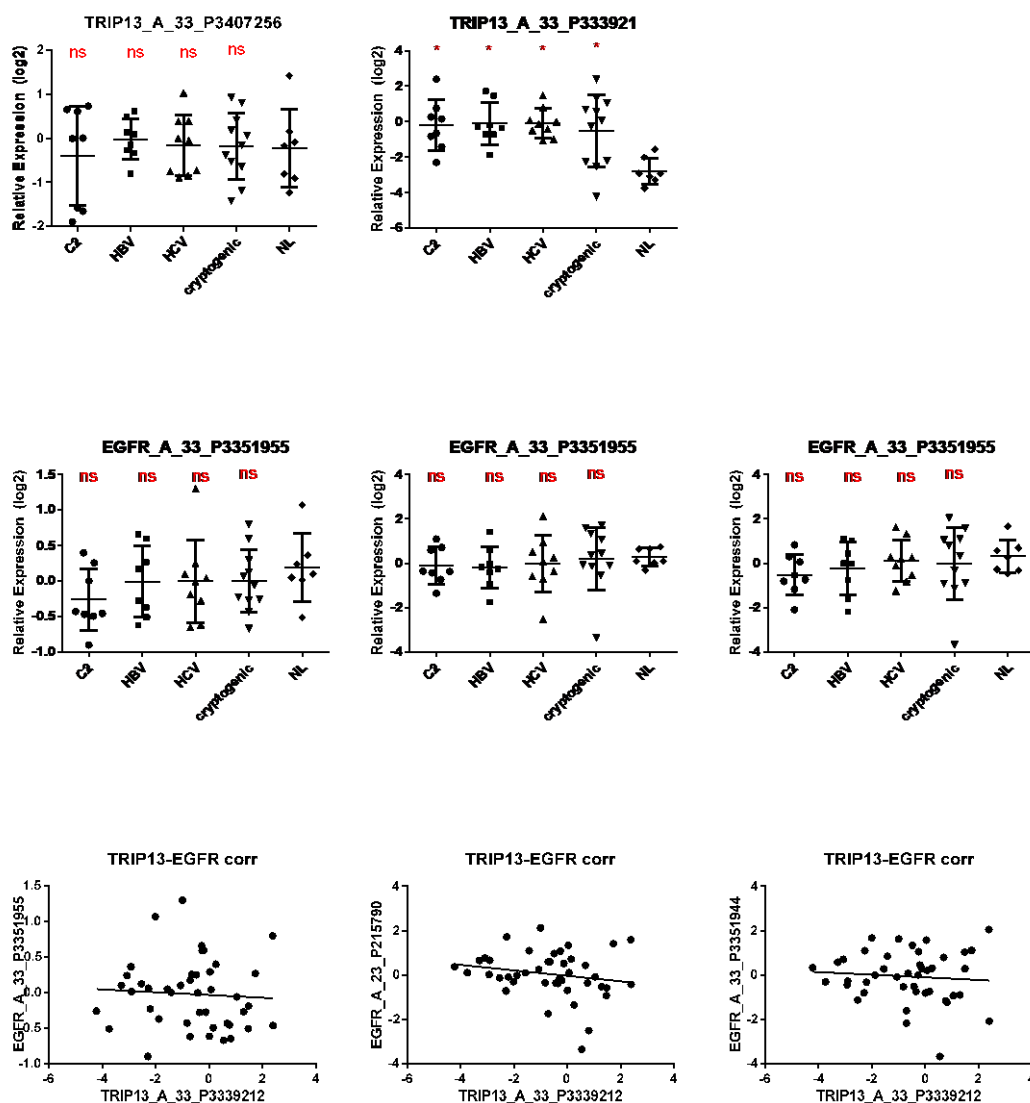
500 mM Tris-HCL, PH7.4, 1.5mM Nacl

5X SDS Sample Buffer

250 mM Tris/HCl pH 6.8, 0.5 M DTT, 10% SDS, 50% glycerol, 0.01% bromophenol blue

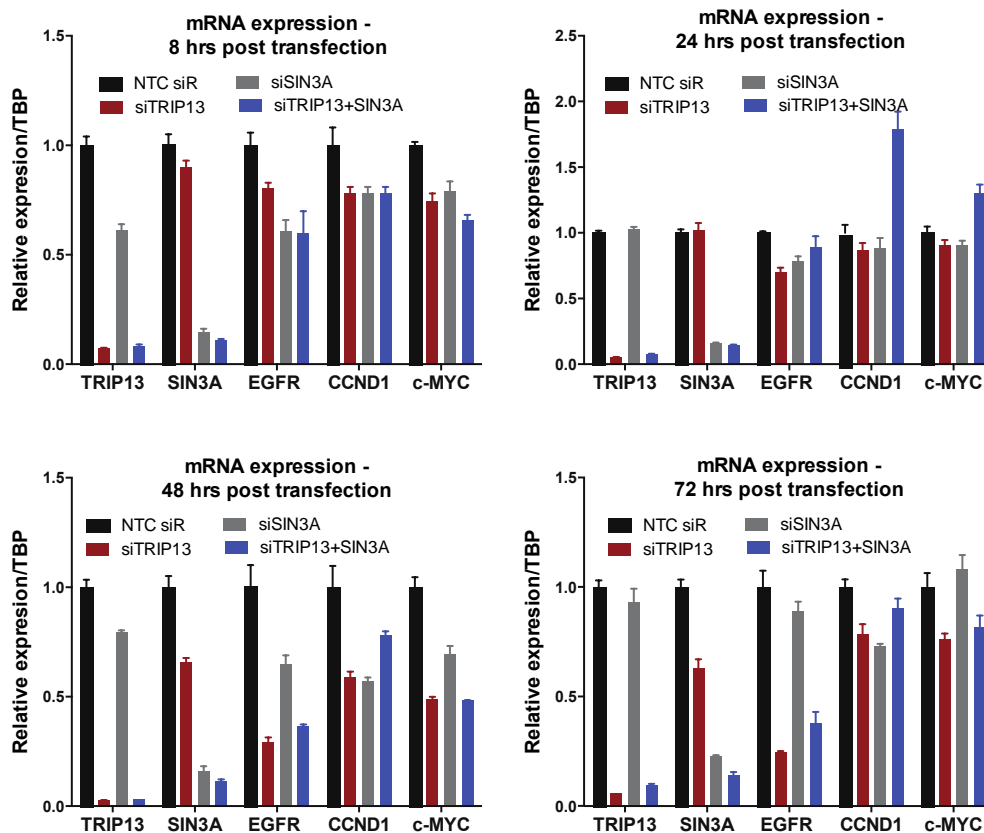
6 Appendices

TRIP13 and EGFR in TL cohort

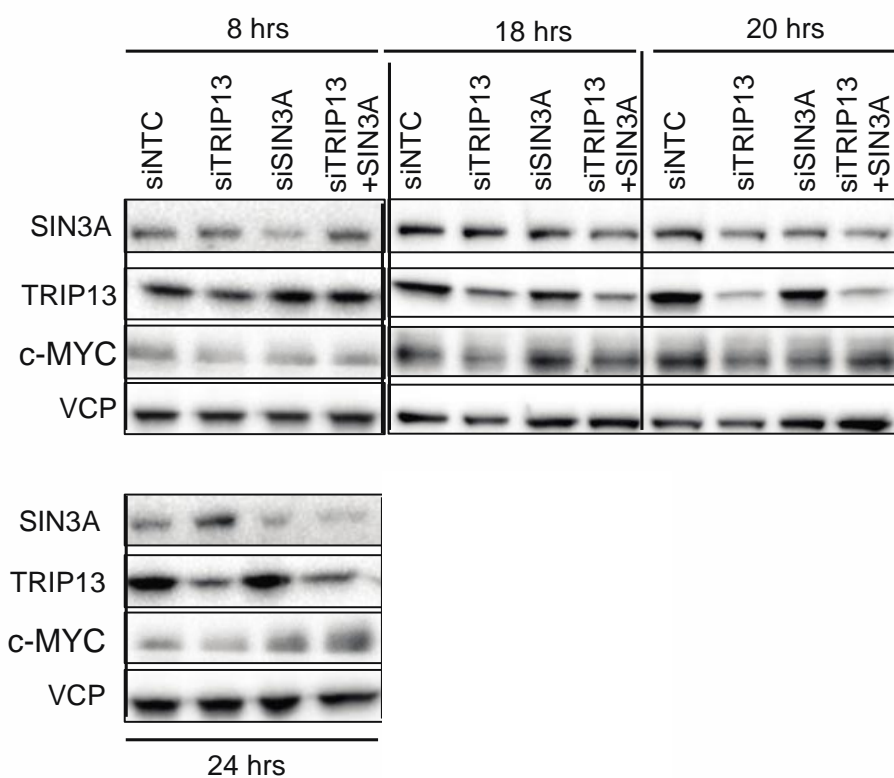


S1 Expression profiling of TRIP13 and EGFR in HCC patient cohorts from different etiology background

One of the patient cohorts A_33_P3407256 was disregarded, as there was no difference in TRIP13 expression across different HCC etiology. TRIP13 expression is upregulated across all HCC etiology from the other patient cohort of A_33_P3339212. EGFR expression remains constant across all HCC etiology groups. No correlation was observed between EGFR and TRIP13 in HCC patient cohorts.



S2 Gene expression levels between 8 hrs-72 hrs post siRNA transfections to knockdown either TRIP13 or SIN3A or both
RNA samples were harvested at 8, 24, 48 and 72 hrs post siRNA transfections. siR KD efficiencies along with expression levels of EGFR, CyclinD1 and c-MYC were quantified via qPCR analysis.



S3 Protein expression levels between 8 hrs-72 hrs post siRNA transfections to knockdown either TRIP13 or SIN3A or both

Cell lysates were harvested at 8, 18, 20, 24 post siRNA transfections. siR KD efficiencies along with expression levels of c-MYC were verified via immunoblotting for SIN3A, TRIP13 and c-MYC using VCP as a loading control

References

1. Ford, E. S., Giles, W. H. & Mokdad, A. H. Increasing prevalence of the metabolic syndrome among u.s. Adults. *Diabetes Care* **27**, 2444–2449 (2004).
2. Calle, E. E., Rodriguez, C., Walker-Thurmond, K. & Thun, M. J. Overweight, Obesity, and Mortality from Cancer in a Prospectively Studied Cohort of U.S. Adults. *New England Journal of Medicine* **348**, 1625–1638 (2003).
3. Nair, S. Is obesity an independent risk factor for hepatocellular carcinoma in cirrhosis? *Hepatology* **36**, 150–155 (2002).
4. Regimbeau, J. M. *et al.* Obesity and diabetes as a risk factor for hepatocellular carcinoma. *Liver Transplantation* **10**, S69–S73 (2004).
5. Neuschwander-Tetri, B. A. & Caldwell, S. H. Nonalcoholic steatohepatitis: summary of an AASLD Single Topic Conference. in **37**, 1202–1219 (W.B. Saunders, 2003).
6. Marchesini, G. Nonalcoholic fatty liver, steatohepatitis, and the metabolic syndrome. *Hepatology* **37**, 917–923 (2003).
7. Matteoni, C. A. *et al.* Nonalcoholic fatty liver disease: a spectrum of clinical and pathological severity. *YGAFT* **116**, 1413–1419 (1999).
8. Siegel, A. B. & Zhu, A. X. Metabolic syndrome and hepatocellular carcinoma. *Cancer* **115**, 5651–5661 (2009).
9. Solinas, G. & Karin, M. JNK1 and IKKbeta: molecular links between obesity and metabolic dysfunction. *FASEB J.* **24**, 2596–2611 (2010).
10. Park, E. J. *et al.* Dietary and Genetic Obesity Promote Liver Inflammation and Tumourigenesis by Enhancing IL-6 and TNF Expression. *Cell* **140**, 197–208 (2010).
11. Nawrocki, A. R. & Scherer, P. E. Keynote review: The adipocyte as a drug discovery target. *Drug Discovery Today* **10**, 1219–1230 (2005).
12. Calle, E. E. & Kaaks, R. Overweight, obesity and cancer: epidemiological evidence and proposed mechanisms. *Nature Reviews Cancer* **4**, 579–591 (2004).
13. Ahmed, M. & Gaffen, S. L. IL-17 in obesity and adipogenesis. *Cytokine & Growth Factor Reviews* **21**, 449–453 (2010).
14. Bruun, J. M. Regulation of Interleukin 8 Production and Gene Expression in Human Adipose Tissue in Vitro. *Journal of Clinical Endocrinology & Metabolism* **86**, 1267–1273 (2001).
15. Schwarzenberg, S. J. & Sinaiko, A. R. Obesity and inflammation in children. *Paediatr Respir Rev* **7**, 239–246 (2006).
16. Wellen, K. E. & Hotamisligil, G. S. Inflammation, stress, and diabetes. *J. Clin. Invest.* **115**, 1111–1119 (2005).
17. Berg, A. H. & Scherer, P. E. Adipose tissue, inflammation, and cardiovascular disease. *Circ. Res.* **96**, 939–949 (2005).
18. Forner, A. & Bruix, J. Biomarkers for early diagnosis of hepatocellular carcinoma. *Lancet Oncol.* **13**, 750–751 (2012).
19. Luedde, T., Kaplowitz, N. & Schwabe, R. F. Cell Death and Cell Death Responses in Liver Disease: Mechanisms and Clinical Relevance. *Gastroenterology* **147**, 765–783.e4 (2014).
20. Boege, Y. *et al.* A Dual Role of Caspase-8 in Triggering and Sensing Proliferation-Associated DNA Damage, a Key Determinant of Liver Cancer Development. *Cancer Cell* **32**, 342–359.e10 (2017).

-
21. Ruhl, C. E. & Everhart, J. E. Elevated Serum Alanine Aminotransferase and γ -Glutamyltransferase and Mortality in the United States Population. *Gastroenterology* **136**, 477–485.e11 (2009).
 22. McPherson, S., Henderson, E., Burt, A. D., Day, C. P. & Anstee, Q. M. Serum immunoglobulin levels predict fibrosis in patients with non-alcoholic fatty liver disease. *Journal of Hepatology* **60**, 1055–1062 (2014).
 23. Hyeon, C. K. *et al.* Normal serum aminotransferase concentration and risk of mortality from liver diseases: prospective cohort study. *BMJ* **328**, 983 (2004).
 24. Hanson, P. I. & Whiteheart, S. W. AAA+ proteins: have engine, will work. *Nat. Rev. Mol. Cell Biol.* **6**, 519–529 (2005).
 25. Bhalla, N. & Dernburg, A. F. A conserved checkpoint monitors meiotic chromosome synapsis in *Caenorhabditis elegans*. *Science* **310**, 1683–1686 (2005).
 26. Joyce, E. F. & McKim, K. S. Chromosome Axis Defects Induce a Checkpoint-Mediated Delay and Interchromosomal Effect on Crossing Over during *Drosophila* Meiosis. *PLoS Genet* **6**, e1001059 (2010).
 27. Zanders, S., Sonntag Brown, M., Chen, C. & Alani, E. Pch2 modulates chromatid partner choice during meiotic double-strand break repair in *Saccharomyces cerevisiae*. *Genetics* **188**, 511–521 (2011).
 28. Wang, K. *et al.* Thyroid Hormone Receptor Interacting Protein 13 (TRIP13) AAA-ATPase Is a Novel Mitotic Checkpoint-silencing Protein. *Journal of Biological Chemistry* **289**, 23928–23937 (2014).
 29. Eytan, E. *et al.* Disassembly of mitotic checkpoint complexes by the joint action of the AAA-ATPase TRIP13 and p31comet. *Proceedings of the National Academy of Sciences* **111**, 12019–12024 (2014).
 30. Sudakin, V., Chan, G. K. T. & Yen, T. J. Checkpoint inhibition of the APC/C in HeLa cells is mediated by a complex of BUBR1, BUB3, CDC20, and MAD2. *The Journal of Cell Biology* **154**, 925–936 (2001).
 31. Mapelli, M., Massimiliano, L., Santaguida, S. & Musacchio, A. The Mad2 Conformational Dimer: Structure and Implications for the Spindle Assembly Checkpoint. *Cell* **131**, 730–743 (2007).
 32. Yang, M. *et al.* p31comet blocks Mad2 activation through structural mimicry. *Cell* **131**, 744–755 (2007).
 33. Teichner, A. *et al.* p31comet Promotes disassembly of the mitotic checkpoint complex in an ATP-dependent process. *Proc. Natl. Acad. Sci. U.S.A.* **108**, 3187–3192 (2011).
 34. Ma, H. T. & Poon, R. Y. C. TRIP13 Regulates Both the Activation and Inactivation of the Spindle-Assembly Checkpoint. *Cell Rep* **14**, 1086–1099 (2016).
 35. Martin, K. J., Patrick, D. R., Bissell, M. J. & Fournier, M. V. Prognostic breast cancer signature identified from 3D culture model accurately predicts clinical outcome across independent datasets. *PLoS ONE* **3**, e2994 (2008).
 36. Rhodes, D. R. *et al.* Large-scale meta-analysis of cancer microarray data identifies common transcriptional profiles of neoplastic transformation and progression. *Proceedings of the National Academy of Sciences* **101**, 9309–9314 (2004).
 37. Carter, S. L., Eklund, A. C., Kohane, I. S., Harris, L. N. & Szallasi, Z. A signature of chromosomal instability inferred from gene expression profiles predicts clinical outcome in multiple human cancers. *Nat Genet* **38**, 1043–1048 (2006).
 38. Lengauer, C., Kinzler, K. W. & Vogelstein, B. Genetic instabilities in human cancers. *Nature* **396**, 643–649 (1998).
 39. Weiler, S. M. E. *et al.* Induction of Chromosome Instability by Activation of Yes-Associated Protein and Forkhead Box M1 in Liver Cancer. *Gastroenterology* **152**, 2037–2051.e22 (2017).
-

-
40. Wilkens, L. *et al.* Induction of aneuploidy by increasing chromosomal instability during dedifferentiation of hepatocellular carcinoma. *Proceedings of the National Academy of Sciences* **101**, 1309–1314 (2004).
 41. Plentz, R. R. *et al.* Hepatocellular telomere shortening correlates with chromosomal instability and the development of human hepatoma. *Hepatology* **40**, 80–86 (2004).
 42. Yimlamai, D., Fowl, B. H. & Camargo, F. D. Emerging evidence on the role of the 39/YAP pathway in liver physiology and cancer. *Journal of Hepatology* **63**, 1491–1501 (2015).
 43. Kang, J. U., Koo, S. H., Kwon, K. C., Park, J. W. & Kim, J. M. Gain at chromosomal region 5p15.33, containing TERT, is the most frequent genetic event in early stages of non-small cell lung cancer. *Cancer Genetics and Cytogenetics* **182**, 1–11 (2008).
 44. Tipton, A. R. *et al.* Identification of novel mitosis regulators through data mining with human centromere/kinetochore proteins as group queries. *BMC Cell Biol.* **13**, 15 (2012).
 45. Banerjee, R. *et al.* TRIP13 promotes error-prone nonhomologous end joining and induces chemoresistance in head and neck cancer. *Nature Communications* **5**, 1–16 (1AD).
 46. Silverstein, R. A. & Ekwall, K. Sin3: a flexible regulator of global gene expression and genome stability. *Current Genetics* **47**, 1–17 (2004).
 47. Nasmyth, K. Both positive and negative regulators of HO transcription are required for mother-cell-specific mating-type switching in yeast. *Cell* **48**, 579–587 (1987).
 48. Kadamb, R., Mittal, S., Bansal, N., Batra, H. & Saluja, D. Sin3: Insight into its transcription regulatory functions. *European Journal of Cell Biology* **92**, 237–246 (2013).
 49. Bansal, N., David, G., Farias, E. & Waxman, S. *Emerging Roles of Epigenetic Regulator Sin3 in Cancer. Advances in Cancer Research* **130**, 113–135 (Elsevier Inc., 2016).
 50. Grzenda, A., Lomberk, G., Zhang, J.-S. & Urrutia, R. Sin3: Master scaffold and transcriptional corepressor. *Biochimica et Biophysica Acta (BBA) - Gene Regulatory Mechanisms* **1789**, 443–450 (2009).
 51. Baymaz, H. I., Karemaker, I. D. & Vermeulen, M. Perspective on unraveling the versatility of ‘co-repressor’ complexes. *Biochimica et Biophysica Acta (BBA) - Gene Regulatory Mechanisms* **1849**, 1051–1056 (2015).
 52. Baltus, G. A., Kowalski, M. P., Tutter, A. V. & Kadam, S. A positive regulatory role for the mSin3A-HDAC complex in pluripotency through Nanog and Sox2. *Journal of Biological Chemistry* **284**, 6998–7006 (2009).
 53. Garcia-Sanz, P. *et al.* Sin3b Interacts with Myc and Decreases Myc Levels. *Journal of Biological Chemistry* **289**, 22221–22236 (2014).
 54. Dannenberg, J.-H. *et al.* mSin3A corepressor regulates diverse transcriptional networks governing normal and neoplastic growth and survival. *Genes Dev.* **19**, 1581–1595 (2005).
 55. Cultraro, C. M., Bino, T. & Segal, S. Function of the c-Myc antagonist Mad1 during a molecular switch from proliferation to differentiation. *Molecular and Cellular Biology* **17**, 2353–2359 (1997).
 56. Das, T. K., Sangodkar, J., Negre, N., Narla, G. & Cagan, R. L. Sin3a acts through a multi-gene module to regulate invasion in Drosophila and human tumours. *Oncogene* **32**, 3184–3197 (2013).
 57. Hudis, C. A. & Gianni, L. Triple-negative breast cancer: an unmet medical need. *Oncologist* **16 Suppl 1**, 1–11 (2011).
-

-
58. André, F. & Zielinski, C. C. Optimal strategies for the treatment of metastatic triple-negative breast cancer with currently approved agents. *Ann. Oncol.* **23 Suppl 6**, vi46–51 (2012).
 59. Bansal, N. *et al.* Targeting the SIN3A-PF1 interaction inhibits epithelial to mesenchymal transition and maintenance of a stem cell phenotype in triple negative breast cancer. *Oncotarget* **6**, (2015).
 60. Kwon, Y.-J. *et al.* Selective Inhibition of SIN3 Corepressor with Avermectins as a Novel Therapeutic Strategy in Triple-Negative Breast Cancer. *Mol. Cancer Ther.* **14**, 1824–1836 (2015).
 61. Farias, E. F. *et al.* Interference with Sin3 function induces epigenetic reprogramming and differentiation in breast cancer cells. *Proceedings of the National Academy of Sciences* **107**, 11811–11816 (2010).
 62. Yu, J., Shen, J., Sun, T. T., Zhang, X. & Wong, N. Obesity, insulin resistance, NASH and hepatocellular carcinoma. *Semin. Cancer Biol.* **23**, 483–491 (2013).
 63. Ye, Q. *et al.* TRIP13 is a protein-remodeling AAA+ ATPase that catalyzes MAD2 conformation switching. *eLife* **4**, 213 (2015).
 64. Ferlay, J. *et al.* Cancer incidence and mortality worldwide: Sources, methods and major patterns in GLOBOCAN 2012. *Int. J. Cancer* **136**, E359–E386 (2015).
 65. Yang, J. D. & Roberts, L. R. Hepatocellular carcinoma: a global view. *Nature Reviews Gastroenterology & Hepatology* **7**, 448 EP —1341.e23 (2017).
 66. Zucman-Rossi, J., Villanueva, A., Nault, J.-C. & Llovet, J. M. Genetic Landscape and Biomarkers of Hepatocellular Carcinoma. *Gastroenterology* **149**, 1226–1239.e4 (2015).
 67. Nahon, P. & Zucman-Rossi, J. Single nucleotide polymorphisms and risk of hepatocellular carcinoma in cirrhosis. *Journal of Hepatology* **57**, 663–674 (2012).
 68. Romeo, S. *et al.* Genetic variation in PNPLA3 confers susceptibility to nonalcoholic fatty liver disease. *Nat Genet* **40**, 1461–1465 (2008).
 69. Singal, A. G. *et al.* The Effect of PNPLA3 on Fibrosis Progression and Development of Hepatocellular Carcinoma: A Meta-analysis. *The American Journal of Gastroenterology* **109**, 325–334 (2014).
 70. Nault, J.-C. *et al.* High frequency of telomerase reverse-transcriptase promoter somatic mutations in hepatocellular carcinoma and preneoplastic lesions. *Nature Communications* **4**, 1245 (2013).
 71. Hartmann, D. *et al.* Telomerase gene mutations are associated with cirrhosis formation. *Hepatology* **53**, 1608–1617 (2011).
 72. Stratton, M. R., Campbell, P. J. & Futreal, P. A. The cancer genome. *Nature* **458**, 719–724 (2009).
 73. La Coste, de, A. *et al.* Somatic mutations of the beta-catenin gene are frequent in mouse and human hepatocellular carcinomas. *Proceedings of the National Academy of Sciences* **95**, 8847–8851 (1998).
 74. Hsu, I. C. *et al.* Mutational hotspot in the p53 gene in human hepatocellular carcinomas. *Nature* **350**, 427–428 (1991).
 75. Satoh, S. *et al.* AXIN1 mutations in hepatocellular carcinomas, and growth suppression in cancer cells by virus-mediated transfer of AXIN1. *Nat Genet* **24**, 245–250 (2000).
 76. Fujimoto, A. *et al.* Whole-genome sequencing of liver cancers identifies etiological influences on mutation patterns and recurrent mutations in chromatin regulators. *Nat Genet* **44**, 760–764 (2012).
 77. Li, M. *et al.* Inactivating mutations of the chromatin-remodeling gene ARID2 in hepatocellular carcinoma. *Nat Genet* **43**, 828–829 (2011).
-

-
78. Sporn, M. B. & Liby, K. T. NRF2 and cancer: the good, the bad and the importance of context. *Nature Reviews Cancer* **12**, 564–571 (2012).
 79. Villanueva, A. *et al.* Pivotal role of mTOR signaling in hepatocellular carcinoma. *Gastroenterology* **135**, 1972–83– 1983.e1–11 (2008).
 80. Law, P. T.-Y. *et al.* Deep sequencing of small RNA transcriptome reveals novel non-coding RNAs in hepatocellular carcinoma. *Journal of Hepatology* **58**, 1165–1173 (2013).
 81. Vader, G. Pch2TRIP13: controlling cell division through regulation of HORMA domains. *Chromosoma* **124**, 333–339 (2015).
 82. Llovet, J. M. *et al.* Sorafenib in advanced hepatocellular carcinoma. *N. Engl. J. Med.* **359**, 378–390 (2008).
 83. Abdel-Rahman, O. Impact of baseline characteristics on outcomes of advanced HCC patients treated with sorafenib: a secondary analysis of a phase III study. *J. Cancer Res. Clin. Oncol.* **11**, 183 (2018).
 84. Zhou, K. *et al.* Loss of thyroid hormone receptor interactor 13 inhibits cell proliferation and survival in human chronic lymphocytic leukemia. *Oncotarget* **8**, 25469–25481 (2017).
 85. Lee J. W. *et al.* Two classes of proteins dependent on either the presence or absence of thyroid hormone for interaction with the thyroid hormone receptor. *Molecular endocrinology* **9**, 243–254 (1995).
 86. Yasugi T. *et al.* Two classes of human papillomavirus type 16 E1 mutants suggest pleiotropic conformational constraints affecting E1 multimerization, E2 interaction, and interaction with cellular proteins. *Journal of virology* **71**, 5942–5951 (1997)
 87. Roig I. *et al.* Mouse TRIP13/PCH2 is required for recombination and normal higher-order chromosome structure during meiosis. *PLoS genetics* **6**, 1001062 (2010)
 88. Pressly, J. D. *et al.* TRIP13-deficient tubular epithelial cells are susceptible to apoptosis following acute kidney injury. *Science Report* 1–13, (2017)
 89. Marinkovic, D. *et al.* Identification of novel Myc target genes with a potential role in lymphomagenesis. *Nucleic Acids Research* **32**, 5368–5378 (2004).
 90. Wanzel, M., Herold, S. & Eilers, M. Transcriptional repression by Myc. *Trends Cell Biol.* **13**, 146–150 (2003).
 91. Tu, W. B. *et al.* Myc and its interactors take shape. *Biochim. Biophys. Acta* **1849**, 469–483 (2015).
 92. Nascimento, E. M. *et al.* The opposing transcriptional functions of Sin3a and c-Myc are required to maintain tissue homeostasis. *Nat Cell Biol* **13**, 1395–1405 (2011).
 93. Natarajan A, *et al.* The EGF receptor is required for efficient liver regeneration. *Proc Natl Acad Sci USA* **104**:17081- 1708 (2014)
 94. Lanaya H, Natarajan A, Komposch K, *et al.* EGFR has a tumour-promoting role in liver macrophages during hepatocellular carcinoma formation. *Nat Cell Biol* **16**, 972-981 (2014).
 95. Lopez-Luque J, Caballero-Diaz D, Martinez-Palacian A, *et al.* Dissecting the role of the epidermal growth factor receptor catalytic activity during liver regeneration and hepatocarcinogenesis. *HEPATOLOGY* **63**, 604-619 (2016)
 96. Berasain, C. & Avila, M. A. Further evidence on the janus-faced nature of the epidermal growth factor receptor: From liver regeneration to hepatocarcinogenesis. *Hepatology* **63**, 371–374 (2016).
 97. Whitfield, J. R. & Soucek, L. Tumour microenvironment: becoming sick of Myc. *Cell. Mol. Life Sci.* **69**, 931–934 (2012).
 98. Meyer, N. & Penn, L. Z. Reflecting on 25 years with MYC. *Nature Reviews Cancer* **8**, 976–990 (2008).
-

-
99. Miller, D. M., *et al.* c-Myc and Cancer Metabolism. *Clinical Cancer Research* **18**, 5546–5553 (2012).
 100. Zheng, K., Cubero, F. J. & Nevzorova, Y. A. c-MYC-Making Liver Sick: Role of c-MYC in Hepatic Cell Function, Homeostasis and Disease. *Genes (Basel)* **8**, 123 (2017).
 101. Dauch, D. *et al.* A MYC-aurora kinase A protein complex represents an actionable drug target in p53-altered liver cancer. *Nat. Med.* **22**, 744–753 (2016).
 102. Kira, S. *et al.* Expression of transforming growth factor alpha and epidermal growth factor receptor in human hepatocellular carcinoma. *Liver* **17**, 177–182 (2008).
 103. Bejarano, P. A. Epidermal Growth Factor Receptor Expression and Gene Copy Number in Conventional Hepatocellular Carcinoma. *Yearbook of Pathology and Laboratory Medicine* **2010**, 42 (2010).
 104. Harada, K.-I., Shiota, G. & Kawasaki, H. Transforming growth factor- α and epidermal growth factor receptor in chronic liver disease and hepatocellular carcinoma. *Liver International* **19**, 318–325 (1999).
 105. Baselga, J. & Arteaga, C. L. Critical Update and Emerging Trends in Epidermal Growth Factor Receptor Targeting in Cancer. *Journal of Clinical Oncology* **23**, 2445–2459 (2005).
 106. Marshall, J. Clinical implications of the mechanism of epidermal growth factor receptor inhibitors. *Cancer* **107**, 1207–1218 (2006).
 107. Höpfner, M. *et al.* Targeting the epidermal growth factor receptor by gefitinib for treatment of hepatocellular carcinoma. *Journal of Hepatology* **41**, 1008–1016 (2004).
 108. Shachaf, C. M. *et al.* MYC inactivation uncovers pluripotent differentiation and tumour dormancy in hepatocellular cancer. *Nature* **431**, 1112–1117 (2004).
 109. Beer, S. *et al.* Hepatotoxin-Induced Changes in the Adult Murine Liver Promote MYC-Induced Tumorigenesis. *PLoS ONE* **3**, e2493 (2008).
 110. Anderson, D. J. *et al.* Targeting the AAA ATPase p97 as an Approach to Treat Cancer through Disruption of Protein Homeostasis. *Cancer Cell* **28**, 653–665 (2015).
 111. Tong Zhou, Jeff Chou. *et al.* (2007) Identification of Primary Transcriptional Regulation of Cell Cycle-Regulated Genes upon DNA Damage, *Cell Cycle*, **6:8**, 972-981 (2007)
 112. Van der Meijden CM, Lapointe DS, Luong MX, *et al.* Gene profiling of cell cycle progression through S-phase reveals sequential expression of genes required for DNA replication and nucleosome assembly. *Cancer Res* **62**, 3233-43 (2002)
 113. Ren B, Cam H, Takahashi Y, *et al.* E2F integrates cell cycle progression with DNA repair, replication, and G (2)/M checkpoints. *Genes Dev.* **16** 245-56 (2002)
 114. Barna M, Pusic A, Zollo O, *et al.* Suppression of Myc oncogenic activity by ribosomal protein haploinsufficiency. *Nature* **456**, 971-5 (2008)
 115. Berasain, C. & Avila, M. A. The EGFR signalling system in the liver: from hepatoprotection to hepatocarcinogenesis. *J. Gastroenterol.* **49**, 9–23 (2014).
 116. Buckley, A. F., Burgart, L. J., Sahai, V. & Kakar, S. Epidermal Growth Factor Receptor Expression and Gene Copy Number in Conventional Hepatocellular Carcinoma. *American Journal of Clinical Pathology* **129**, 245–251 (2008)
-